2018

Condition based bridge management with SHM integration: A novel approach to remaining life estimation of bridges

Sameera Tharanga Jayathilaka
Iowa State University

Condition based bridge management with SHM integration: A novel approach to remaining life estimation of bridges

by

Sameera Tharanga Jayathilaka

A dissertation submitted to the graduate faculty

in partial fulfillment of the requirements for the degree of

DOCTOR OF PHILOSOPHY

Major: Civil Engineering (Structural Engineering)

Program of Study Committee:
Brent Phares, Major Professor
Behrouz Shafei
Alice Alipour
Vinay Dayal
David Herzog

The student author, whose presentation of the scholarship herein was approved by the program of study committee, is solely responsible for the content of this dissertation. The Graduate College will ensure this dissertation is globally accessible and will not permit alterations after a degree is conferred.

Iowa State University

Ames, Iowa

2018

TABLE OF CONTENTS

LIST OF FIGURES

LIST OF TABLES

ACKNOWLEDGMENTS

I would like to express my sincere gratitude to my major professor, Dr. Brent Phares. I appreciate the freedom, guidance, support and encouragement which he has given to me throughout the course my graduate student life. I would like to thank Dr. Shafei Behrouz, Dr. Alice Alipour, Dr. Vinay Dayal and Dr. David Herzog for being my PhD committee members. I am always very grateful to former Civil Engineering Department Chair at Iowa State University, Professor Emeritus Lowell Greimann for his excellent guidance and support given to me throughout my graduate research projects while battling with Cancer. I would also like to thank the former Civil Engineering Department Chair at Iowa State University, Dr. Terry Wipf's help throughout the preparation of my PhD dissertation. Without you all this work would have been far from complete.

I am grateful to Bridge Engineering Center at Iowa State University, Iowa DOT, Wisconsin DOT, Illinois DOT, FHWA, and USDA which have funded my project and also its engineers, who have helped in various aspects of the project. I would also like to acknowledge the Department of Civil Construction and Environmental Engineering of Iowa State University and all of its professors for molding my mind into what it is today.

Finally, I would like to thank my wife, Chathurika Karunathilake, and my family, friends for all their help, encouragement and their valuable company throughout my life. Thank You.

ABSTRACT

Bridge deterioration and aging are important problems in the United States. According to the infrastructure report card from the American Society of Civil Engineers, as of 2016, almost one in 11 (9.1%) bridges are structurally deficient and approximately 4 out of 10 (40%) bridges are older than 50 years. Rehabilitation cost for these bridges are estimated to be about $123 billion, pointing to the need for proper bridge management plans. There are many bridge management systems in the world. All of these lack of an integrated SHM system and are subject to criticism of being subjective. Condition-Based Maintenance (CBM) coupled with the Structural Health Monitoring (SHM) data can be used to actively manage bridges while minimizing subjective effects.

The current research work consisted of two primary tasks. The first task was to update the current automated CBM-SHM framework developed at the Bridge Engineering Center (BEC) at Iowa State University (ISU), by improving its current load rating calculation process. The current load rating approach underestimates the rating factor of a bridge by 20% to 40%. The load rating calculation process was improved by developing a relationship between moment of inertia and flexural strength of bridges. An extensive experimental program was conducted to validate the relationship. The proposed method may significantly improve the rating factor of a bridge.

The second task was to develop a novel condition rating prediction model to predict future condition ratings of the bridges. The condition rating information in the National Bridge Inventory (NBI) database was used in this development. The research group developed two different types of future condition rating prediction models, Current Practice Model (CPM) and Deterioration Prediction Model (DPM). CPM is capable of simulating the effects of

historical maintenance activities and DPM does not consider the effects of historical maintenance activities when predicting the future condition rating probabilities. Both CPMs and DPMs were quantitatively and qualitatively validated.

CHAPTER 1. INTRODUCTION

1.1. Background

Bridges constitute the most expensive assets, by mile, for transportation agencies around the United States and World. Most of the bridges in the United States were constructed between the 1950's and the 1970's. There is, consequently, an increasing number of bridges that are getting old and requiring much more frequent inspections, repairs, or rehabilitations to keep them safe and functional. However, due to constrained construction and maintenance budgets, bridge owners are faced with the difficult task of balancing the condition of their bridges with the cost of maintaining them. According to the infrastructure report card from the American Society of Civil Engineers (ASCE) [1], as of 2016, out of 614,387 bridges in the United States, approximately 245,755 bridges (4 out of 10) are older than 50 years, in most cases the design life is 50 years. Also, it states that 56,007 bridges (1 out of 11) are considered structurally deficient and on average, 188 million trips across structurally deficient bridges on each day were recorded. Further, more than 83,557 bridges (1 out of 8) in the nation do not serve current traffic demand or meet current standards. Rehabilitation of these bridges could cost about $123 billion.

1.1.1 Bridge Management Systems

Bridge maintenance strategies depend upon the information used to estimate future condition and remaining life of bridges. The purpose of the future condition assessment is to determine when to undertake repairs or maintenance to keep its condition within acceptable limits. Also, the estimation of residual or remaining life is an important input for budgeting and setting longer-term repairs and maintenance priorities. To better manage bridge inventories, therefore, tools that can accurately predict the future condition of a bridge, as well

as its remaining life (i.e., when a bridge will become substandard in terms of load carrying capacity, serviceability, and/or functionality), are required. It goes without saying that essential to estimating future condition of structures is having a very strong and accurate understanding of the current condition of the structure.

The AASHTO Manual for Bridge Evaluation [2], together with software PONTIS and BRIDGIT [3], are fundamental for the Bridge Management System (BMS) used by many states in the United States. BMS accurately document the current and future condition of bridges, are required, by the 1991 Intermodal Surface Transportation Efficiency Act (ISTEA) and the 1998 Transportation Equity Act for 21st Century (TEA-21), for public safety. Even more, bridge owners are mandated in other bridge preservation areas that include inspection scheduling, cost analysis, and rehabilitation planning.

The Manual for Bridge Evaluation [2] characterizes the condition of bridges across the United States following highly prescribed processes and procedures. The components of a bridge are visually inspected biennially and the standardized four condition states (good, fair, poor, and severe) are assigned to each of the relevant components. The condition states are used subsequently to determine bridge condition, appraisal, and sufficiency ratings. These ratings then become an important parameter in the bridge management approach typically used by each state. Although the bridge condition states reflect deterioration or damage, they do not quantify the structural deficiency of a bridge or its components.

An approach to predict the future condition of bridge components could be to use a "back of the envelope" linear model that assume one drop in deck condition rating every eight years and one drop in superstructure and substructure condition rating every ten years. This approach has a significant limitation that is it does not quite capture the actual aging process

and it does not reflect any difference between individual bridges. Aging is a continuous accumulation of deleterious chemical and mechanical reactions (observed and unobservable) throughout the life of the bridge due to weather, service conditions (traffic, deicing, etc.), and their interactions [4] [5]. The linear deterioration model does not account for the nonlinear behavior caused by the impacts of traffic volume, weight, structure and material type, environmental impacts, and interactions between these variables specific to any given bridge, and this might result in unreliable prediction of bridge future condition.

1.1.2 Structural Health Monitoring

The desire for many Department's of Transportation (DOT's) is to augment the existing inspection process and maintenance system with a system that is capable of objectively and more accurately quantifying the state of bridge health in terms of condition and performance, aiding in inspection and maintenance activities, and able to estimate the remaining life of its bridge inventory in real time. As early as the 1980's bridge engineers have had the vision for an intelligent infrastructure system [6] [7] [8] capable of, (1). Sensing its own load environment, its responses and any ongoing damage and deterioration, (2). Assessing its condition regarding its capacity and performance needs and the actual capacity that is being delivered, (3). Determining if and when behavior thresholds are exceeded or compromised such that the structural capacity, traffic volume capacity, environmental limiting conditions, and others have exceeded predetermined criteria.

In terms of alerts, the bridge owner is ideally alerted by the system when a diversion of traffic is required, when posting of the bridge is required to prevent infractions from accelerated deterioration, when bridge repairs are needed, and when the bridge needs to be closed. To this end it has been identified [9] that one of the key requirements for an effective

infrastructure management system is the establishment of Structural Health Monitoring (SHM) system consisting of a network of monitoring sensors, data acquisition, and communication hardware and software for carrying out bridge condition assessments in real time and capable of accurately and objectively predicting the health of the infrastructure components and systems. It is also held by many researchers [10] [11] and the FHWA long-term bridge performance (LTBP) program [12] that the other important component is the establishment of indices or thresholds for the critical structural elements through, for instance, calibration of finite element analytical models that compute strains, stresses, forces, reactions, and boundary conditions. In this conceptualization a SHM system serves as the tool that enables the bridge owner to understand and evaluate the interactions between environmental conditions, bridge boundary conditions, bridge component mechanical conditions, and the impact of damage and deterioration on the mechanical characteristics of the bridge elements.

1.1.3 Bridge Maintenance Prioritization Strategies

1.1.3.1. State of the Art of Practice of Bridge Maintenance Prioritization

Corrective maintenance and preventative maintenance are the most common maintenance prioritization approaches utilized by most bridge owners. Sometimes these two approaches are combined using engineering judgement. Within the corrective maintenance framework, a bridge is operated until a defect appears, then a decision needs to be made to determine if the defect is critical or non-critical. Prompt action is needed for critical defects. This approach has been used by bridge owners for years in prioritizing maintenance activities. However, some defects have developed that have gotten so significant that they were very expensive to fix and/or had safety threatening conditions. This approach is sometimes

criticized because it does not use maintenance funding in an optimized way. In other words, some (minor) maintenance should have been performed before severe damage can even occur.

Preventive maintenance includes periodic maintenance or maintenance based on condition prediction. This is fairly commonly used in the bridge community. This involves looking at the bridge rating history and available bridge deterioration models to find an optimized time for maintenance activities but before failures occur. Due to limitations of currently available bridge deterioration models and the lack of quantitative data, accurately predicting the performance of a specific bridge is hard, if not impossible. Therefore, preventive maintenance is still used more commonly for preventing failure rather than optimizing maintenance activities. Even so, there is a cost associate with this approach. Generally, this strategy advises that maintenance be performed more often than is absolutely necessary and, as such, can lead to an over maintenance scenario.

1.1.3.2. Condition-Based Maintenance (CBM) Approach

Condition-Based Maintenance (CBM) [13] [14] is a maintenance strategy used to actively manage the condition of assets/equipment in order to perform maintenance only when it is needed and at the most opportune times. CBM is accomplished by integrating all available data to predict impending failures of assets as well as to avoid costly maintenance activities. This process depends, largely, on the ability of the manager or managing algorithm to recognize undesirable operating conditions as measured by diagnostic monitoring systems. The process also allows an asset to continue operating in an undesirable, yet safe, condition while it is being monitored until maintenance can be scheduled and performed. CBM can reduce maintenance costs, improve availability and reliability, and enhance life span of the asset. This strategy has been widely used in the management of weapon systems, nuclear power

plants, jet engines, marine engines, wind turbine generators, natural gas compression, and others [15]. However, its application in bridge management is limited because current bridge inventory data, which are collected biennially through scheduled bridge inspection, are not sufficient to implement CBM. With the development of SHM, more and more bridges are being continuously monitored. By integrating the real-time or near real-time bridge condition data collected by SHM system into bridge inventory data, a SHM facilitated CBM (SHM-CBM) framework is possible.

1.2. Objective

The research described here consisted of two primary tasks. The first task was to update the current automated SHM framework developed by the BEC of ISU by improving its current load rating calculation process. The second task was to develop a novel condition rating prediction model to predict the future condition ratings of bridges in the United States. The condition rating prediction model along with the SHM framework is intended to be used as a SHM facilitated CBM strategy for the United States bridge management. A method to combine the condition rating prediction model into the current SHM framework is briefly discussed, but presented in detail elsewhere. Due to the somewhat limited availability of installed SHM systems, the condition rating prediction model, which is based on the biennial bridge inspections in the NBI database still play a notable role in the maintenance decision making process with the SHM data functioning as a "tuner" to refine the maintenance priority up or down to a reasonable and user controllable degree when such data are available.

1.3. Report Organization

In this report, Chapter 2 reviews sample of current SHM systems and Chapter 3 illustrates the overview of the current SHM framework, which has been developed by the

authors and is becoming more widely adopted. Also; Chapter 3 briefly describes truck detection, damage detection and the automated load rating of the current SHM framework. Chapter 4 presents the improved load rating calculation process along with improved capacity estimation of steel-concrete composite sections. Chapter 5 illustrates the development of condition rating prediction models using biennial bridge inspections in the NBI database. Chapter 6 summarizes this work and presents several concluding remarks.

CHAPTER 2. LITERATURE REVIEW

A literature review was conducted to investigate the currently available different types of asset management systems in different areas, including pavements, vehicle systems, tall buildings and bridges. The current bridge management methodology of the Iowa Department of Transportation (IADOT) was also discussed at the end of the literature review.

2.1. Pavements Management Systems

In Pavement Management Systems (PMS) some owners use the Pavement Condition Index (PCI) as the controlling factor for scheduling of maintenance and repair activities. PCI is a number between 0 and 100, with 0 being the worst condition. For instance, a PCI of less than 60 means the pavement needs reconstruction while a PCI between 80 and 85 means the pavement is in very good condition [16]. The PCI is a function of road surface distresses such as cracking, ride quality, structural capacity, and friction. The predictive variables for pavement condition in regression and deterministic mechanistic algorithms used in PMS include traffic loading, climatic conditions, pavement structural properties, and past rate of pavement deterioration. These algorithms are in essence damage mathematical tools that predict the time or cumulative traffic to reach a failure criterion. This information is then used to plan and schedule maintenance and repair activities for pavement systems.

2.2. Aerospace and Other Vehicle Management Systems

In the aircraft industry one fleet asset management system is referred to as the Integrated Vehicle Health Management (IVHM) system [17]. The goal of IVHM is to assess present and to predict future vehicle condition. This information is used to enhance operational decisions, support corrective actions, and subsequent continued use of the aircraft [18]. In this framework, IVHM consists of four main blocks, namely, (1). SHM systems to measure the

state of the aircraft while in flight for damage prone stress concentration areas, for unanticipated aerial events such as impacts, and for aging effects such as fatigue and cracking, to establish the current state of the fleet. Structural health measurement is primarily through the use of fiber optic sensors for state parameter metrics such as strain, temperature, pressure load, and aircraft components accelerations. Probabilistic models for the state parameters and failure models are also established at this stage [19] [20]. (2). A Prognostics and Health Management (PHM) block that uses the current stochastic state parameters together with damage growth characteristics to form failure probability models. This is followed by calibration of a model to produce a probabilistic prognosis of damage evolution in terms of damage versus time or number of cycles the aircraft is in use. The calibrated structural model can also be used to assess failure probabilities in areas not instrumented by sensors. If the failure probabilities established above are lower than the pre-set levels, the fleet of aircraft is kept in service. The processed structural damage parameters include strain time histories, power spectral densities, and Root Mean Square (RMS) values of the state parameters. As fatigue is the biggest problem in aircraft, the processed data are primarily used in designing repair patches with increased damping properties for installation on the aircraft body. These patches lead to reduced structural responses and, thus, extending the service life of the aircraft fleet. (3). Non-Destructive Inspections (NDI) are also used on aircraft while they are on the ground. When the probability of failure is higher than the pre-set levels the fleet of aircraft is further subjected to non-destructive inspections, and, if needed, repairs are carried out at the aircraft maintenance facility. (4). The IVHM architecture finally includes an Information Technology (IT) block for communication of the obtained knowledge base to the flight crew,

operations and maintenance personnel, regulatory agencies, and the Original Equipment Manufacturers (OEM).

Today the acronym IVHM also includes other types of vehicle systems such as cars, trucks, ships, trains, helicopters, submarines, tanks, etc. In this broader sense, it is meant, therefore, to be an advanced system capable of carrying out health monitoring, diagnosis, prognosis, and computation of reactive planning decision making tools for corrective and preventive measures for the numerous components and subsystems such as, structural frame, engine performance, electronics, hydraulics, fuel systems, and electric power systems.

2.3. Tall Building Management Systems

The issues of importance in tall buildings are safety and comfort of the occupants. Tall buildings are normally designed using state-of-the art structural analyses coupled with wind tunnel testing on scaled models. Wind speed and direction are the primary parameters for wind tunnel prediction models. In this framework the impetus for structural health monitoring is the need for establishing the accuracy and validity of the design methods. The results of the analyses must be in conformity with the monitored building performance [21] [22] [23] as determined by sensors monitoring ground accelerations, damping, strains, deflections, gravity loads, and meteorological site conditions. From the SHM knowledge base, structural control, in terms of limiting states, is then established via the use of structural control devices such as Active Mass Dampers (ADM), Active Variable Stiffness (AVS) systems, Hybrid Mass Dampers (HMD), and Active Gyroscopic Stabilizers (AGS) [24] [25].

2.4. Bridges Management Systems

2.4.1 Basis of Bridge Management Systems

Estimation of remaining service life of bridges are very important, yet it is a very complex problem as bridges deteriorate due to many reasons. Many researchers developed different methods, from simple linear regressions to artificial neural networks, to predict the remaining service life of bridges. Also, many of the researchers focused on estimating the remaining service life of bridge decks over the other bridge components. Because, the bridge decks get deteriorate faster than the other bridge components due to its continuous exposure to environmental changes and traffic conditions. According to a survey of bridge decks in Korea, Oh et. al. [26] stated that bridge decks are repaired 5 years after the opening and most bridge decks get repaired every 10 to 15 years. This section summarizes some of the research work conducted to estimate the remaining service life of bridges.

Most bridge decks get cracks and then reinforcement get corrode due to freeze thaw effect and deicing salt. The deck cracking could lead to reduce the remaining service life and the ultimate capacity of the bridge. Therefore, many researchers focused on bridge deterioration due to deck reinforcement corrosion. Kirkpatrick et. al. [27] developed a model to estimate the time to first repair the concrete bridge decks which are subjected to cold weather condition and deicing salts. Ten bridges in State of Virginia considered during the study. Probabilistic models along with statistical parameters used to predict the repair times and results validated with another bridges. According to the results, time to first repair concrete bridge decks takes about 13 years. Liang et. al. [28] conducted a study to compare the estimations of the remaining service life given by several different mathematical models. The mathematical models used to estimate both corrosion initiation time and corrosion propagation time. Liang et. al. [28] suggested to use AJMF prediction method to estimate corrosion

initiation time and Modified Bazant method to predict the corrosion propagation time. Oh et. al. [26] developed a model to realistically assess the service life of concrete bridge decks based on both corrosion effect and moving traffic loads. D. Chen and S. Mahadevan [29] proposed a model to simulate the reinforcement corrosion, and later a finite element model used to simulate the concrete cracking due to rust expansion. Song et. al. [30] also proposed a numerical simulation method to predict the remaining service life of bridge decks due to chloride ingress through concrete deck. Even though many researchers looked at the bridge deck deterioration due to chloride diffusion, the primary idea behind each research work is to use of Fick's second law model the chlorine diffusion with different statistical parameters. The ultimate results are useful to draw baseline for the remaining service life of a bridge, it highly depends on the statistical parameters and assumptions used in the analysis. The results obtained using this method represent generic number for the remaining service life of a bridge deck. Therefore, this method does not consider the unique characteristic of any bridge and the historical behavior of the bridge. Hence, these models are more suitable to use in newly constructed bridge decks to estimate the time to carry out the first repair and maintenance activities and these models are not appropriate to estimate the service life of old bridges in the transportation network.

Another important factor that affects the remaining life of bridges is fatigue of bridge components. The basic concept of estimating cumulative fatigue damage is based on Miner rule proposed by Miner [31] in 1945. Since the Miner rule is often unsatisfactory for estimating fatigue damage due to variable amplitude loading, many researchers tried to come up with some modifications to Miner rule or innovative methods to estimate the remaining fatigue life of structures. Li et. al. [32] developed strategy to assess the fatigue damage and estimate the

remaining fatigue life of existing bridges using structural health monitoring data. Theory of Continuum Damage Mechanics (CDM) used to develop the damage accumulation due to the fatigue. A modified version of Miner rule also considered to calculate the fatigue damage accumulation and compared with the CDM fatigue damage model results. Later, Li et. al. [33], validated the proposed CDM fatigue damage model using structural health monitoring data coming from an actual bridge. Y. Zhou [34] also worked on estimating the remaining fatigue life of bridges using field strain measurements. Zhou concluded that use of actual data coming from a bridge site is more accurate and efficient in estimating the remaining fatigue life of existing bridges. K. Kwon and D. M. Frangopol [35] assessed the performance of aging steel bridges due to fatigue based on three different prediction models, (1). Fatigue Reliability Model (FRM), (2). Crack Growth Model (CGM), and (3). Probability of Detection (POD) model. The combined model is used to evaluate the fatigue damage of an existing bridge. Estimation of remaining fatigue life is important, and the proposed models are very useful in predicting the remaining fatigue life. However, fatigue damage alone does not govern the remaining life of a bridge. Especially, when estimating remaining life of a prestressed concrete girder bridges, the remaining fatigue life is not significant.

The estimation of the remaining service life of bridges based on the overall condition of each primary component is very important. Many researchers used NBI bridge condition rating database to model the future bridge condition ratings and estimate of remaining service life of bridges. The NBI bridge condition rating database consist of historical conditions of each bridge component, based on biannual visual inspections. The NBI bridge condition rating database contains historical condition rating data over past three decade and it is the best database which describe the historical behavior of bridges in the United States. Researchers

used the NBI bridge condition rating database in three different ways to predict the remaining service life of bridges, namely, (1) Regression method, (2) Markov-Chain Theory and (3) Artificial neural networks.

In Turkey, bridge inspections are conducted based on as-needed basis and Alp Caner et. al. [36] proposed very simple method to estimate the remaining service life of bridges in Turkey. The remaining life estimated by establishing a relationship between the age and condition of the bridges. Each component of 29 bridges inspected for the first time and age and condition rating of the bridge recorded. A regression line of the 29 data points used as the future condition perdition and it was used to define the remaining service life of the bridges. Even though the procedure is simple Alp Caner et. al. [36] stated that the deck condition deteriorates faster that the superstructure and substructure components. Bolukbasi et. al. [37] used NBI bridge condition rating database to develop deterioration models for different types of bridges and different bridge components. The NBI database used for the analysis involved 2601 bridges built during 1976 to 1998 in the State of Illinois. Typically, the condition rating data in the NBI bridge condition rating database carry large uncertainty, mainly due to different inspection routines of different bridge inspectors and unrecorded repair and maintenance events. Bolukbasi et. al. [37] used two different set of rules to remove possible uncertainties of the NBI database and regression methods used to develop the future condition rating prediction models.

It is a well-known fact that, the condition rating data in NBI bridge condition rating database carry large uncertainty. However, filtering NBI condition rating data to remove uncertainty, may disturb the actual representation of the condition rating behavior of the bridges. The future condition rating prediction models develop based on regression theory

illustrate a generic condition rating models that can be applied only to newly constructed bridges. Therefore, these models may or may not represent the future condition of an existing bridge in the nation's transportation network.

Development of future condition rating prediction models using Markov-Chain theory is one step advanced than the regression method. Markov-Chain Theory is used to calculate the transition probabilities of the condition ratings. The transition probabilities are found based the NBI historical condition rating database. Morcous [38] developed transition probability of bridge decks using Markov-Chain theory. Bocchini et. al. [39] developed an improved version of future condition rating predication models using Markov-Chain Theory. Hopper et. al. [40] proposed a Semi-Markov-Chain theory model to predict the deterioration of bridge decks. Hopper et. al. [40] used more than 20,000 bridge condition rating histories of Pennsylvania State in the analysis. The data filtered to remove any uncertainties due to inspector subjectivity and unrecorded repair and maintenance data. Sojourn Time, the time spent at each condition rating before transitioning to another condition rating along with Weibull distribution used to develop transition probabilities of the model.

Even though many researchers tend to use traditional and improved versions of Markov-Chain theory to develop future condition rating prediction models, the Markov- Chain models depend on two primary assumptions, (1). Bridge inspections are carried out at fixed time intervals and (2). The future bridge conditions depend on the present condition of the bridge, but not the past condition of the bridge. Therefore, the predicted future condition rating may not clearly represent the historical behavior of the bridges.

2.4.2 Current Bridge Management Systems

There are roughly 21 Bridge Management Systems (BMS) in the world [41]. These management systems are used for quantification of, (1). Deterioration and performance indicators, (2). Formulation of corrective intervention strategies with respect to cost and time, and (3). Quantification of changes following an intervention program. What all of these have in common is a lack of an integrated SHM system. Hence, they are all subject to criticism of being subjective. The general organizational structure of a bridge management system with an integrated SHM system is a self-contained entity comprising, in the minimum, of the following main features [42], such as personnel consisting mainly of the scientific team, the technical team, and general staff, the physical bridge, information technology, analytical division, decision making wing, and influence of the non-technical sector.

All the most advanced BMSs (e.g., the Federal Highway Administration (FHWA) PONTIS and BRIDGIT in the US, NYSDOT in New York, US, OBMS in Ontario, Canada, QBMS in Quebec, Canada, KUBA in Germany), tend to use Markov probabilistic models based on linear transition probabilities that specify the likelihood that the condition of a bridge component will change from one state to another in a specified interval of time. They have been found very useful in predicting the percentage of bridges in any given deterioration state, and in estimating the expected condition of a bridge at some given future time.

In the US, PONTIS is the BMS used by many states. In PONTIS a bridge is subdivided into many structural elements instead of just three components that have been the focus of historical National Bridge Inventory inspections (i.e., deck, superstructure, and substructure). Each element is evaluated separately and later combined at the project level to determine the best maintenance repair and rehabilitation, improvement, and replacement strategy for the bridge. PONTIS is a federally-funded BMS that uses probabilistic modelling techniques and

optimization procedures coupled with the NBI database. The database is an accumulation of inventory, inspection, and supplemental data from traffic and bridge accident reports. All these data are fed into PONTIS to, (1). Predict bridge deterioration for each bridge element, (2). Find the most cost-effective MR&R action to solve the deterioration problem, (3). Quantify any necessary functional improvements in terms of user cost and convenience, and weighing them against the cost of MR&R, (4). Select the most appropriate bridge improvement and replacement, (5). Help in scheduling of the work to be undertaken using state based statistical Markov models and solution methods that predict future bridge conditions. However, none of the data in PONTIS comes from a structural health monitoring system. PONTIS is, therefore, a subjective tool.

2.4.3 Implementation of a SHM System in BMS

The planed objectives for introduction of a SHM system are well known (i.e. to provide objective quantitative data in real time that can be used to assess structural damage and deterioration, structural capacity, and which can be synthesized through algorithms to aid bridge owners make decisions regarding bridge closures, posting, and maintenance, repairs and rehabilitation) [43]. The actual process involves monitoring and capturing critical inputs and responses of a structural system. These system descriptors might include physical dimensional properties, strains levels, vibration properties, material properties, damping properties, and boundary conditions. Collectively, these inputs and responses can be used to understand the root causes of the problems as well as to track responses to predict the future behavior of a bridge. There is no one SHM system that fits all bridges. A setting or application has to be defined for a SHM plan. Each bridge setting normally pre-determines a unique set of

parameters to be measured and monitored so that a bridge may be accurately and completely characterized for reliable simulation.

2.4.4 Current Bridge Management System of the Iowa DOT

According to the FHWA, bridges must be given a condition rating and bridge overall sufficiency rating in accordance with the "Recording Guide for the Structure Inventory and Appraisal of the Nation's Bridges" Report No. FHWA-PD-96-001 [44]. A condition rating is an integer number from 0 and 9, with 9 representing a component in excellent condition while a 0 rating is given to a failed bridge, out of service and beyond any corrective action. A bridge with condition ratings 5 or better is structurally adequate requiring only cosmetic routine maintenance for section loss, cracking, spalling or scour. The Iowa DOT BMS is based on the biennial visual inspection reports generated and required to update the NBI database. These inspection reports, including other levels of inspections deemed necessary by Iowa DOT, include detailed descriptions of type and extent of deteriorations observed by inspectors using photographs, construction drawings and sketches. Bridge issues requiring immediate attention are also noted in the reports by the inspectors. Iowa DOT conducts around 2500 bridge inspections annually. These inspections are most commonly completed using Iowa DOT personnel. Once each bridge inspection is complete, together with the FHWA required bridge inventory and operating rating by the Bridge Office, a Structure Inventory and Appraisal Sheet is prepared for FHWA biennial NBI reporting compliance. In addition, all bridge issues reported by inspectors as requiring immediate actions are reviewed by the Iowa DOT Maintenance Office. Based on the review, repairs orders are issued to the District Office with jurisdiction over the bridge. The DOT determines the type of repairs to be conducted, and whether the repairs are to be done in-house or through a contract.

Bridges requiring contract-based repairs are entered into a five-year program of repair and replacement overseen by the Iowa Transportation Commission (ITC), although the commission cannot preclude a bridge from repairs. Six times annually the Iowa DOT conducts meetings to review and prioritize the bridges for repair and to determine type of continued monitoring for those bridges that cannot be repaired with the current budget. A bridge repair ranking system has been developed by Iowa DOT for funding purposes. The ranking is based on the Average Daily Traffic (ADT) and a number of issues at the bridge reported by the inspector. The Iowa DOT BMS is similar in many respects to what it was twenty-five years ago [45]. However, since 2014, Iowa DOT has been developing a bridge element condition index classification as well as a modified sufficiency rating formula for bridge elements. This sufficiency rating is to help in the decision-making process when a large number of bridges are reported with varying element deterioration levels. One of the features the Iowa DOT is looking for in an SHM system, therefore, is a capability to help document the varying levels of deterioration in bridge elements.

2.4.5 SHM Framework for the Iowa DOT

The Iowa DOT in conjunction with the Bridge Engineering Center (BEC) at Iowa State University (ISU) has embarked on developing an SHM system to help collect on site quantitative bridge measurements for use in their current bridge management system. Iowa DOT conceptualization of an SHM is a system that would have the following characteristics, (1). Generates significant bridge performance parameters and their thresholds that may assist them in their current bridge management system. These parameters and thresholds, for the most part, will be dictated by or set in collaboration with Iowa DOT. (2). Includes rate of change of performance parameters for comparison with other bridges in the system. (3). Allows

querying the system for specific bridge performance parameters at any time. (4). Helps in bridge life cycle cost computations, e.g. life lost while a bridge is awaiting repairs, knowledge of preventable part of lost bridge life, annual loss of value of bridges in its inventory, etc., and (5). Communications go through personnel in their Bridge Maintenance Office.

CHAPTER 3. STRUCTURAL HEALTH MONITORING (SHM) FRAMEWORK

3.1. Introduction to SHM Framework

The Bridge Engineering Center (BEC) at Iowa State University (ISU) developed a Structural Health Monitoring (SHM) framework called Bridge Engineering Condition Assessment System (BECAS), which eliminates the subjectivity of current inspection approaches, increases evaluation frequency from once every two years to continuously, virtually remove human error, bias, and limitations, and provides feedback that can be used to perform proactive, rather than reactive, preventative maintenance. BECAS consists three important components, (1). BECAS hardware, (2). BECAS software, and (3). Finite element model of the bridge in which BECAS SHM system is installed. This chapter is intended to describe the primary components of the BECAS SHM Framework and a brief overview of its capabilities.

3.1.1 BECAS Hardware

The BECAS hardware consists of off-the-shelf components integrated together to form a network of state-of-the-art sensors, data collection equipment, data storage, and an N-tier data processing hub. There are three sensor types that make-up every BECAS installation, (1). Resistance strain sensors, (2). Temperature sensors, and (3). GPS signal collectors. In addition, sensors of multiple types can be integrated into the system (tilt, deflection, corrosion, acceleration, etc.) depending upon any unique monitoring needs. The sensors are connected to an on-site data logger that has high speed data collection and integrated data filtering capabilities. To temporarily store, initially process, and then transfer the data to the main data processing hub, a mid-level desktop PC is connected to the data logger via wired Ethernet. An IP-based video camera is also installed at each BECAS site. This camera is setup to record

(and temporarily store) a live video feed of the bridge (including traffic crossing the bridge). Another important piece of the on-site hardware is an IP-based power switch. This power switch has multiple features that make it a useful part of the system. For example, the power switch allows remote uses to power up or down individual system components from anywhere in the world. Second, in the event that the on-site system loses connection with the internet, the power switch will automatically reboot the on-site cellular modem until the system comes back on-line fully.

The ISU BEC has installed the BECAS SHM system on several bridges, including the bridge on Interstate 80 over Sugar Creek near Colfax, IA (FHWA No: 22380), hereafter referred to as I-80 Bridge (Figure 3.1) which is utilized here to explain the typical aspects of the BECAS SHM system. The bridge was built in 1966, and it is 200 ft. long, 40 ft. wide, 15 degrees skewed to right eastbound and carries two lanes of I-80 Eastbound traffic. It has 7.5 in. thick cast-in-place reinforced concrete deck, which is supported by five continuous steel girders (three W36×150 interior girders and two W36×136 exterior girders). The bridge consists of two 61 ft. outer spans and one 78 ft. middle span, where the girders are continuous over the both piers. Within the negative moment region, the exterior and interior girder flanges have cover plates with dimensions of 14 in. × 9/16 in. × 18.5 ft. and 14 in. × 5/8 in. × 18.5 ft., respectively. The girders are spliced at locations 17.5 ft. away from both piers. The spacing between the girders is 9.5 ft. The substructure consists of two end concrete stub abutments, and two intermediate open column concrete piers with cantilevers. Roller supports were placed at both abutments and at the east pier. Whereas, pinned supports were designed at the west pier of the bridge.

Figure 3.1. I-80 Bridge, on Interstate 80 over Sugar Creek

The SHM system developed for the I-80 Bridge consists of 71 electrical resistance strain gauges installed on the steel girders as shown in Figure 3.2. In Figure 3.2, the red disks represent a total of 35 strain gauges installed only on the top of the bottom flange of the steel girders, whereas green disks represent total of 36 strain gauges installed on both top of the bottom flange and bottom of the top flange of the steel the girders. The bridge cross-sections with instrumentation were labeled from A to O and the girder lines were labeled from 1 to 5. The sensor designation nomenclature represents strain gauge location by cross-section, girder line and flange location. For instance, sensor designation B2_BF represents a sensor installed at the intersection of Cross-Section B and Girder Line 2 (B2), and at the Bottom Flange (BF) of the girder, whereas sensor designation G1_TF represents a sensor installed at the intersection of Cross-Section G and Girder Line 1 (G1), and at the Top Flange (TF) of the girder. The SHM system on the I-80 Bridge also consists of eight electrical resistance strain gauges installed on the bottom of the concrete deck (Figure 3.3). These strain gauges are in

two rows of four strain gauges in each, and are located 23.59 ft. and 47.34 ft. from the northwest corner of the I-80 Bridge. For each deck strain gauges line, two gauges were installed in the south and north lanes. The deck strain gauges are used to identify vehicle travel lane, number of axles, axle spacing, and vehicle speed.

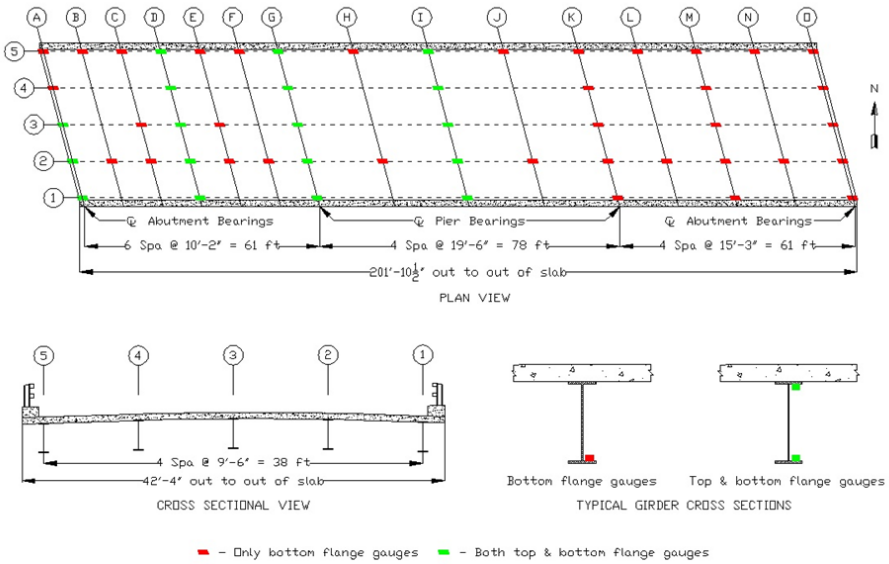

Figure 3.2. I-80 Bridge, Instrumentation Plan Girder Gauges

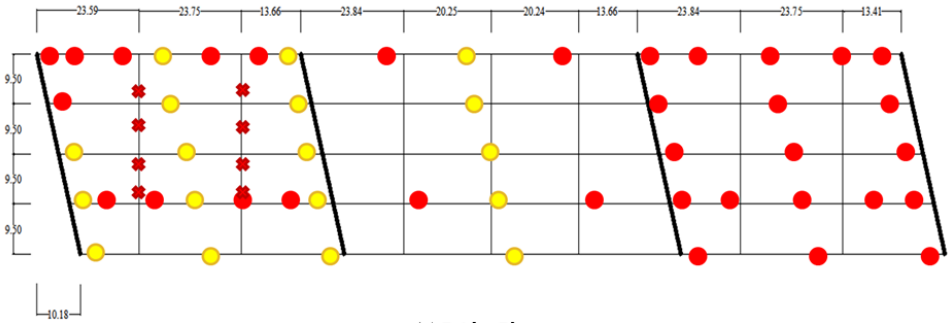

(a) Bridge Plan

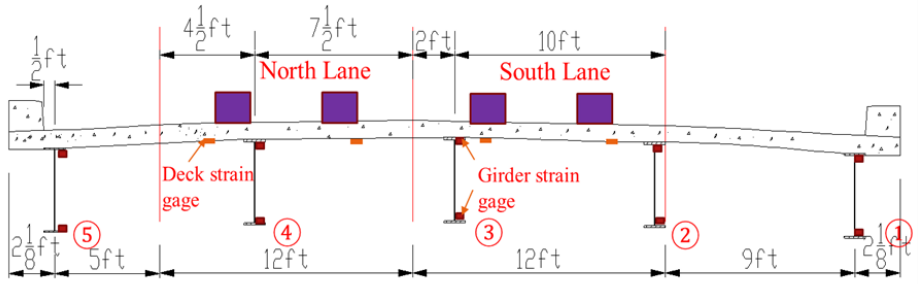

(b) Bridge Cross-section

Figure 3.3. I-80 Bridge, Instrumentation Plan Deck Gauges

3.1.2 BECAS Software

The BECAS Software package consists of several programs which are intended to carry out different tasks. Most BECAS SHM framework installations require multiple data loggers and BECAS Merge creates time sequenced data files with concatenated columns from multiple input files produced from multiple data loggers. BECAS Distributor continuously monitors a specified data repository to maintain the specific number of files. The program called BECAS Processing Engine checks the continuous data stream for anomalies and then analyzes the time sequenced data and evaluates the data to determine if a catastrophic event has occurred and then assesses the presence of user specified truck events on the bridge. BECAS Training trains the damage detection algorithm and BECAS Damage Detection program detects any condition changes in bridge condition based on user specified predefined settings. BECAS Load Rating uses the SHM data to calculate the load ratings of bridges.

3.1.3 Finite Element Model (FEM) of Demonstration Bridge

The Finite Element Model (FEM) of I-80 Bridge was developed using a commercially available software application called WinGen [46] and shown in Figure 3.4. The girders and diaphragms were modeled using two-node beam elements, which have three translational and three rotational degrees of freedom at each node. The deck was modeled using four-node quadrilateral shell elements, which have three translational and three rotational degrees of freedom at each node and incorporates bending behavior (ignore tension membrane behavior). Girder restraints at the abutment supports were modeled using spring elements. As shown in Figure 3.4(b), the beam elements share common nodes with the deck shell elements at the centroid locations. The composite section of the girder incorporating the transformed deck was

utilized for the section properties of each beam element. Linear elastic material models are used for the concrete and steel.

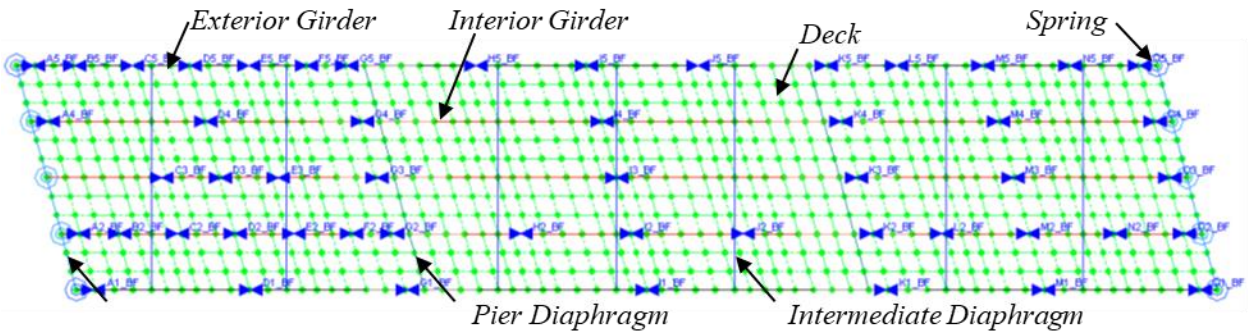

(a) Bridge Model and Sensors

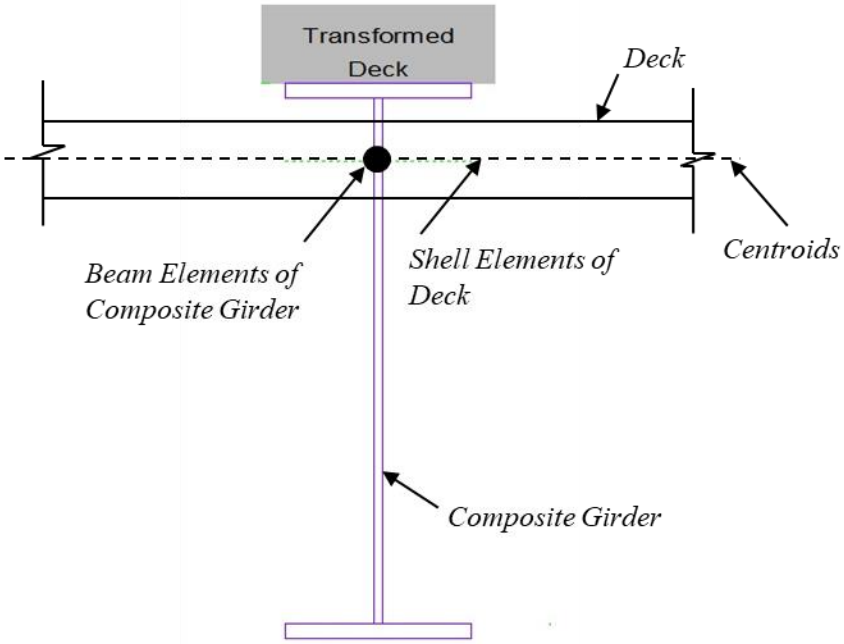

(b) Modeling of Girder and Deck

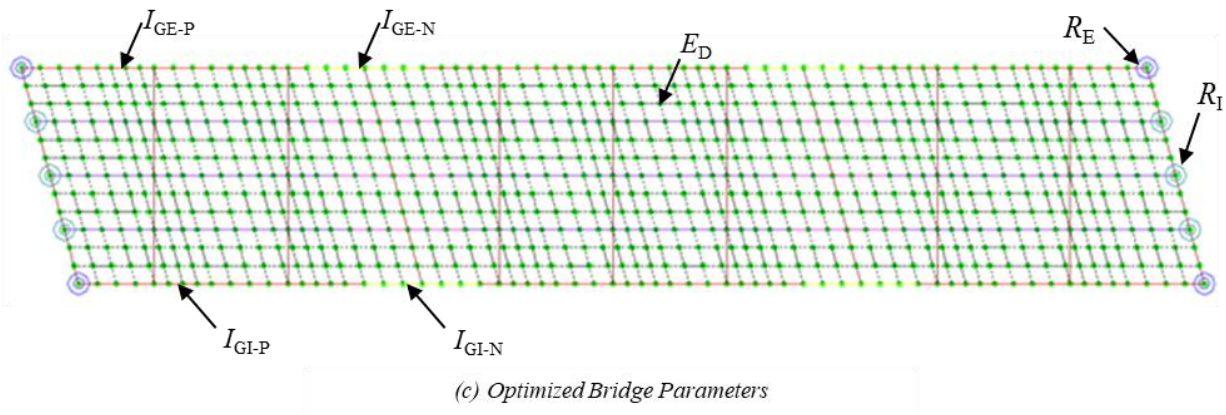

Figure 3.4. Details of FEM of I-80 Bridge

3.2. Truck Detection of SHM Framework

Truck Detection is a critical component of the BECAS SHM Framework. The damage detection and load rating portions of the SHM Framework (described later) primarily depend on the truck detection and associated responses of the bridge. The truck detection method was developed to detect single truck events with associated travel lane. A single truck event is defined as a scenario in which only a single truck travels in a single lane of a multi-lane bridge. Concurrent events, such as side-by-side trucks and/or one-after-other trucks traveling across a multi-lane bridge simultaneously, when detected, are not considered in further analysis. As an example, on a two lane bridge, the single truck event is shown in Figure 3.5(a) and Figure 3.5(b). The side-by-side concurrent events are illustrated in Figure 3.5(c), Figure 3.5(d), and Figure 3.5(e). Whereas Figure 3.5(f) and Figure 3.5(g) represent the one-after-another concurrent events.

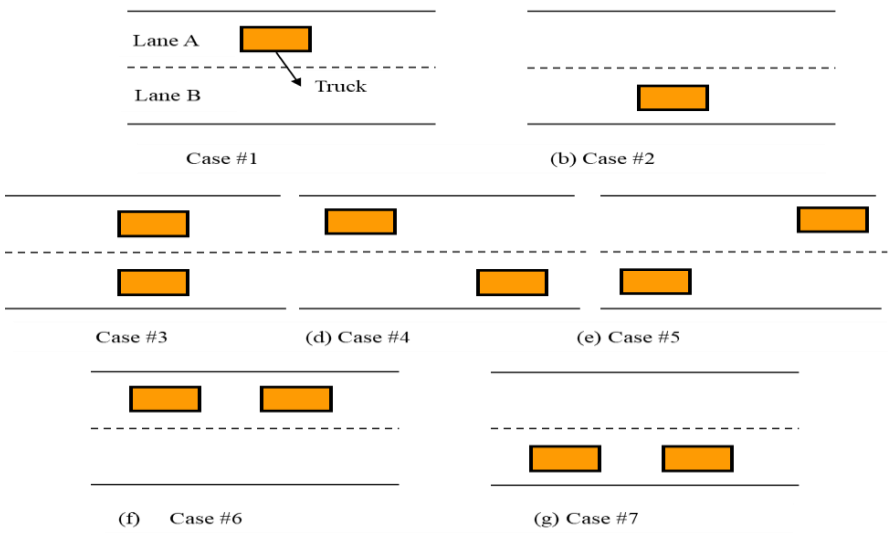

Figure 3.5. Scenarios of Trucks Traveling on a Two-lane Bridge

The single truck events can be detected using strains from strategically placed strain gauges on the bottom of the concrete deck of the bridge. When considering the ambient traffic, most trucks tend to travel and stay in the center of a lane. Accordingly, to detect trucks on each lane of a bridge, two gauges are placed under or close to the wheel lines of each truck. When each axle passes over the strain gauges, it induces a strain response spikes and such strain responses are used to identify the truck events on the bridge. The truck detection methodology consists of three important parts, (1). Event detection – extract single lane event, (2). Lane detection – determine the lane that the truck travels on, (3). Axle detection – determine the number of axles of the detected trucks. This method can be applied to bridges with different configurations, dimensions, and number of girders. For this project, the single truck events with a five-axle truck are extracted from the SHM system to perform damage detection and bridge load rating because, (1). Five-axle trucks have the largest truck population, (2). Five-axle trucks generally induce large absolute strains in bridges with relatively small influence due to noise.

3.3. Damage Detection SHM Framework

As a part of SHM Framework, an automated damage detection method based on strain responses of a bridge was developed [47]. The bridge on US 30 over South Skunk River near Ames, IA was used to develop the damage detection system. Total of 40 fiber-optic strain gauges were installed on the bridge to measure strain responses under ambient traffic. An algorithm called cross prediction method was quantified using traditional linear regression together with statistical control charts [48]. To validate the cross-prediction method, an experiment was conducted with a sacrificial specimen mounted to the bridge and exposed to real traffic loads to induce fatigue cracks [48]. The results showed that the damage detection algorithm detects structural damage well. However, a relatively high false indication rate was also observed. To further improve the damage detection method, the SHM Framework on I-80 Bridge was used. The statistical F-test along with the orthogonal linear regression was proposed as a means to improve overall system performance [48].

3.4. Load Rating Factor Determination of SHM Framework

3.4.1 Finite Element Model (FEM) Calibration

A set of bridge parameters significantly correlated to the bridge response, such as, moments of inertia of girders, the elastic modulus of the deck, and spring constants at supports were selected to calibrate the FEM. The bridge parameters are calibrated through a process of minimizing the difference between the measured and computed strains using a least squares approach. Four different statistical values, Absolute Error (AE), Percent Error (PE), Scale Error (SE) and Correlation Coefficient (CC), were used to describe the FEM's ability to represent the actual structure, and can be determined by Equation 1, 2, 3, and 4, respectively. Where, ε_R is measured strain, ε_C is strain calculated using the FEM, $\max|\varepsilon_R - \varepsilon_C|_{\text{gauge}}$ is

maximum absolute strain differences between measured and calculated strains in each gage, $|\varepsilon_R|_{gauge}$ is maximum absolute strain in each gauge, μ_{ε_R} is average recorded strain in each gauge, μ_{ε_C} is average calculated strain in each gage. The calibrated FEM was later used to estimate the load rating factor of the bridge.

$$AE = \sum |\varepsilon_R - \varepsilon_C| \quad \ldots.(1)$$

$$PE = \frac{\sum(\varepsilon_R - \varepsilon_C)^2}{\sum \varepsilon_R^2} \quad \ldots.(2)$$

$$SE = \frac{\sum \boldsymbol{max}|\boldsymbol{\varepsilon_R} - \boldsymbol{\varepsilon_C}|_{\boldsymbol{gage}}}{\sum|\boldsymbol{\varepsilon_R}|_{\boldsymbol{gage}}} \quad \ldots.(3)$$

$$CC = \frac{\sum(\varepsilon_R - \mu_{\varepsilon_R})(\varepsilon_C - \mu_{\varepsilon_C})}{\sum\sqrt{(\varepsilon_R - \mu_{\varepsilon_R})^2(\varepsilon_C - \mu_{\varepsilon_C})^2}} \quad \ldots.(4)$$

3.4.2 Load Rating

The FEM, which consists of calibrated bridge parameters, was used to determine the load rating factor of the bridge. Commercially available software application called WinSac [46] was used in the calculation process. The inventory load rating was performed and load rating factor, simply the Rating Factor (RF) was calculated using the Load Factor Rating (LFR) Method per AASHTO Standard Specifications [49], and given in Equation 5, where, C is capacity and D is dead load effect of the member. The L is live load effect on the member. The factor for dead load, A_1 and the factor for the live load, A_2 were taken as 1.3 and 2.17, respectively. The impact factor for live load effect, I is expressed in Equation 6 [49], where, l is length in meters of the portion of the span that is loaded to produce the maximum stress in the member.

$$RF = \frac{C - A_1 D}{A_1 L(1 + I)} \quad \ldots.(5)$$

$$I = \frac{15}{l + 38} \leq 0.3 \quad \ldots.(6)$$

The live load effect on bridge members were calculated using AASHTO HS20 trucks. The dead loads consist of self-weights of the concrete deck, parapets, and the superstructure components including steel girders, stringers, floor beams. The capacity of the bridge members was calculated based on the Appendix D6.1 of the AASHTO LRFD Bridge Design Specification [50]. The nominal material properties given in the bridge plans were used to in the capacity calculation. The load rating calculation process was automated such that the rating factor of the bridge can be determined based on ambient traffic condition in near real-time. However, in the current approach, the capacity calculation is still based on the AASHTO LRFD Bridge Design Specification [50] guidelines and nominal properties of the bridge, which may not represent the flexural strength of the bridge, and thereby the Rating Factor at the time of the load rating. An improved estimation of the capacity can be used to further improve the automated load rating calculation of the SHM framework and introduced in the next chapter. A detailed description of the SHM framework related to truck detection, damage detection and load rating can be found in an accompanied report.

CHAPTER 4. IMPROVED LOAD RATING FACTOR CALCULATION

4.1. Overview

The load rating calculation can be used to estimate the safe load carrying capacity of a bridge. It helps to increase the public safety by reducing the risk of structural damage and collapse. The load rating factor, known as the rating factor (RF), is also a tool used to issue permits to heavy trucks and load postings on bridges. The American Association of State Highway Transportation Officials (AASHTO) Manual of Bridge Evaluation (MBE) [2] recommends two primary methods to calculate the rating factor of a bridge, the non-destructive load rating method and analytical load rating method. The non-destructive load rating method involve load testing in the field, where the load tests are required traffic closures on bridges. The Allowable Stress Rating (ASR), Load Factor Rating (LFR) and Load and Resistant Factor Rating (LRFR) are three different general rating factor calculation methods. The main difference between these analytical load rating methods are the design philosophies underlying the associate rating specification. The basic idea of the rating factor is that the safety at a critical section, and can be expressed in Equation 7, which is a simplified version of AASHTO MBE Equation 6A.4.2.1-1 [2].

$$\boldsymbol{RF = \frac{Strength\ Reduction\ Factor \cdot M_n - Load\ Factor\ for\ Permanent\ Loads \cdot M_{DL}}{Load\ Factor\ for\ Live\ Loads \cdot M_{LL+IM}}} \quad \ldots.(7)$$

In Equation 7, M_n represents the nominal flexural strength at a critical section. The M_{DL} and M_{LL+IM} are dead load moment and live load moment at the section, respectively. Analytical methods are used to calculate the M_{DL} and M_{LL+IM} in the above equation. The M_n can be calculated using theory of strength of materials and plastic moment principles given in

Appendix D6.1 of the AASHTO Load and Resistance Factor Design (LRFD) Bridge Design Specification [50]. Typically, the M_{DL}, M_{LL+IM} and M_n are calculated based on nominal parameters, such as the section dimensions and the material properties listed in the bridge plans. The rating factor calculated in this way reflects the load rating of the bridge at the time of construction. However, the rating factor of the bridge could also be based on the section dimensions and the material properties at the time of the load rating.

4.1.1 Load Rating Using BECAS SHM System

In an attempt to improve the rating factor calculation, the Bridge Engineering Center (BEC) of the Iowa State University (ISU) developed a Structural Health Monitoring (SHM) based approached. Figure 4.1 shows the current approach to calculate the rating factor based on SHM data. The truck detection program (Section 3.2) is capable of detecting and then characterizing five axle semi-trucks as they cross a bridge. Even though the truck detection program is capable of detecting the five axle semi-trucks as well as determining truck speed and longitudinal position on the bridge, the program cannot precisely determine the gross weight of the trucks and axle weights. Thus, a single batch of strain data from the monitoring system and truck information from a Weigh-in-Motion (WIM) database are sampled to calibrate a Finite Element Model (FEM) of the bridge (Section 3.4.1). The calibration is done by minimizing the percent error between measured and calculated strains by optimizing different bridge parameters. The calibrated FEM is used to obtain the M_{DL} and the M_{LL+IM}. The nominal moment capacity is calculated based on the AASHTO LRFD Bridge Design Specification [50]. With the above information the load rating factor can be calculated as per the AASHTO Standard Specification [49]. By sampling many different batches of strain data

combined with different truck information from the WIM database, a probability distribution for the rating factor can be found.

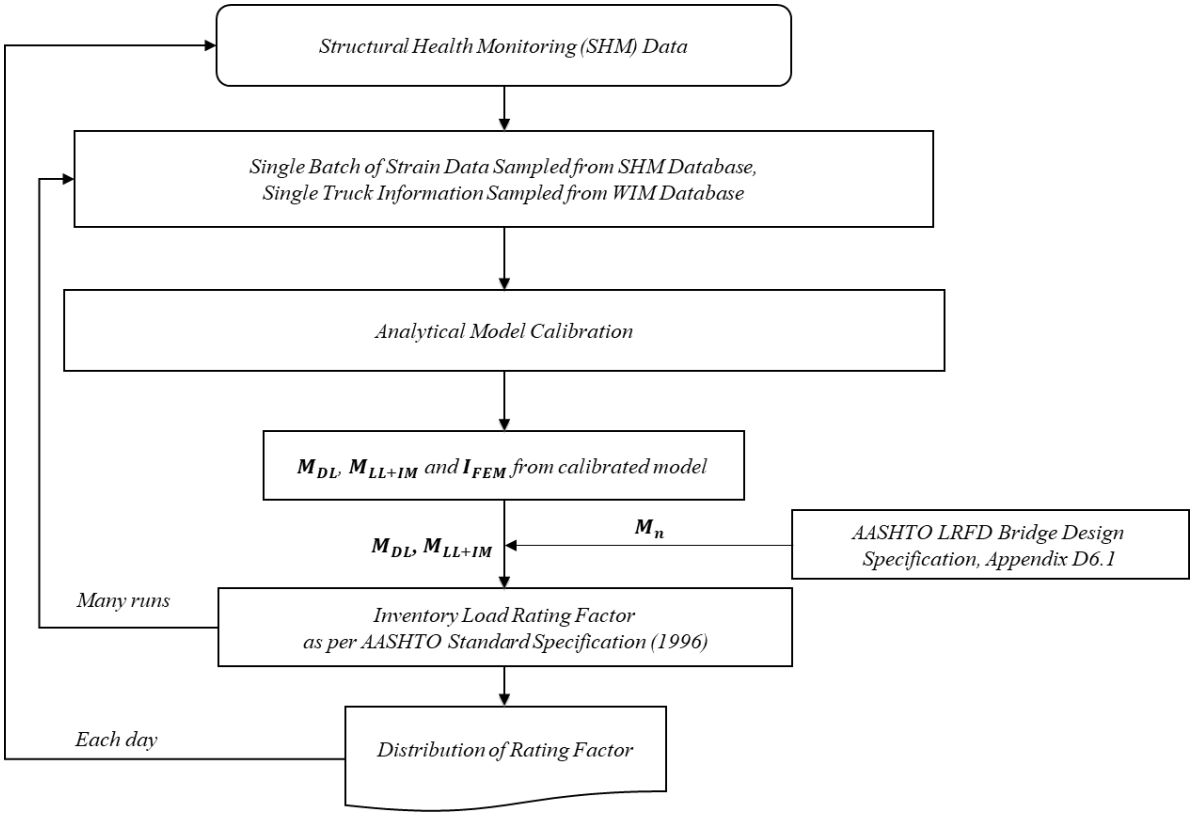

Figure 4.1. Current Load Rating Process Using SHM Data

In the current approach, the M_{DL} and M_{LL+IM} are estimated using the calibrated FEM of the bridge. As such, they represent the dead load moment and live load moment based on the section dimensions and the material properties at the time of the load rating. However, the above approach still uses the M_n, which is calculated based on AASHTO LRFD Bridge Design Specification [50] guidelines and nominal properties of the bridge, which may not represent the flexural strength at the time of current load rating.

The material properties and section dimensions significantly affect the M_n of a bridge. Mans et.al. [51] conducted two full-scale experiments on steel-concrete composite sections to investigate the effects of material properties on the flexural strength under positive bending

moment. Both specimens were 40 ft. long and loaded with a concentrated load at mid-span. Specimen 1 consisted of 2.5 ft. deep plate girder with a 5 ft. wide, 7.25 in. thick concrete slab. Specimen 2 consisted of similar plate girder, but a narrower bottom flange and a 7 ft. wide, 7.25 in. thick concrete slab. Both girders had nominal yield strength of steel 70 ksi. However, the measured steel material properties indicated that the yield strength of steel was between 80-85 ksi. Even though the specified strength of the concrete slab was not mentioned, the measured strength of the concrete was about 4.5 ksi for Specimen 1, whereas Specimen 2 was 7.5 ksi. The author used these section dimensions and material properties to calculate the M_n of Specimen 1 and Specimen 2 and compared them with the experimentally estimated flexural strength, M_{exp}. The results indicated that the M_n of Specimen 1 is 14% lower than the M_{exp} of the section and Specimen 2 showed 22% lower strength compared to the M_{exp}.

Gupta et.al. [52] carried out an experiment to evaluate the ultimate flexural strength of a composite section. The steel-concrete composite section consisted of 4 ft. deep beam with 1.5 ft. wide 7 in. thick concrete slab. Two concentrated loads were applied at approximately the 1/3 location of a 33 ft. long beam. The measured yield strength of the steel was about 47 ksi. The minimum specified strength of the concrete was not given in the article. However, the measured strength of the concrete is given as 6.5 ksi. The test results indicate that the M_{exp} was 7% higher than the M_n of the section.

Roberts [53] conducted an experiment to understand the ductile behavior of steel-concrete composite sections under positive bending. The experiment consists of three full scale composite sections. The first specimen was an 18 ft. long simply supported beam with a 2 ft. deep rolled steel beam with 3.5 ft. wide, 7 in. thick concrete slab. Specimen 2 was a 30 ft. long simply supported beam with 2 ft. deep plate girder. Specimen 1 and 2 had the same slab

dimension. Specimen 3 was similar to Specimen 2 except the top flange and web of Specimen 3 consisted of grade 50 steel, whereas the bottom flange consisted of HPS70W steel. The material test results indicated that the experimentally evaluated material properties were significantly higher than the nominal values. Probably due to this reason, Specimen 1 showed a 14% higher M_{exp} and Specimen 2 showed a 24% higher M_{exp} compared to their M_n values. Specimen 3 did not reach ultimate state during testing. However, the moment capacity at the maximum load was 10% higher than the M_n.

According to the above, typically the M_{exp} is significantly higher than the M_n of steel-concrete composite sections under positive bending moment. The probable reason for this difference is the measured material strength of both steel and concrete are significantly higher than the nominal values prescribed in the plans. However, there is no direct way to determine the material properties of a bridge component without doing a destructive test.

4.1.2 Objective

The objective of this part of the project was to further improve the rating factor calculation process by improving the estimate for flexural strength of steel-concrete composite sections. As mentioned in Section 4.1.1, the M_n value in the current rating factor calculation process is the only value which depends upon nominal bridge parameters. According to the experimental results shown in Section 4.1.1, typically the M_n is significantly smaller than the M_{exp}, which could lead to underestimating the rating factor of a bridge. By improving the estimate for flexural strength a more meaningful value for the rating factor can be obtained.

4.2. Methodology

4.2.1 Hypothesis

As an insight, Figure 4.2 shows the relationship between flexural strength and moment of inertia for non-composite sections obtained from the American Institute of Steel Construction Manual, hereafter referred to as AISC Specification [54]. According to Figure 4.2(a) there is a trend, such that when flexural strength increases the moment of inertia increases and vice versa. It also noted that the relationship between strength and stiffness is not unique. The research group suspected that there is a similar trend between flexural strength and moment of inertia of steel-concrete composite sections. If that statement is true, then that relationship along with the I_{FEM} can be used to get an improved estimate for the flexural strength of the section, where the I_{FEM} is the moment of inertia from calibrated FEM and it represents the moment of inertia of the section based on the existing section dimensions and the material properties at the time of the load rating (Figure 4.1).

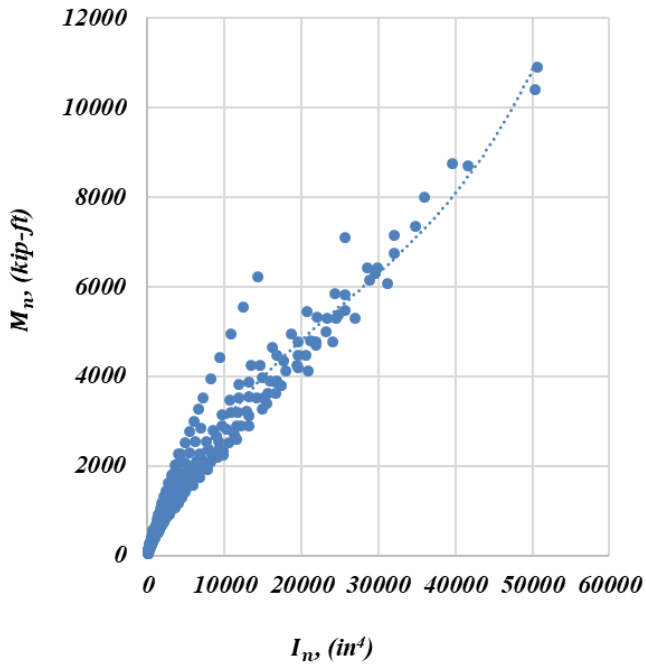

Figure 4.2. Relationship of Capacity and Moment of Inertia of Non-Composite Sections

The relationship between flexural strength and moment of inertia was proposed to be developed using a Monte Carlo simulation. Figure 4.3 shows a schematic diagram of the expected relationship. The improved flexural strength, M_{imp} would be estimated from the I_{FEM} of the section. It is important to note that the M_{imp} does not necessarily mean a higher flexural strength compared to the M_n of a section. The M_{imp} could be smaller than or equal to the M_n of a section depending on its I_{FEM}. The M_{imp} would replace the M_n value in the current rating factor calculation process (Equation 7). The proposed improved rating factor calculating process using SHM data is shown in Figure 4.4.

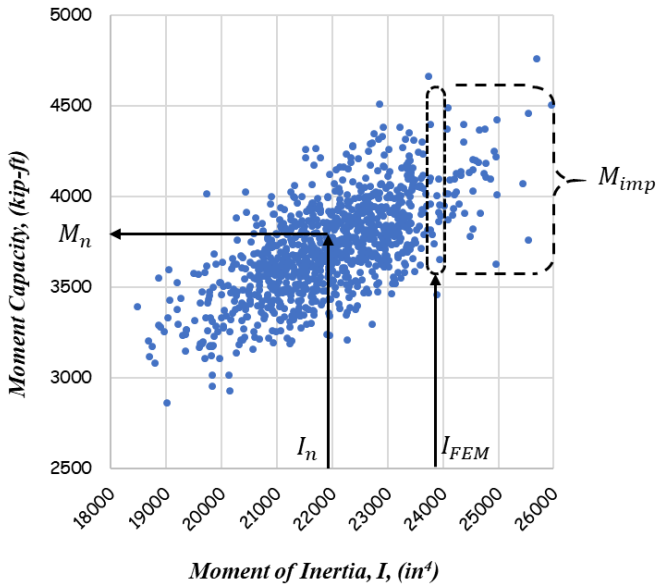

Figure 4.3. Relationship of Capacity and Moment of Inertia of Composite Sections

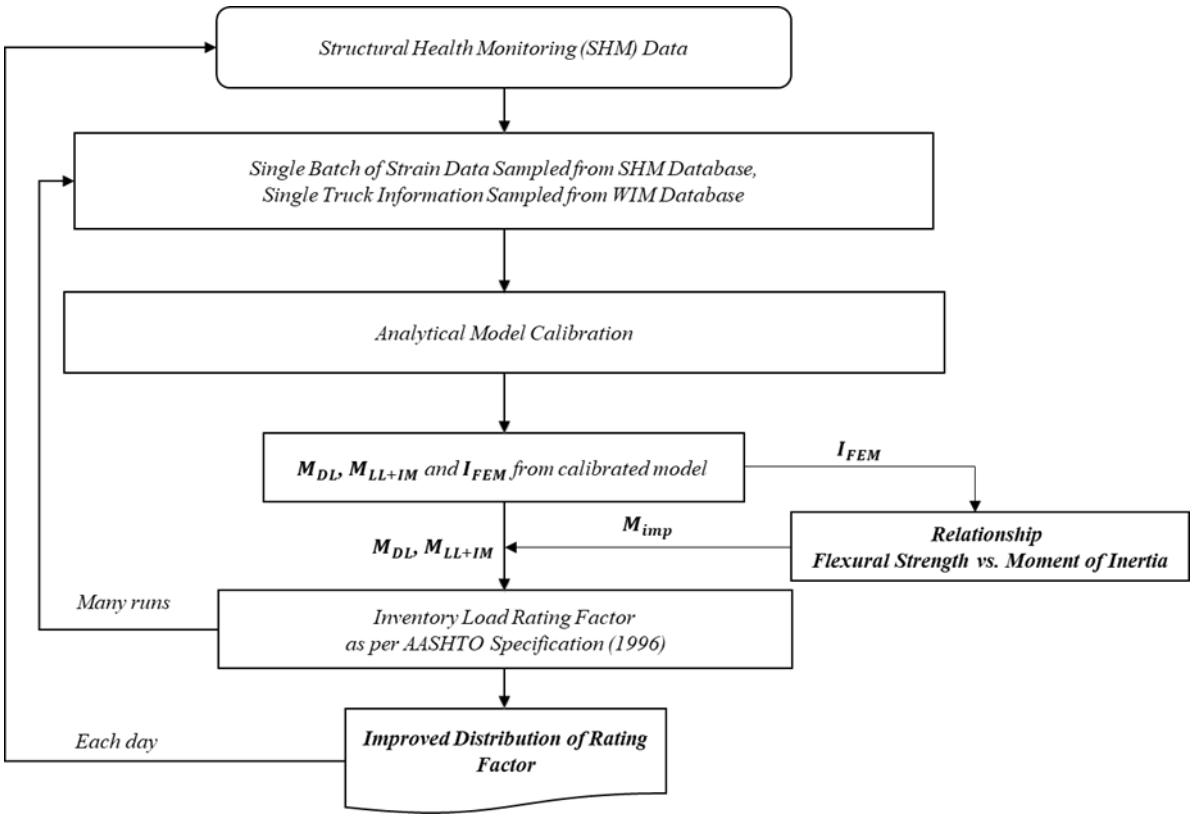

Figure 4.4. Improved Load Rating Process Using SHM Data

4.2.2 Monte Carlo Simulation

When the existing material and geometric properties of a bridge element are known, the theory of strength of materials and the equations given in the AASHTO LRFD Bridge Design Specification [50] can be used to develop a relationship between the moment of inertia and flexural strength of a section. However, the existing material properties of a bridge can't be determined without performing material tests on the bridge components. To overcome the uncertainty of the existing section dimensions and material properties, statistical distributions of section dimensions and material properties can be used to represent the possible values for existing section dimensions and material properties. An extensive literature review was conducted by the research group to determine the parameters of the statistical distribution of

section dimensions and material properties of bridge components. Significant research has proposed statistical distributions for material properties based on experiments [55] [56]. As an example, Table 4.1 shows possible statistical parameters for Specimen A. The nominal material properties of Specimen A were used as the mean. The mean (μ) and COV were then used to determine the standard deviation (σ) of the lognormal distribution for each material property.

Table 4.1. Statistical Distribution Parameters of Material Properties

Parameter	*Nominal Value*	*Mean, (μ)*	$COV = \sigma/\mu$	*Standard Deviation, (σ)*	*Type of Distribution*
f'_c, (ksi)	4	4	0.20	0.8	Lognormal
F_y, (ksi)	50	50	0.05	2.5	
E_s, (ksi)	29000	29000	0.04	1160	

However, minimal research data were found regarding the statistical distribution of section dimensions [57]. The COV and type of distribution is used to describe the section dimensions as was used for the material properties. The nominal dimension of the section was used as the mean value and the COV was used to calculate the standard deviation of each lognormal distribution (Table 4.2).

Table 4.2. Statistical Distribution Parameters of Section Properties

Parameter	*Nominal Value*	*Mean, (μ)*	$COV = \sigma/\mu$	*Standard Deviation, (σ)*	*Type of Distribution*
b_s, (in.)	108	108	0.05	5.4	Lognormal
t_s, (in.)	8	8	0.05	0.4	
t_{tf}, (in.)	0.79	0.79	0.09	0.07	
b_{tf}, (in.)	12	12	0.02	0.25	
t_w, (in.)	0.6	0.6	0.08	0.05	
h_w, (in.)	34.02	34.02	0.02	0.68	
t_{bf}, (in.)	0.79	0.79	0.09	0.07	
b_{bf}, (in.)	12	12	0.02	0.25	

The Monte Carlo simulation along with the statistical distributions of section dimensions and material properties could be used to simulate the possible values moment of inertia and flexural strength such that a relationship between the moment of inertia and flexural strength can be developed. The equations given in in Appendix D6.1 of the AASHTO LRFD Bridge Design Specification [50] were automated to perform the Monte Carlo simulation. The Monte-Carlo simulation was carried out using @Risk computer program version 7.5.1 Industrial Version using 50,000 iterations.

Figure 4.5 shows the probability distribution of moment of inertia of all four specimens obtained from the Monte-Carlo simulation. Results show that the moment of inertia generally is normally distributed.

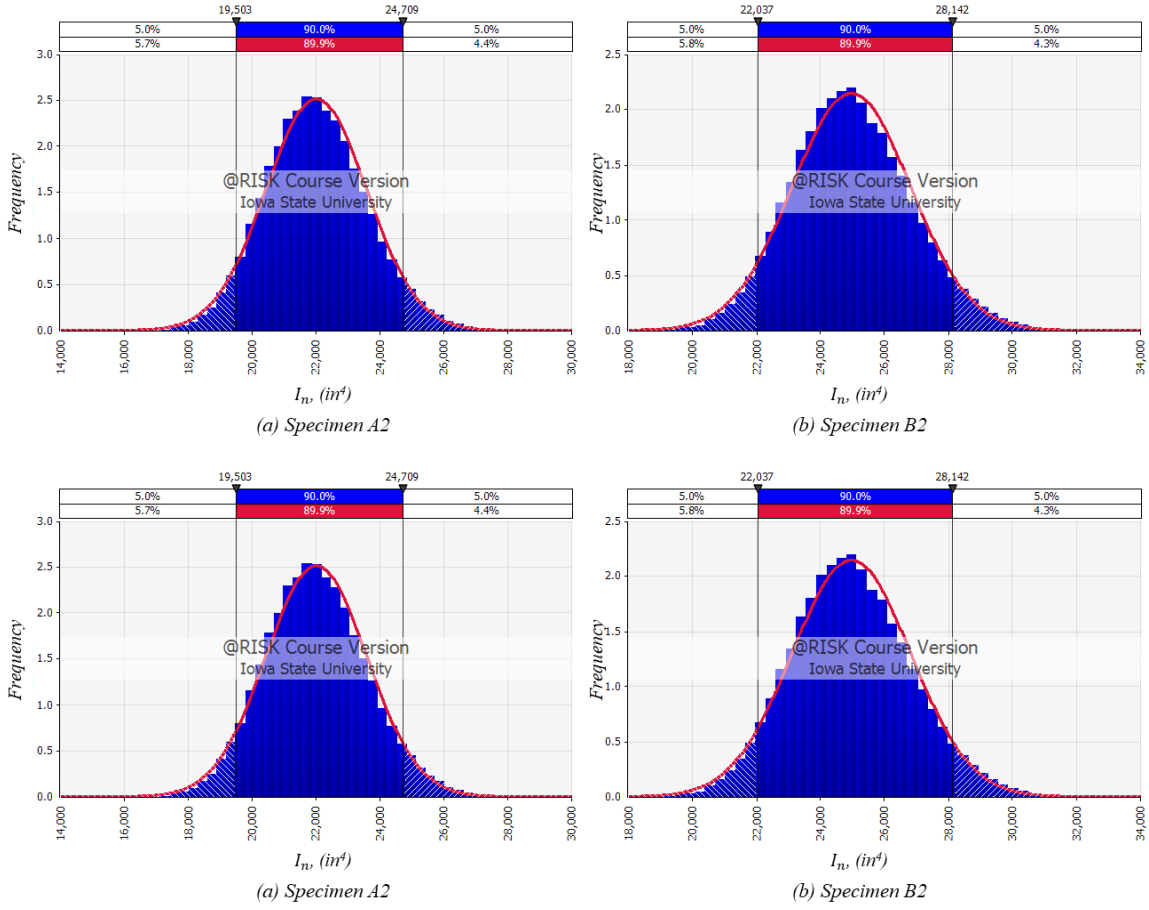

Figure 4.5. Monte Carlo Simulation of Composite I_n

Similarly, Figure 4.6 shows the Monte-Carlo simulation results for flexural strength of all four specimens. Results indicate that the flexural strength of all four specimens are normally distributed.

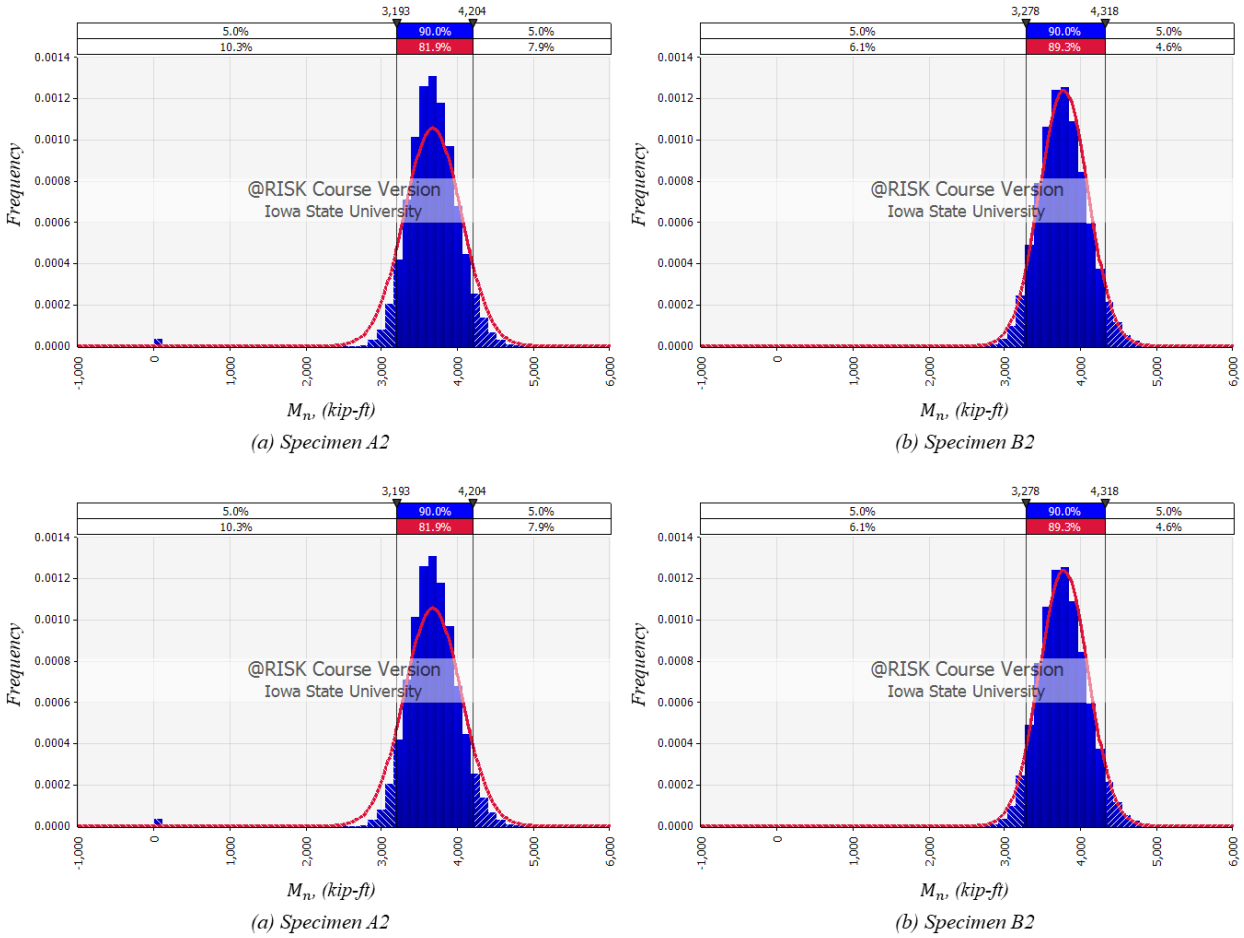

Figure 4.6. Monte Carlo Simulation of Composite M_n

The probability distributions of moment of inertia (Figure 4.5) and flexural strength (Figure 4.6) of each specimen were combined to develop the relationship between moment of inertia and flexural strength of the sections. Figure 4.7 shows the relationship between moment of inertia and flexural strength of all four specimens involved in the experimental study. According to the relationships shown in Figure 4.7, when the flexural strength increases then moment of inertia increases and vice versa, as suspected (Section 4.2.1). The experimental

program described next was conducted to provide validation of the use of I_{FEM} to get M_{imp} for the proposed rating factor calculation process.

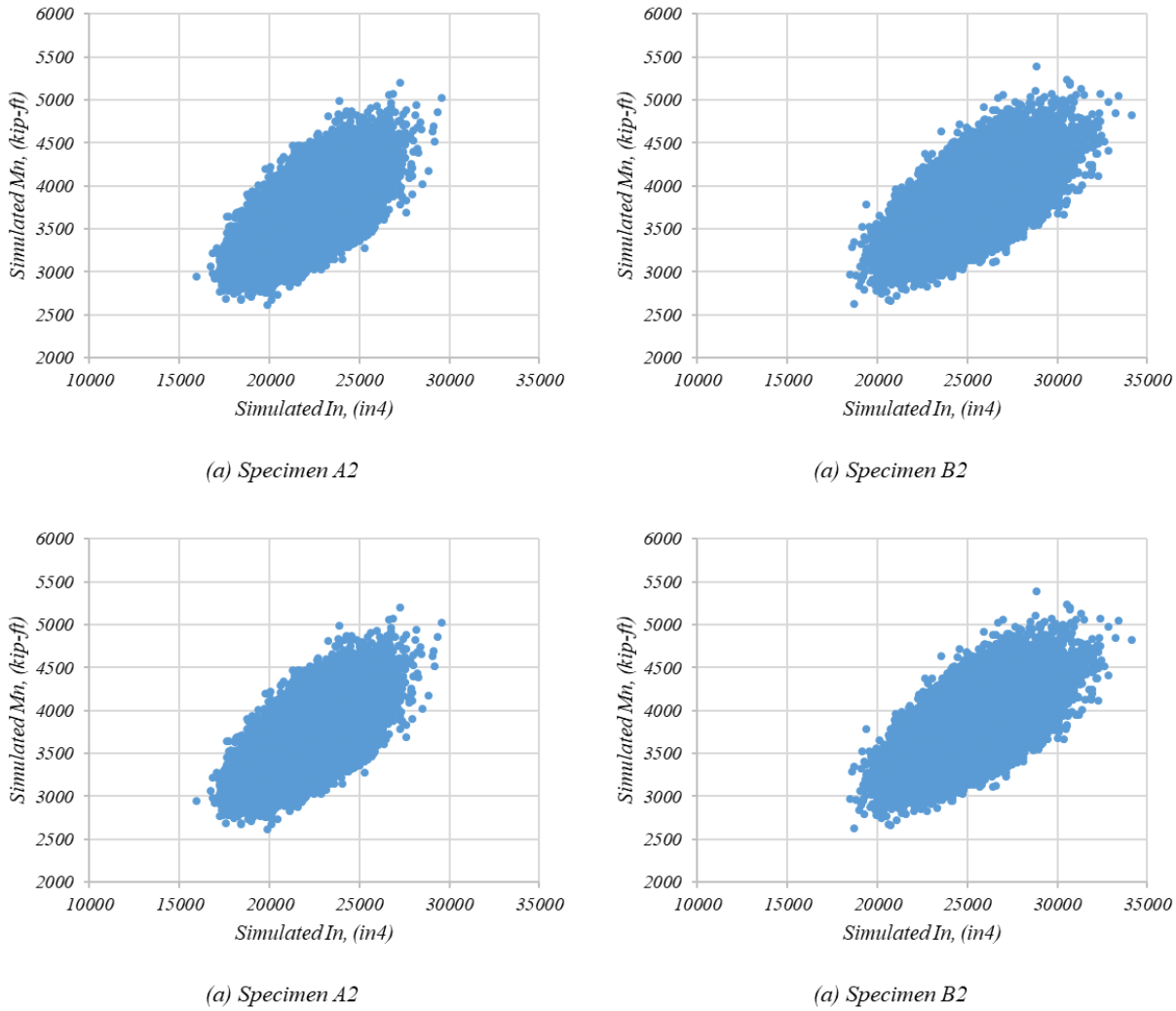

(a) Specimen A2 (a) Specimen B2

(a) Specimen A2 (a) Specimen B2

Figure 4.7. Relationship between M_n and I_n

4.3. Experimental Program

4.3.1 Layout

An experimental program was conducted at the Iowa State University Structural Engineering Laboratory to validate the hypothesis associated with this project objective. The experimental program consisted of the testing of four different steel-concrete composite

specimens (Figure 4.8). The moment of inertia and flexural strength of each specimen were experimentally determined to validate the, (1). Relationship between moment of inertia and flexural strength of steel-concrete composite sections, and (2). Use of moment of inertia from calibrated FEM, I_{FEM} to estimate flexural strength, M_{imp} for the proposed rating factor calculation process.

Specimen A (Figure 4.8(a)) was a 40 ft. long W36×135 mild-steel (A992 Steel) beam with a 9 ft. wide and an 8 in. thick concrete deck, whereas Specimen B (Figure 4.8(b)) was a 50 ft. long stainless-steel (A1010 Steel) plate-girder with a 7.5 ft. wide and an 8 in. thick concrete deck. Specimen C and Specimen D (Figure 4.8(c)) consisted of a 45 ft. long W36×135 mild-steel (A709 Steel) beam with a cover plate attached to the bottom flange and a 4.5 ft. wide, 7 in. thick concrete deck. Compared to the cross-section of Specimen A, deck width of Specimen C and D were half as wide with a cover plate at the bottom flange. Theoretically, the narrower deck width and cover plate on the bottom flange should move the Plastic Neutral Axis (PNA) of the cross-section from the deck towards the steel girder. The only difference between Specimen C and Specimen D is that Specimen D was constructed with lesser strength concrete to simulate the effects of a deteriorated concrete deck in the field. The rebar arrangement of the concrete deck of all four specimens were same as those given in typical bridge plans. The shear studs were designed according to the AASHTO LRFD Bridge Design Specification [50] Section 6.10.10.4, such that fully composite action can be achieved between the concrete and steel sections.

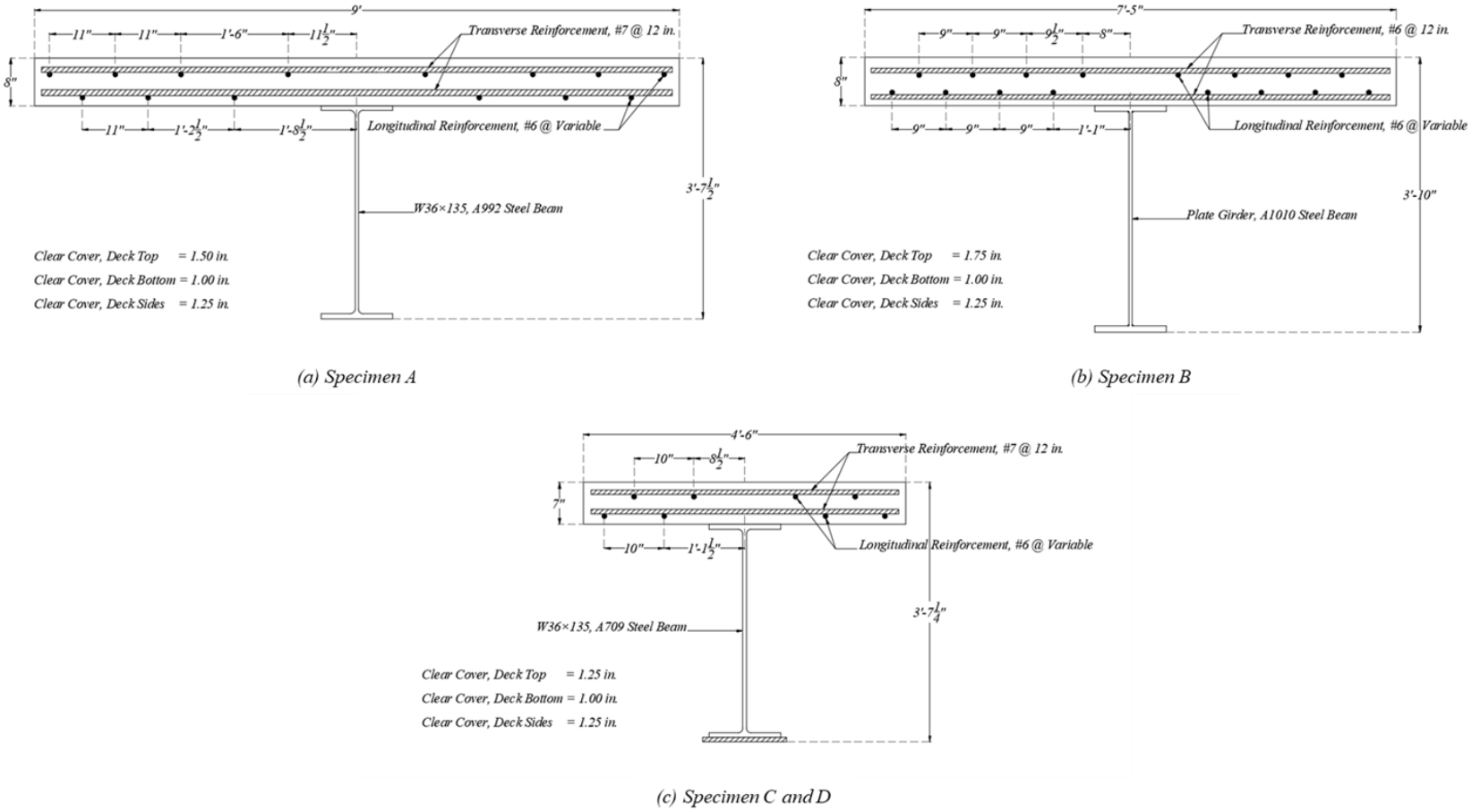

Figure 4.8. Cross-Sectional Details

4.3.2 Section Dimensions

Table 4.3 shows the nominal dimensions of each specimen. The actual dimensions of each specimen were measured to investigate the effects of actual dimensions on moment of inertia and flexural strength of each specimen. The difference between nominal and measured dimensions are significantly small. It should be pointed out that in an actual bridge, the effective deck width is highly variable and mostly unknown. Therefore, the nominal dimensions given in Table 4.3 were used to initially estimate the moment of inertia and flexural strength of each specimen.

Table 4.3. Nominal Dimensions of Specimens

Nominal Dimensions, (in.)	*Specimen A*	*Specimen B*	*Specimen C*	*Specimen D*
Deck Width, b_s	*108*	*89*	*54*	*54*
Deck Thickness, t_s	*8*	*8*	*7*	*7*
Top Flange Width, b_{tf}	*12*	*12*	*12*	*12*
Top Flange Thickness, t_{tf}	*0.79*	*1.00*	*0.79*	*0.79*
Web Thickness, t_w	*0.60*	*0.44*	*0.60*	*0.60*
Web Height, h_w	*34.02*	*36*	*34.02*	*34.02*
Bottom Flange Width, b_{bf}	*12*	*12*	*12*	*12*
Bottom Flange Thickness, t_{bf}	*0.79*	*1.00*	*0.79*	*0.79*
Cover Plate Width, b_{cp}	-	-	*14*	*14*
Cover Plate Thickness, t_{cp}	-	-	*0.75*	*0.75*
Span Length, L	*39×12*	*51.75×12*	*44×12*	*44×12*

4.3.3 Material Properties

The nominal material properties of the concrete deck, steel girders and cover plates for each specimen are listed in Table 4.4. The nominal strength of the concrete deck, $f'_{c,n}$ was obtained from the associated construction drawings of I-80 Bridge. The nominal modulus of

elasticity of the concrete deck, $E_{c,n}$ was calculated based on the equation given in Section C5.4.2.4 of the AASHTO LRFD Bridge Design Specification [50]. The nominal strength of steel girder $F_{y,n}$ and cover plate, $F_{y,cp,n}$ were obtained from the corresponding American Society for Testing and Materials (ASTM) Standards [58] [59] [60]. The nominal modulus of elasticity of the steel girder $E_{s,n}$ and cover plate, $E_{s,cp,n}$ were obtained based on AASHTO LRFD Bridge Design Specification [50] Section 6.4.1.

Table 4.4. Nominal Material Properties

Nominal Material Properties, (ksi)	***Specimens A, B, C and D***
Strength of Concrete Deck, $f'_{c,n}$	*4.00*
Modulus of Concrete Deck, $E_{c,n}$	*3640*
Strength of Steel Girder, $F_{y,n}$	*50*
Modulus of Steel Girder, $E_{s,n}$	*29000*
Strength of Steel Cover Plate, $F_{y,cp,n}$	*50*
Modulus of Steel Cover Plate, $E_{s,cp,n}$	*29000*

The nominal material properties listed in Table 4.4 were experimentally determined to investigate the effects of measured material properties on moment inertia and flexural strength of each specimen. The material property experiments were conducted according the ASTM Standards. The material properties of reinforcement in the concrete deck were not evaluated, since its contribution to the moment inertia and flexural strength of each specimen is small under positive bending behavior. ASTM A370 [61] and ASTM E8/E8M [62] were followed to determining the yield strength of steel girders, $F_{y,m}$, the Young's modulus of steel girders, $E_{y,m}$, the yield strength of cover plates, $F_{y,cp,m}$ and the Young's modulus of the cover plates, $E_{y,cp,m}$. Figure 4.9 shows the dimensions of the steel coupons

used to conduct both yield strength and Young's modulus experiments. Three coupons from each specimen were tested.

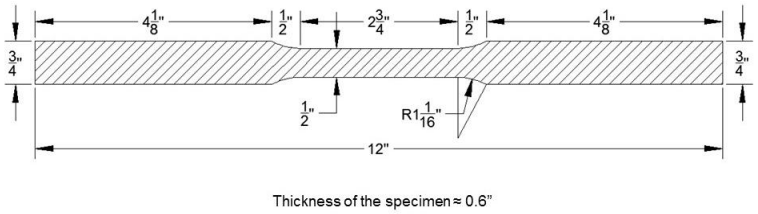

Figure 4.9. Rectangular Tension Coupon Details

Two 6 mm (≈ 0.25 in.) foil strain gauges were attached on opposite sides at the middle of each coupon. A hydraulic test machine was used to apply a tensile load to each coupon until its failure. The applied load and average strain of two strain gauges were used to develop the engineering stress-strain response for each specimen. Figure 4.10(a) shows a sample stress-strain response obtained during the coupon tests of Specimen A, C and D. The stress-strain curve shows a distinct yielding behavior. Figure 4.10(b) shows a typical stress-strain response obtained in the coupon tests of Specimen B. No distinct yielding behavior can be observed. The 0.2% offset method stated in ASTM A370 [61] and ASTM E8/E8M [62] was used to estimate the yield strength of the steel. The slope of the linear elastic region was used to calculate the Young's modulus of the steel. The experimentally determined material properties of steel are tabulated in Table 4.5. The average value was used in the calculations.

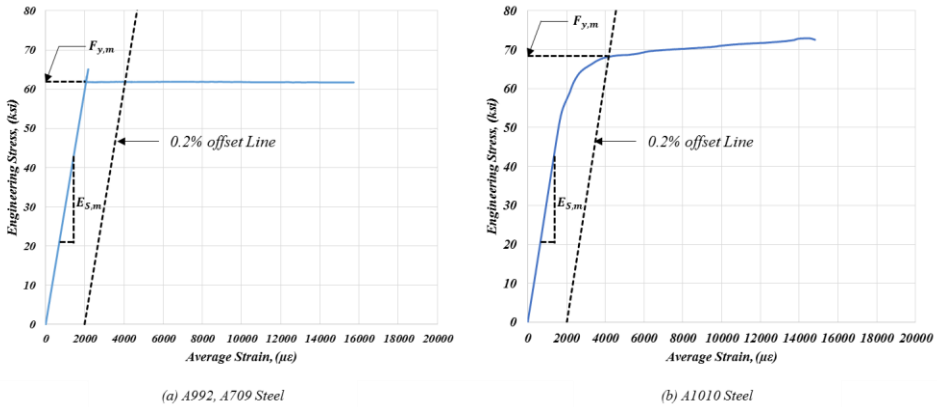

Figure 4.10. Typical Applied Load vs Average Strain Variation of a Test Specimen

Table 4.5. Material Test Results in ksi, Steel

Coupon No:	Experiment A		Experiment B		Experiment C				Experiment D			
	$F_{y,m}$	$E_{s,m}$	$F_{y,m}$	$E_{s,m}$	$F_{y,m}$	$E_{s,m}$	$F_{y,cp,m}$	$E_{s,cp,m}$	$F_{y,m}$	$E_{s,m}$	$F_{y,cp,m}$	$E_{s,cp,m}$
1	61.9	30010	68.2	31414	52.1	29884	60.5	30154	52.1	29884	60.5	30154
2	61.0	29742	68.0	31264	54.0	30161	62.2	29316	54.0	30161	62.2	29316
3	61.2	30753	70.9	31638	53.6	30010	61.0	30054	53.6	30010	61.0	30054
Average	61.4	30168	69.0	31439	53.2	30018	61.2	29841	53.2	30018	61.2	29841

The compressive strength of the concrete deck, $f'_{c,m}$ was experimentally determined based on the guidelines given in ASTM C39/C39M [63]. Following ASTM C469 [64], a compressometer was used to experimentally determining the Young's modulus of the concrete, $E_{c,m}$. Three 4 in. diameter and 8 in. height concrete cylinders were prepared from each specimen's concrete. Each cylinder was attached to the compressometer and loaded to 40% of $f'_{c,n}$ to obtain the stress-strain response of concrete. The slope of the linear elastic region was used to calculate the Young's modulus of the concrete. Since the Young's modulus experiment is non-destructive, the same cylinders were used to measure the compressive strength of each concrete deck, $f'_{c,m}$. The cylinders were removed from the compressometer and loaded until failure. The maximum load was recorded and used to calculate the compressive strength of the concrete. The $f'_{c,m}$ and $E_{c,m}$ of each specimen are tabulated in Table 4.6. The average value was used in the calculations.

Table 4.6. Material Test Results in ksi, Concrete

Cylinder No:	***Experiment A***		***Experiment B***		***Experiment C***		***Experiment D***	
	$f'_{c,m}$	$E_{c,m}$	$f'_{c,m}$	$E_{c,m}$	$f'_{c,m}$	$E_{c,m}$	$f'_{c,m}$	$E_{c,m}$
1	*5.602*	*4807*	*6.509*	*6695*	*7.783*	*6280*	*3.710*	*5427*
2	*5.710*	*4621*	*6.460*	*6933*	*7.828*	*6144*	*3.529*	*5887*
3	*5.469*	*4724*	*6.322*	*6577*	*7.929*	*6019*	*3.740*	*5035*
Average	*5.594*	*4717*	*6.430*	*6735*	*7.847*	*6148*	*3.615*	*5450*

Table 4.7 shows the experimentally evaluated material properties as a ratio to the nominal material properties. The experimentally measured material properties of Specimen A, B and C are significantly greater than corresponding nominal material properties. The $f'_{c,m}$ of Specimen D is in the vicinity of its nominal value, because, Specimen D was constructed with a week concrete deck to simulate the deteriorated concrete deck in the field.

Table 4.7. Measured Material Properties

Measured / Nominal	*Specimen A*	*Specimen B*	*Specimen C*	*Specimen D*
$f'_{c,m}/f'_{c,n}$	*1.40*	*1.61*	*1.96*	*0.90*
$E_{c,m}/E_{c,n}$	*1.30*	*1.85*	*1.69*	*1.50*
$F_{y,m}/F_{y,n}$	*1.23*	*1.38*	*1.06*	*1.06*
$E_{s,m}/E_{s,n}$	*1.04*	*1.08*	*1.04*	*1.04*
$F_{y,cp,m}/F_{y,cp,n}$	-	-	*1.22*	*1.22*
$E_{s,cp,m}/E_{s,cp,n}$	-	-	*1.03*	*1.03*

4.3.4 Experimental Setup and Instrumentation Plan

Figure 4.11(a) shows an elevation view of experimental setup of Specimen A. The specimen was simply supported and two equal concentrated loads (P_a and P_b) were simultaneously applied approximately at the 1/3 span locations to generate a constant moment region in the middle 1/3 of the specimen. Two sections outside the constant moment region (Section 1 and Section 5) and three sections within the constant moment region (Section 2, Section 3 and Section 4) were instrumented to obtain the strain and displacement responses. Figure 4.11(b) shows the instrumentation plan on the concrete deck. Four foil strain gauges were placed across the width of the concrete deck at the sections within the constant moment region to obtain the strain responses and investigate the effective width of the section. Two foil strain gauges were installed at the sections outside the constant moment region to get the strain responses. As mentioned above, the instrumented cross-sections in transverse direction were labeled from 1 to 5. Whereas the instrumented cross-sections in longitudinal direction were labeled as A, B, M, E and F. For an example, CT-A2 indicate the Concrete Top (CT) gauge along Grid Line A at Section 2. During Experiment A, no strain gauges were installed along Grid Line M. Figure 4.11(c) and Figure 4.11(d) represent the instrumentation plan of cross-

sections outside the constant moment region and within the constant moment region, respectively. A similar labeling system was used to identify the strain gauges attached to the steel girder. For an example ST-B1 indicate the Steel Top flange (ST) gauge along Grid Line B at Section 1. Whereas, SB-B1 indicate the Steel Bottom flange (SB) gauge along Grid Line B at Section 1. The steel gauges and concrete gauges along the Grid Line B and E were used to obtain the strain profile at each section. String potentiometers were attached to the bottom of the bottom flange at every section to measure deflection (Figure 4.11(c) and Figure 4.11(d)). Additionally, two string potentiometers were located very close to the supports (8.5 in. towards the mid-span from the support) to investigate displacements at the supports. The string potentiometers at each section were labeled from D-1 to D-5, where D stands for displacement and number stands to identify the instrumented cross-section.

An elevation view of the experimental setup of Experiment B is shown in Figure 4.12(a). Specimen B was simply supported and two equal concentrated loads (P_a and P_b) were simultaneously applied approximately 19 ft. from each side of the beam. The two instrumented sections outside the constant moment region were labeled Section 1 and Section 5. The instrumented section within the constant moment region was labeled Section 3. Figure 4.12(b) shows the instrumentation plan on the concrete deck. Three foil strain gauges were placed across the width of the concrete deck of all three cross-sections to obtain the strain responses. A similar labeling system was used to identify the strain gauges on top of the concrete deck. Figure 4.12(b) shows the cross-sectional instrumentation plan. The average strain of each top and bottom strain gauges along Grid Line B, E and the strain data of concrete gauges along Grid Line M were used to develop the strain profile for each section. Similar to Experiment A,

the string potentiometers were attached to the bottom of the bottom flange at every section to measure displacement (Figure 4.12(b)).

Figure 4.13 illustrates the instrumentation plan and loading arrangement of both Experiment C and D. The concept of the experimental setup shown in Figure 4.13 is similar to the experiment setup of Experiment A (Figure 4.11). However, the strain gauges and displacement gauges are at different locations due to the different section dimensions.

During the experiment, each specimen was loaded within the elastic limits to obtain the experimentally evaluated moment of inertia, I_{exp} of each specimen. Later, the specimens were loaded until the failure to obtain the experimentally evaluated flexural strength, M_{exp} of each specimen.

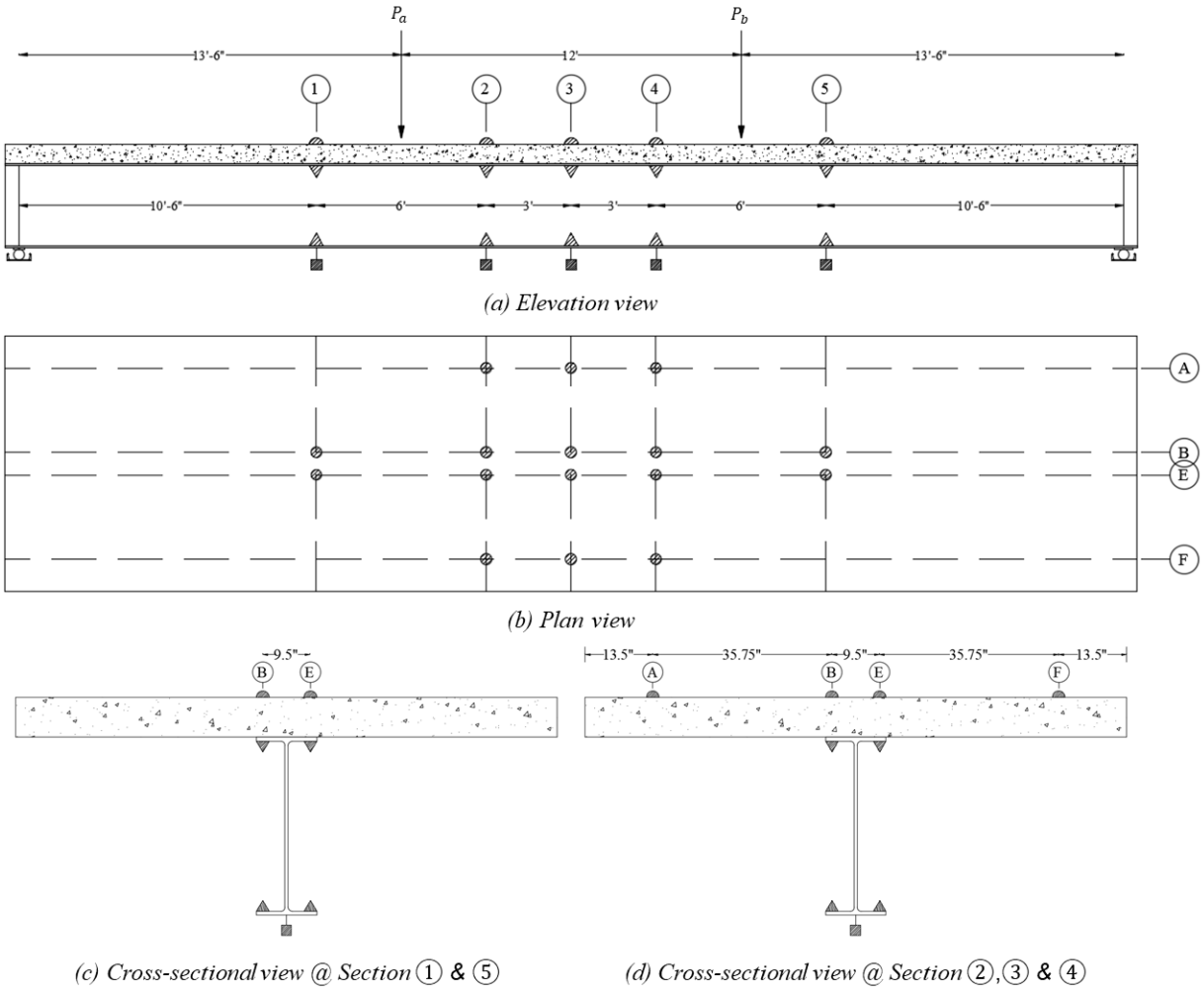

(a) Elevation view

(b) Plan view

(c) Cross-sectional view @ Section ① & ⑤

(d) Cross-sectional view @ Section ②, ③ & ④

Figure 4.11. Experimental Setup and Instrumentation Plan, Experiment A

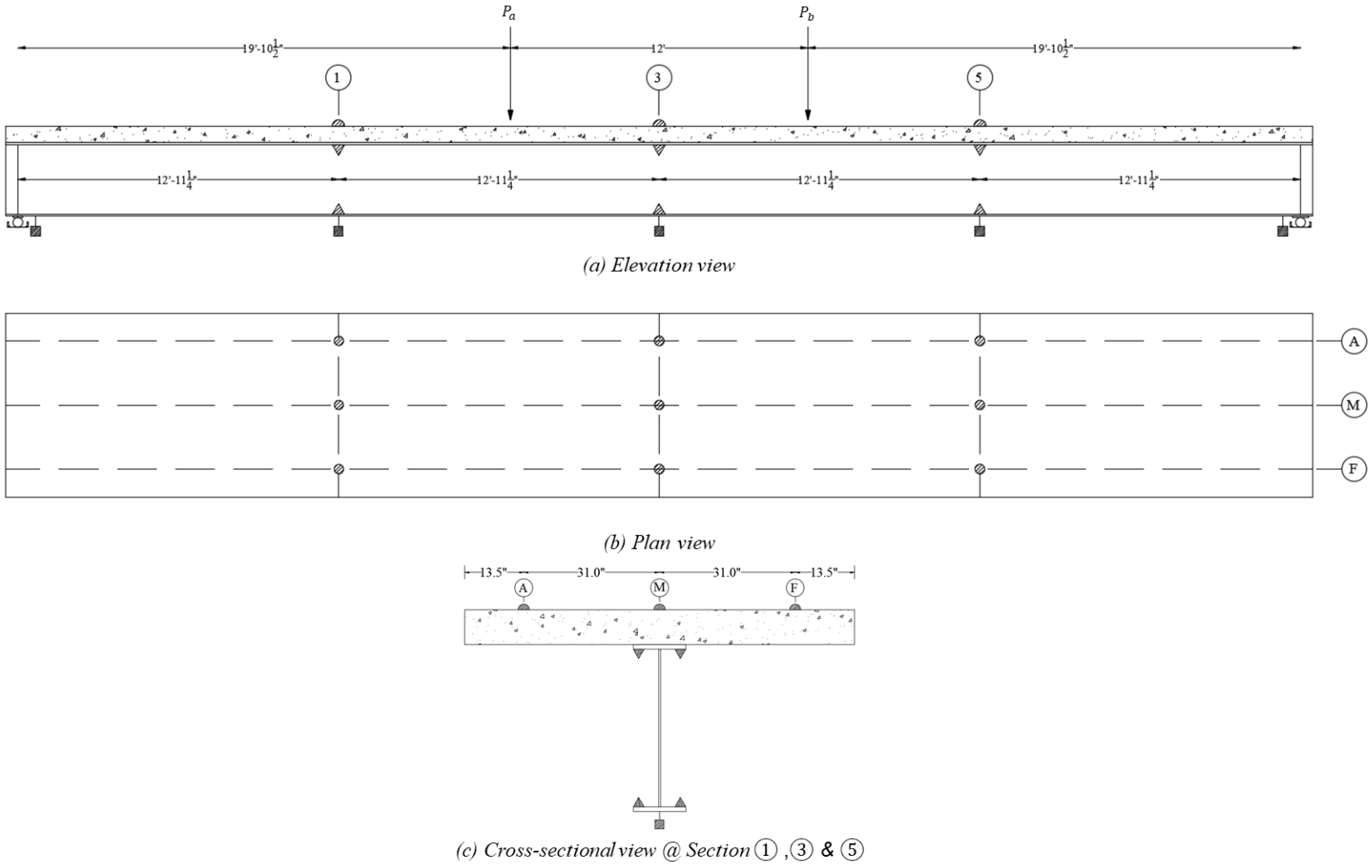

Figure 4.12. Experimental Setup and Instrumentation Plan, Experiment B

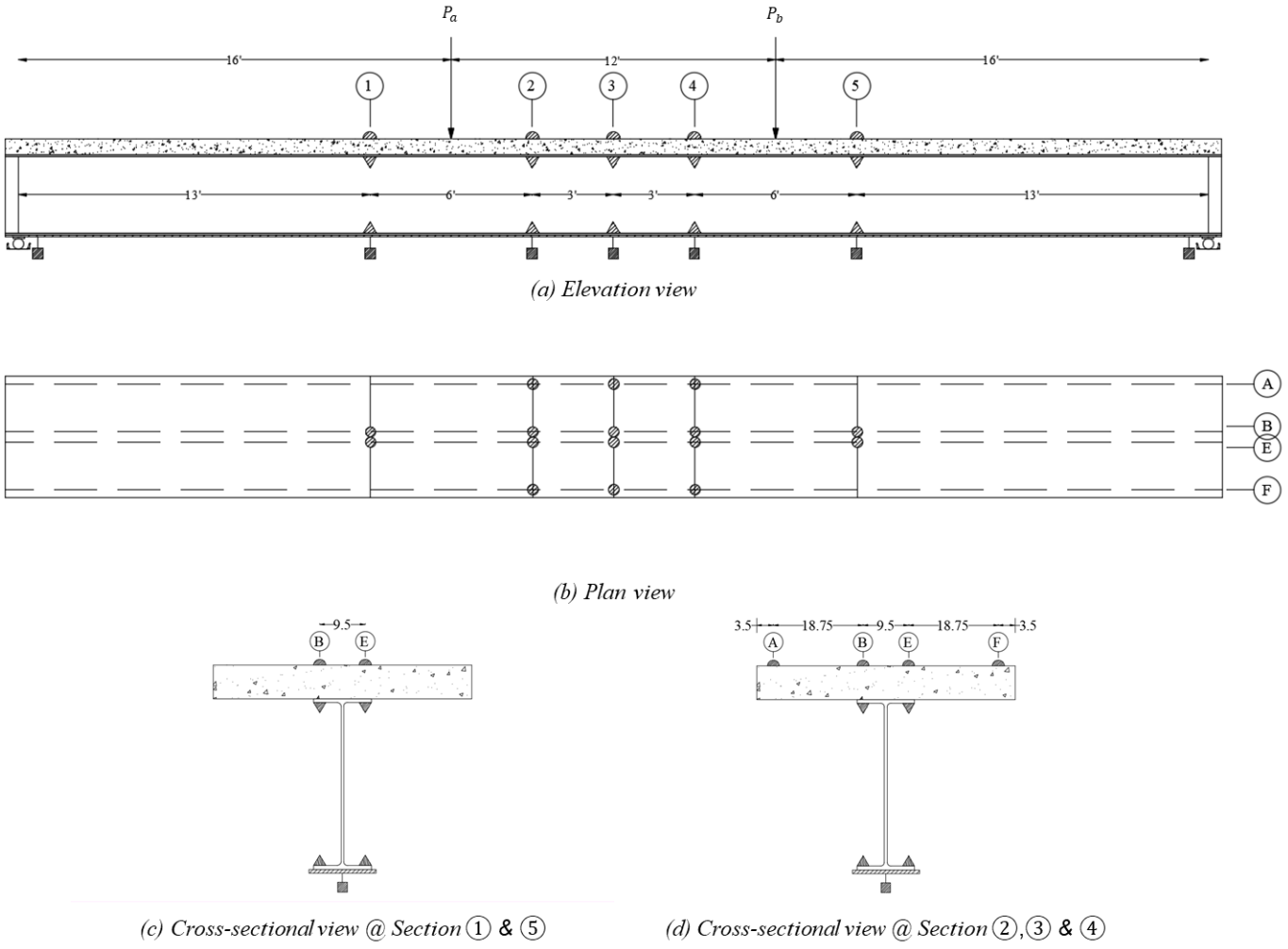

Figure 4.13. Experimental Setup and Instrumentation Plan, Experiment C and D

4.4. Moment of Inertia of a Composite Section

4.4.1 Based on Strength of Materials

When calculating the I_n of the steel-concrete composite sections, the effective width of the concrete deck plays an important role. The strain in the concrete away from the beam lags behind the strain of the concrete in the vicinity of the beam phenomenon known as shear-lag. Due to the shear-lag, the longitudinal stress distribution across the transverse direction of the composite section becomes non-uniform (Figure 4.14). The concept of effective width has been introduced to simplify the calculations, i.e., the non-uniform stress distribution is replaced by a uniform stress distribution with a reduced width of the slab, effective width, b_e (Figure 4.14).

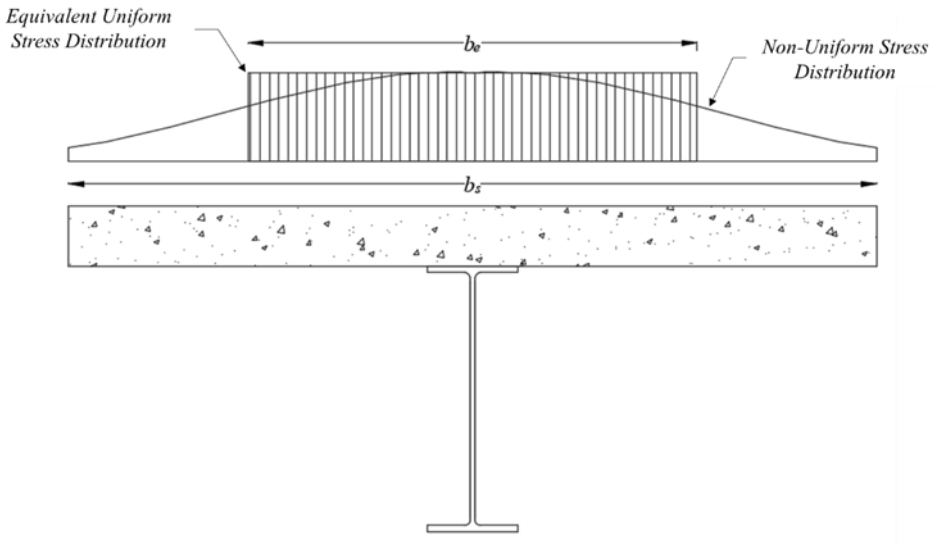

Figure 4.14. Effective Width Concept

Numerous researchers developed different simplified formulas to estimate the effective width of a steel-concrete composite sections under positive bending. Researchers have found that the effective width of a composite section primarily depends on the width of the deck (b_s), span length (L) and the loading condition of the composite section. Also, they have found that

the effective width during the elastic behavior is different from the plastic behavior. Based on analytical investigation of several composite sections, Salama et. al. [65] proposed Equation 8 to calculate the effective width of a steel-concrete composite deck in the elastic range. The b_s/L ratio of all four specimens are less than 0.25 (Table 4.3). Therefore, the full width of the concrete deck was used when calculating I_n of all four specimens.

$$\boldsymbol{b_e/b_s = 1 - 0.5(b_s/L)\ if\ b_s/L > 0.25} \quad \ldots.(8)$$

When estimating the effective width of a steel-concrete composite sections under positive bending at the ultimate limit state, Jian-Guo Nie et. al. [66] suggested that if $b_s/L < 0.5$ then the full width acts as the effective width of the section. Castro et. al. [67] also suggested the same criteria. Salama et. al. [65] have proposed Equation 9 to estimate the effective width of a section at ultimate limit state. According to the b_s/L ratios of all four specimens (Table 4.3), the deck width of every specimens is fully effective in ultimate limit state.

$$\boldsymbol{b_e/b_s = 1 - 0.25(b_s/L)\ if\ b_s/L > 0.25} \quad \ldots.(9)$$

When calculating the I_n of steel-concrete composite sections, the section is transformed in to a single homogenous material, typically, the concrete deck is transformed in to an equivalent steel deck by reducing the effective width of the deck by the ratio of E_s/E_c, which is known as the Modular ratio, n, of the section. Once the steel-concrete composite section is transformed in to a homogeneous section, Equation 10 can be used to calculate the neutral axis location of the cross-section, where $\bar{y}$ is the distance to the neutral axis from a datum, A_i is the

area of a segment, and y_i denotes the centroid of each segment from the datum. For a homogeneous section within the elastic range, the location of the neutral axis coincides with the centroid of the section given that there is no axial force.

$$\bar{y} = \frac{\sum y_i A_i}{\sum A_i} \quad \text{....(10)}$$

A typical steel-concrete composite section usually consists of at least four rectangular segments. Using Parallel Axis Theorem, the second moment of area, or the moment of inertia of a composite section about $\bar{y}$ is defined in Equation 11, where A_i equals to the area of each individual segment. The d_i stands for the perpendicular distance between centroid of each segment and the $\bar{y}$ of the section. The b_i and t_i is equal to the width and thickness of each rectangular segment, respectively.

$$I_n = \sum \left(\frac{1}{12} b_i t_i^3 + A_i d_i^2 \right) \quad \text{....(11)}$$

4.4.2 Using Nominal Material Properties

Equation 10 and Equation 11 along with the nominal section dimensions listed in Table 4.3 and nominal material properties listed in Table 4.4 were used to calculate the I_n of each specimen and tabulated in Table 4.8.

Table 4.8. The I_n of Specimens

Moment of Inertia, (in^4)	*Specimen A*	*Specimen B*	*Specimen C*	*Specimen D*
I_n	*22019*	*24980*	*25996*	*25996*

4.4.3 Using Measured Material Properties

Similarly, Equation 10 and Equation 11 along with the nominal section dimensions listed in Table 4.3 and measured material properties listed in Table 4.5 and Table 4.6 were used to calculate the I_n' of each specimen and listed in Table 4.9. Compared to the I_n, the I_n' is significantly different due to the effects of the measured material properties of each specimen.

Table 4.9. The I_n' of Specimens

Moment of Inertia, (in^4)	*Specimen A*	*Specimen B*	*Specimen C*	*Specimen D*
I_n'	*22922*	*28394*	*29941*	*28991*

4.4.4 Based on Experiment

The moment of inertia of each composite specimen were experimentally evaluated using strain responses. The I_{exp} estimation process is somewhat similar to the I_{FEM} estimation process outlined in the current rating factor calculation process, which involves minimizing the percent error between the measured and the calculated strains or displacements by optimizing single parameter, which is the I_{exp} of the section. During each experiment the strains were measured, ε_m at the top of the concrete deck, bottom of the top flange and top of the bottom flange of each specimen. The moment at each strain gauge location, M_m was calculated based on the equilibrium. The distance to each strain gauge location from the neutral axis, y_m was calculated based on the linear response of measured strains. The strain at any strain gauge location can be calculated using the theory of strength of materials principles, ε_c' (Equation 12) as the I_{exp} is the value to be determined.

$$\varepsilon_c' = \frac{M_m y_m}{E_{s,m} I_{exp}} \quad \ldots.(12)$$

The percent error between ε_m and ε_c' can be calculated using Equation 13. The I_{exp} is selected such that it minimizes the percent error between ε_m and ε_c', a procedure similar to I_{FEM} in the current load rating process explained in Section 3.4.2.

$$\textbf{Percent Error} = \frac{\sum_{all\ gauges}[\varepsilon_c' - \varepsilon_m]^2}{\sum_{all\ gauges}[\varepsilon_m]^2} \quad \ldots.(13)$$

To estimate the I_{exp} of each specimen, the loads P_a and P_b were slowly and simultaneously applied to create 40% the yield moment of each specimen at the mid-span (Crosse-section 3). As an example, the strain responses obtained during Experiment A is used to explain the I_{exp} calculation process. Figure 4.15(a) shows the variation of strain magnitude with the applied load at the top of the concrete deck at Section 3 of Specimen A. Figure 4.15(b) and Figure 4.15(c) show the variation of strain magnitudes of the top and bottom flange strain gauges at cross-section 3 of Specimen A. Since the top flange gauges are very close to the neutral axis of the specimen, the strain responses of the top flange gauges are in the vicinity of the noise level of the strain gauges (5 με) and were not used in the calculation process. According to Figure 4.15(a) and Figure 4.15(c), a liner variation between measured strain vs applied load can be observed. Therefore, a single batch of strain data associated with P_a equals to -66.77 kips and P_b equals to -65.14 kips were selected for further calculations.

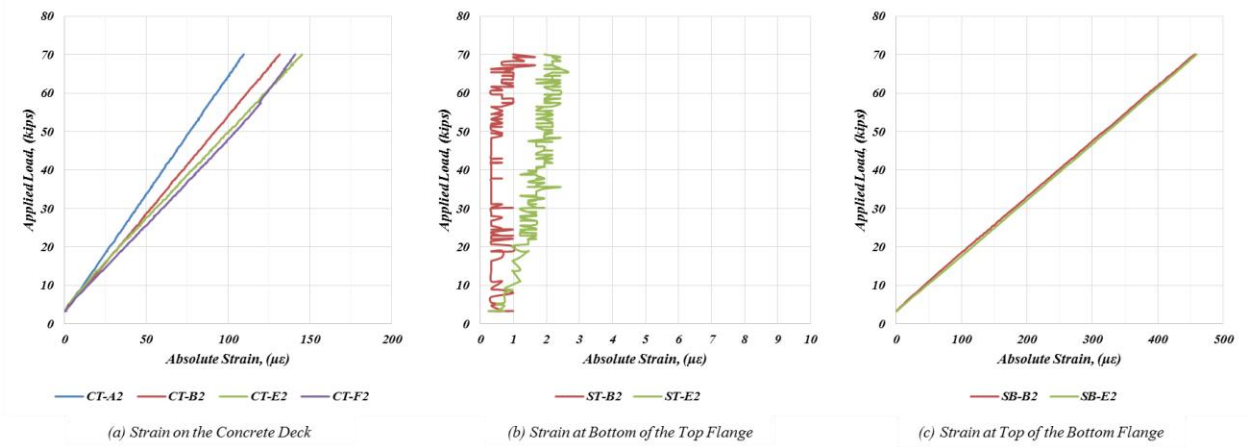

Figure 4.15. Typical Strain Measurements at a Cross-Section

The strains data associated with the above loads are represented in Figure 4.16(a). The strain measurements are non-uniform across the concrete deck, probably due to minor axis bending and torsional effects. The average strains were used to remove the effects of the minor axis bending and torsional effects and Figure 4.16(b) shows the measured strain profile at Section 3 of Specimen A. Later, the strain profile is used to calculate y_m at each section and I_{exp} of the specimen.

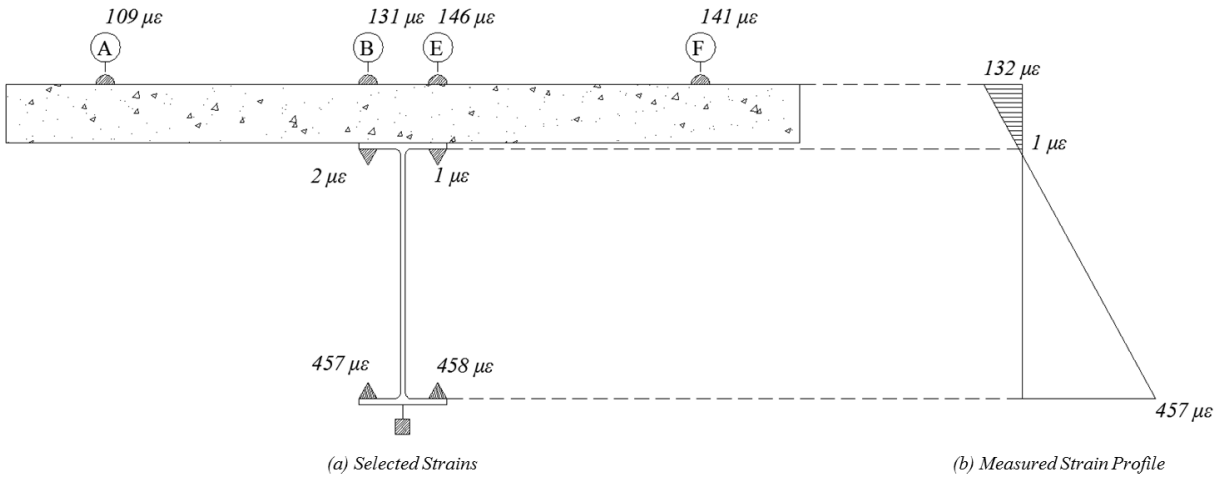

Figure 4.16. Typical Strain Measurements at a Cross-Section

The measured strains of the strain profile of every cross-section of all for specimens are tabulated in Table 4.10 to Table 4.13. For the purpose of comparison, the expected strains values based on nominal parameters, ε_c (use Equation 12 with nominal parameters given in Table 4.3 and Table 4.4, and average of P_a and P_b) are also listed in each table. The data suggest that ε_m is approximately 12% smaller than the ε_c of each specimen.

Table 4.10. Summary of the Average Strains at each Section, Experiment A

Experiment A Section No:	***Strain (με) at P_a= -66.77 kips, P_b= -65.14 kips***			
	Concrete Top (CT)		***Steel Bottom Flange (SB)***	
	ε_c	ε_m	ε_c	ε_m
1	*-133*	*-106*	*424*	*357*
2	*-172*	*-132*	*545*	*457*
3	*-172*	*-132*	*545*	*421*
4	*-172*	*-136*	*545*	*467*
5	*-133*	*-134*	*424*	*360*

Table 4.11. Summary of the Average Strains at each Section, Experiment B

Experiment B Section No:	***Strain (με) at P_a= -50.08 kips, P_b= -49.52 kips***			
	Concrete Top (CT)		***Steel Bottom Flange (SB)***	
	ε_c	ε_m	ε_c	ε_m
1	*-123*	*-86*	*357*	*322*
3	*-189*	*-138*	*549*	*468*
5	*-123*	*-85*	*357*	*301*

Table 4.12. Summary of the Average Strains at each Section, Experiment C

Experiment C Section No:	***Strain (με) at P_a= -39.65 kips, P_b= -40.48 kips***			
	Concrete Top (CT)		***Steel Bottom Flange (SB)***	
	ε_c	ε_m	ε_c	ε_m
1	*-139*	*-103*	*207*	*188*
2	*-172*	*-123*	*255*	*235*
3	*-172*	*-121*	*255*	*233*
4	*-172*	*-118*	*255*	*235*
5	*-139*	*-100*	*207*	*194*

Table 4.13. Summary of the Average Strains at each Section, Experiment D

Experiment D Section No:	***Strain (με) at P_a= -39.73 kips, P_b= -40.78 kips***			
	Concrete Top (CT)		***Steel Bottom Flange (SB)***	
	ε_c	ε_m	ε_c	ε_m
1	*-139*	*-104*	*207*	*201*
2	*-172*	*-134*	*255*	*245*
3	*-172*	*-156*	*255*	*247*
4	*-172*	*-139*	*255*	*236*
5	*-139*	*-118*	*207*	*184*

The above strain data along with Equation 12 and Equation 13 were used to calculate the I_{exp} of each specimen. The I_{exp} value was mathematically determined as a ratio to I_n. Variation of percent error with I_{exp}/I_n ratio for all four specimens are given in Figure 4.17, whereas the I_{exp}/I_n ratios which minimizes the percent error are tabulate in Table 4.14. According to Table 4.14 the I_{exp} value of each specimen is significantly different from I_n of the specimen.

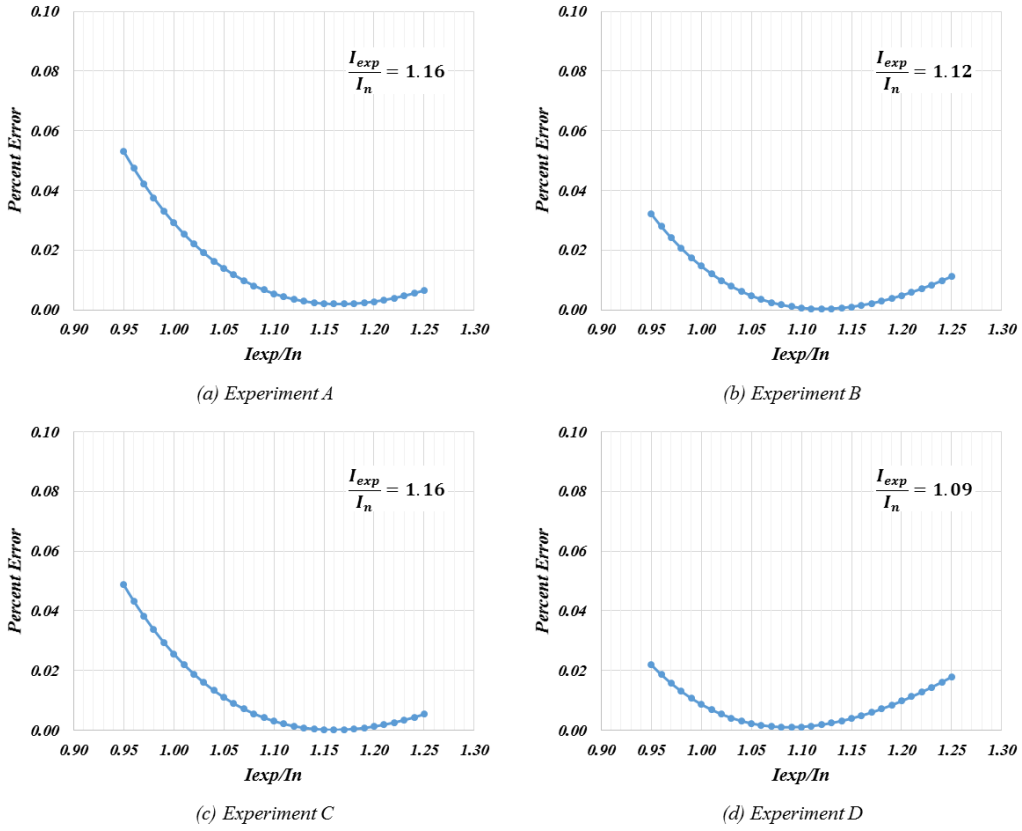

(a) Experiment A (b) Experiment B

(c) Experiment C (d) Experiment D

Figure 4.17. Percent error vs I_{exp}/I_n Variation

Table 4.14. The of I_{exp} of Specimens

Moment of Inertia, (in^4)	*Specimen A*	*Specimen B*	*Specimen C*	*Specimen D*
I_{exp}	*25542*	*27978*	*30155*	*28336*

4.5. Flexural Strength of a Composite Section

4.5.1 Based on Strength of Materials

Steel-concrete composite sections can be divided into three categories as compact, non-compact and slender sections. Typically, compact sections can reach the maximum flexural resistance of the section at the ultimate state, which is the plastic moment capacity, M_p of the section. Non-compact sections have a flexural strength above the yield moment, M_y, but do not reach the M_p. The slender sections will not attain M_y. Most bridges are designed to comply

with the compact section limits recommended in the AASHTO LRFD Bridge Design Specification [50] Section 6.10.6.2.2, such that it can reach the maximum flexural resistance of the section at the ultimate state and reach to the M_p of the section. However, the compact sections under positive moments with the Plastic Neutral Axis (PNA) close to steel-concrete interface may not reach to M_p, because part of the steel section close to the concrete-steel interface may not reach the yield stress. Based on Wittry [68], Yakel and Azizinamini [69] findings, AASHTO LRFD Bridge Design Specification [50] Section 6.10.7.1.2 states that the nominal flexural resistance of a compact section is equal to M_P if $D_P \leq 0.1D_t$, where D_t is total depth of the composite section and D_P is distance from the top of the concrete deck to the plastic neutral axis (PNA). Otherwise the flexural strength of a compact section can be calculated using Equation 14.

$$\boldsymbol{M_n = M_p\left(1.07 - 0.7\frac{D_P}{D_t}\right)\ if\ D_P \geq 0.1D_t} \quad \ldots.(14)$$

According to Equation 14, the flexural strength of a steel-concrete composite section primarily depends on the plastic moment capacity, location of the PNA and total depth of the composite section. In fact, locating the PNA is the first step of determining the M_P of a composite section. Depending on possible PNA locations, seven different equations are given in AASHTO LRFD Bridge Design Specification [50] Table D6.1-1 to calculate the location of the PNA of a composite section under positive bending. However, the definition of the PNA location is somewhat vague as to whether PNA is the depth to the zero-stress location or to the Whitney stress block when the PNA is at the concrete deck. Figure 4.18(a) shows a typical stress distribution of a composite section when the PNA is at the concrete deck. Figure 4.18(b) shows the equivalent stress distribution based on both AASHTO LRFD Bridge Design

Specification [50] Section 5.7.2.2 and American Concrete Institute (ACI) 318 Building Specification [70], hereafter referred to as ACI 318-14 Specification Section 22.2.2.4.1. Both sections define the PNA is at the zero-stress location (Figure 4.18, PNA Location 1). The equations given in Table D6.1-1 of the AASHTO LRFD Bridge Design Specification [50] consider the plastic neutral axis location as depth to the stress block (Figure 4.18, PNA Location 2), which is equal to the factor β_1 times depth to the PNA Location 1. The factor β_1 depends on the f_c' of the concrete slab. (AASHTO LRFD Bridge Design Specification [50] 5.7.2.2. or ACI 318-14 Specification [70] Table 22.2.2.4.3). Depending on the β_1 factor, two PNA locations could be 35% different from each other. Even though M_p of a section does not depend on the PNA location, then M_n could be affected by that as it directly related to the M_n of the section. The AASHTO method is selected for further calculations because it is commonly used in bridge design offices. The AASHTO method denotes the PNA by using either $\bar{Y}$ or D_P.

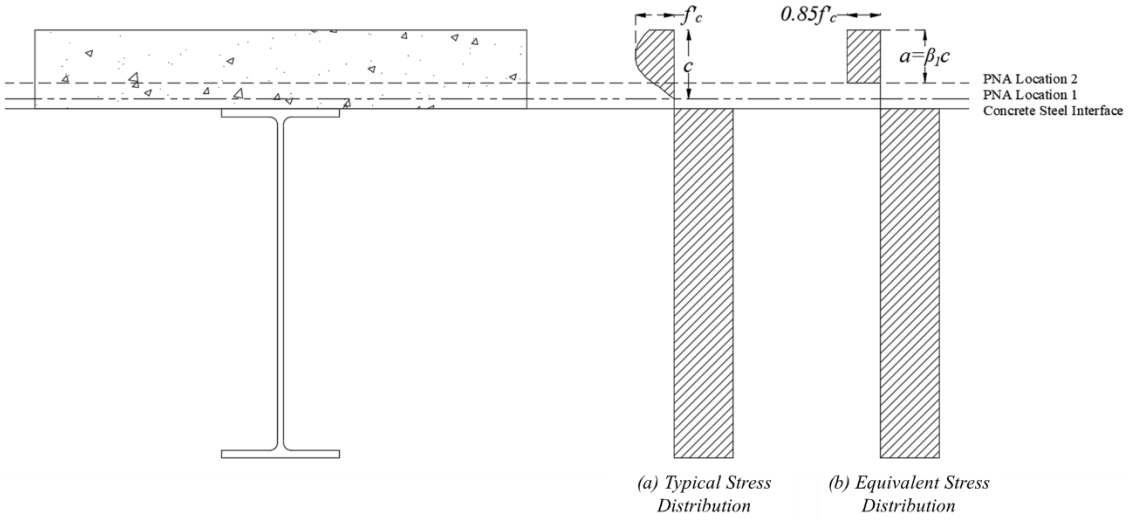

Figure 4.18. Definition of Plastic Neutral Axis (PNA) Location

Equations given in the AASHTO LRFD Bridge Design Specification [50] Table D6.1-1 were used to calculate the M_p of the composite sections. In the equations, the plastic force induced in the concrete slab is calculated by using the equivalent stress block with maximum compressive strength as $0.85f_c'$ (AASHTO LRFD Bridge Design Specification [50] Section 5.7.2.2). The plastic forces of the steel sections are calculated by multiplying the cross-sectional area by the yield strength of the steel. The concrete in tension and the plastic forces induced in the deck reinforcement were neglected.

4.5.2 Using Nominal Material Properties

Each specimen satisfies the compact section requirements given in the AASHTO LRFD Bridge Design Specification [50] Section 6.10.6.2.2. However, the specimens cannot reach the M_p due to ductility limitations. Equation 14 along with the section dimensions given in Table 4.3 and material properties given in Table 4.4 were used to calculate the nominal flexural strength of the section and listed in Table 4.15. The PNA location of Specimen D is about 5 in. below the steel-concrete interface. Therefore, significant reduction in flexural strength can be observed.

Table 4.15. The PNA, M_p and M_n of Composite Specimens

Parameter	*Specimen A*	*Specimen B*	*Specimen C*	*Specimen D*
D_t, *(in.)*	*43.60*	*46.00*	*43.35*	*43.35*
$\bar{Y}$ *or* D_P, *(in.)*	*5.36*	*6.58*	*12.13*	*12.13*
D_P/D_t	*0.12*	*0.14*	*0.28*	*0.28*
$[1.07 - 0.7(D_P/D_t)]$	*0.98*	*0.97*	*0.87*	*0.87*
M_P, *(kip-ft)*	*3793*	*3936*	*4773*	*4773*
M_n, *(kip-ft)*	*3732*	*3817*	*4173*	*4173*

4.5.3 Using Measured Material Properties

Similarly, Equation 14 along with the section dimensions given in Table 4.3 and material properties given in Table 4.5 and Table 4.6 were also used to calculate the flexural strength of each specimen and listed in Table 4.16. According to the results in given in Table 4.16 the M_n' shows a significant difference compared to the M_n value. This could be due to the significant difference shown in the measured material properties of each section (Table 4.7).

Table 4.16. The PNA, M_P' and M_n' of Composite Specimens

Parameter	*Specimen A*	*Specimen B*	*Specimen C*	*Specimen D*
D_t, *(in.)*	*43.60*	*46.00*	*43.35*	*43.35*
$\bar{Y}'$ *or* D_P', *(in.)*	*4.69*	*5.59*	*7.20*	*16.73*
D_P'/D_t	*0.11*	*0.12*	*0.17*	*0.39*
$[1.07 - 0.7(D_P'/D_t)]$	*0.99*	*0.98*	*0.95*	*0.80*
M_P', *(kip-ft)*	*4709*	*5481*	*5845*	*5167*
M_n', *(kip-ft)*	*4684*	*5399*	*5575*	*4133*

4.5.4 Based on Experimental Results

As the final step of the experiment program the experimental flexural strength, M_{exp} of each steel-concrete composite specimen was determined. The loads were applied until the collapse of each specimen. The M_{exp} is defined as the maximum flexural strength right before the collapse. The M_{exp} was calculated using two different methods, (1). Considering the equilibrium at ultimate, (2). Using strain profile at the ultimate.

As an example, the strain responses obtained during Experiment A are used to explain the M_{exp} calculation process. Figure 4.19(a) shows the variation of concrete strain with the applied load. According to Figure 4.19(a), at the collapse the concrete strain reached to the crushing strain (3000 με) of the concrete. Figure 4.19(b) shows the variation of strain at the

bottom of the top flange with the applied load, whereas Figure 4.19(b) shows the variation of strain at the top of the bottom flange with the applied load. The applied loads, P_a and P_b at the collapse were recorded as 342.8 kips and 346.2 kips. The average of P_a and P_b, 344.5 kips and the distance to the loading point from the support, 13.5 ft were used to calculate the M_{exp} of the specimen in the equilibrium method (Table 4.17).

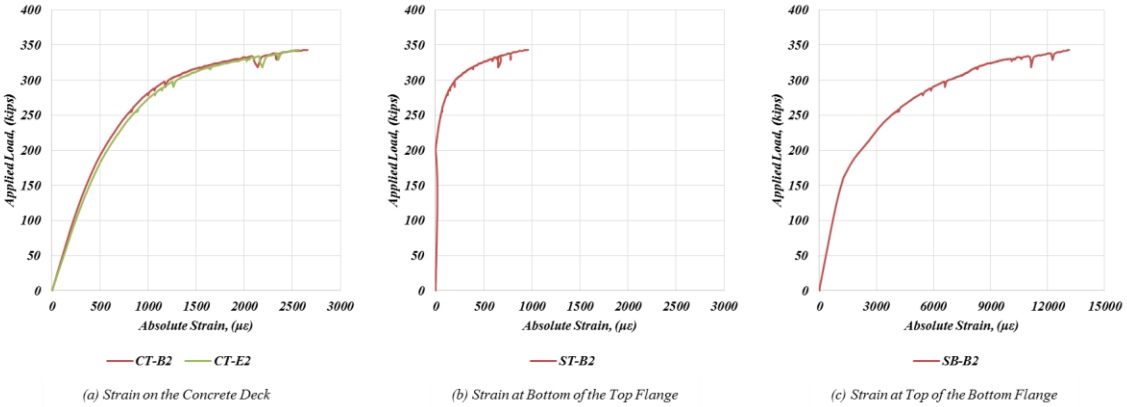

Figure 4.19. Variation of Strain at Each Location at Section 2 of Specimen A

The strains at the ultimate loading condition (P_a = 342.8 kips and P_b = 346.2 kips) are shown in Figure 4.20(a). The average strains of the concrete gauges and the strain of steel gauges were used to develop the strain profile at the ultimate and shown in Figure 4.20(b). Since the strain data are not in a prefect linear relationship, a linear regression line was used to calculate the strains at any location of the cross-section.

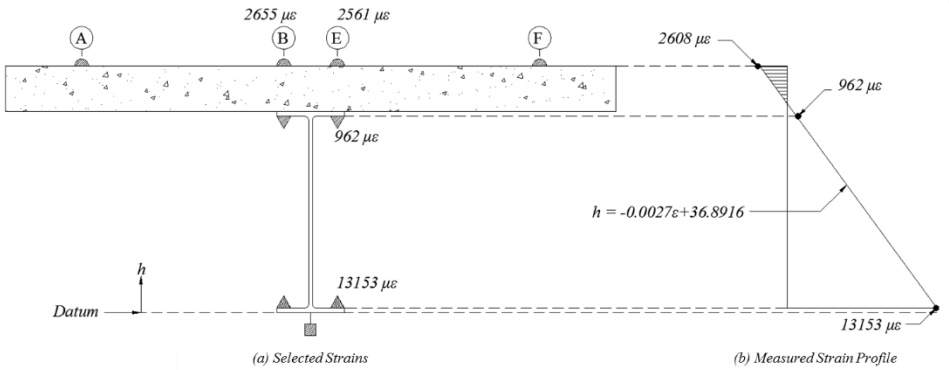

Figure 4.20. Typical Strain Measurements at a Cross-Section

According to the regression line, the strain at the concrete, bottom of the top flange and top of the bottom flange are -2453 με, 761 με, and 13199 με, respectively. Typically, strain of steel at strain hardening is 12000 με. However, during steel material tests no strain hardening was observed at the 12000 με strain level (Figure 4.10). Therefore, any possible strain hardening at the bottom flange was neglected. The stress-strain response obtained during coupon test along with the measured strain profile of the cross-section was used to develop the stress profile of the cross-section (Figure 4.21). According to that, the top flange and about 3.5 in. of the web did not reach the yield limit. The stress profile along with the steel section dimensions (Table 4.3) were used to estimate the tensile force induced in the steel girder. Stress-strain responses were not recorded during the concrete cylinder test. In lieu of stress-strain relationship on concrete, Whitney rectangular stress block with maximum stress of $0.85f_c'$ was considered to calculate the compressive force induced in the concrete deck, where the f_c' is the measured strength of the concrete. The depth of the PNA was adjusted to make the force equilibrium between tensile and compressive forces and the distances to the plastic forces were calculated. The calculated plastic forces and distances were used to calculate the M_{exp} of the section. Strain and stress profiles for used to calculate M_{exp} of each specimen are shown in Figure 4.22 to Figure 4.24.

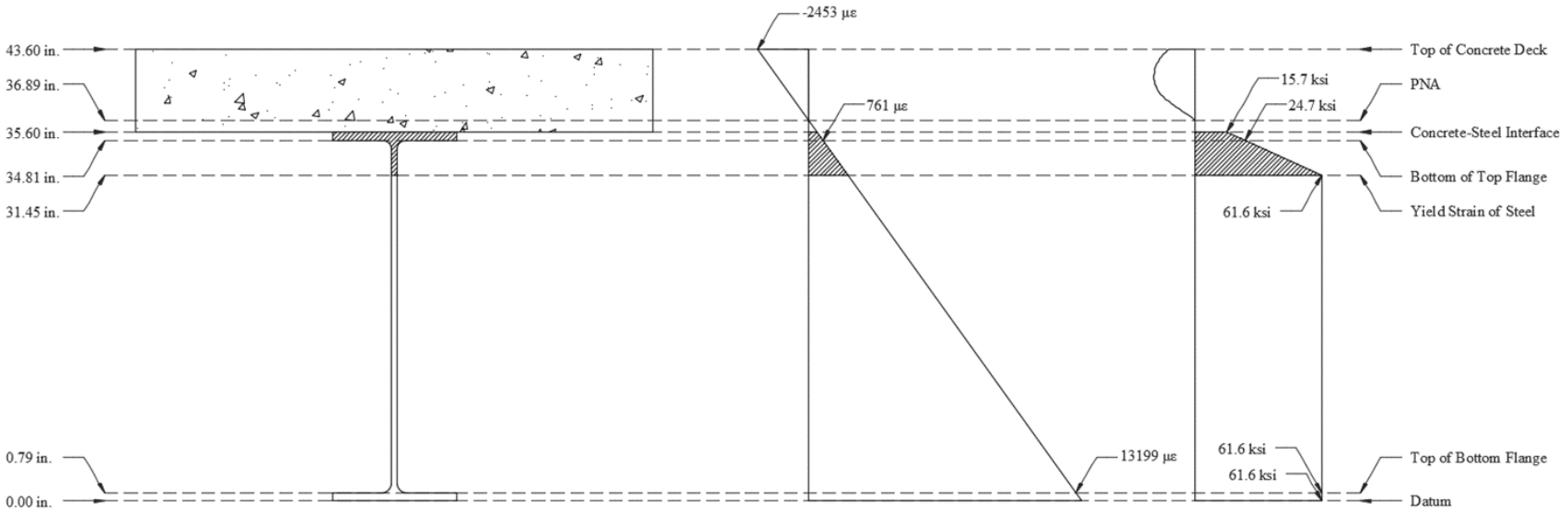

Figure 4.21. Strain and Stress Distribution at Section 2 of Specimen A

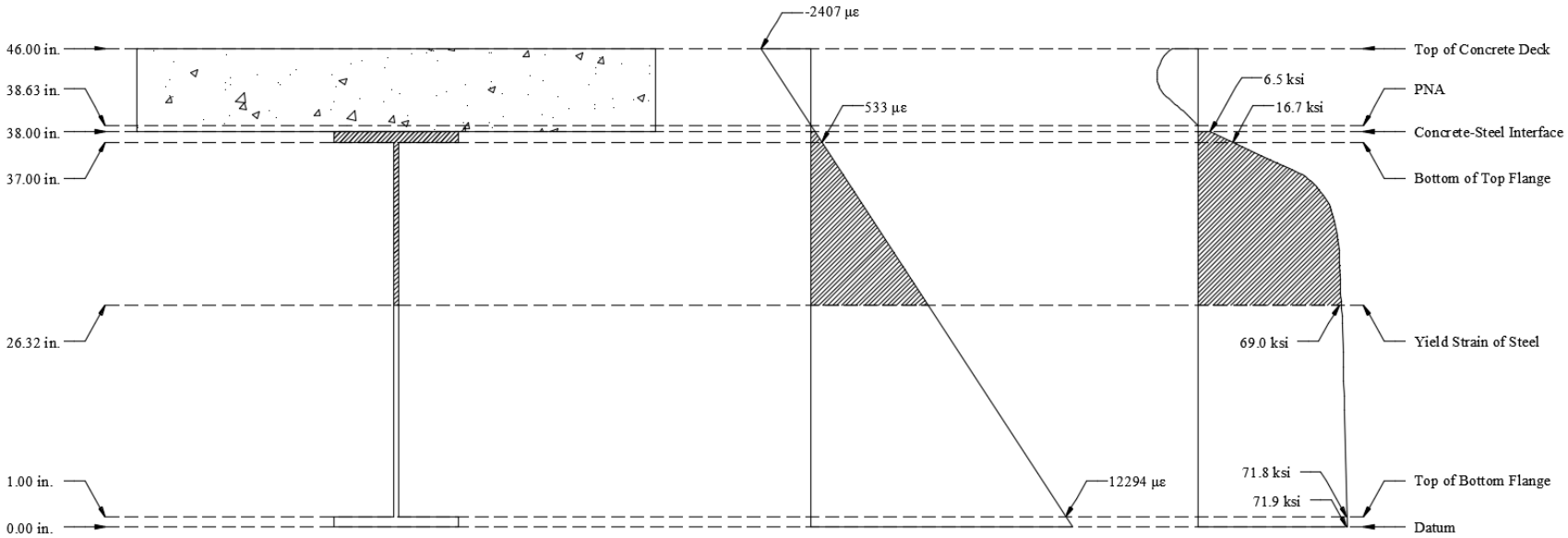

Figure 4.22. Strain and Stress Distribution at Section 2 of Specimen B

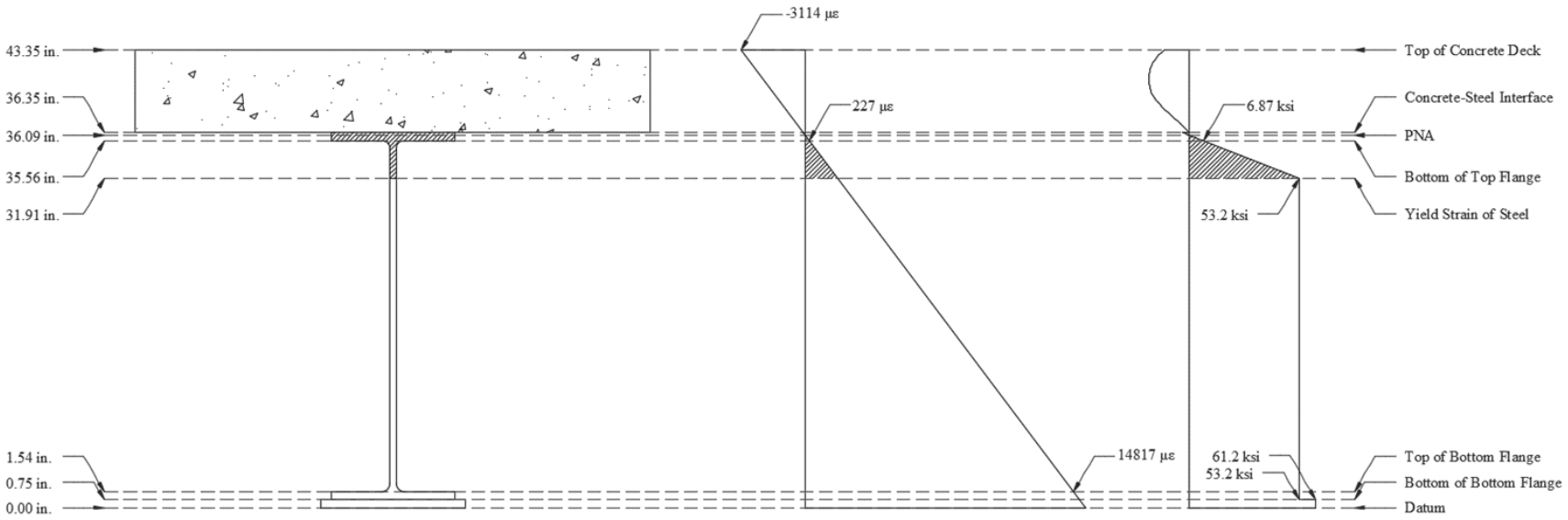

Figure 4.23. Strain and Stress Distribution at Section 2 of Specimen C

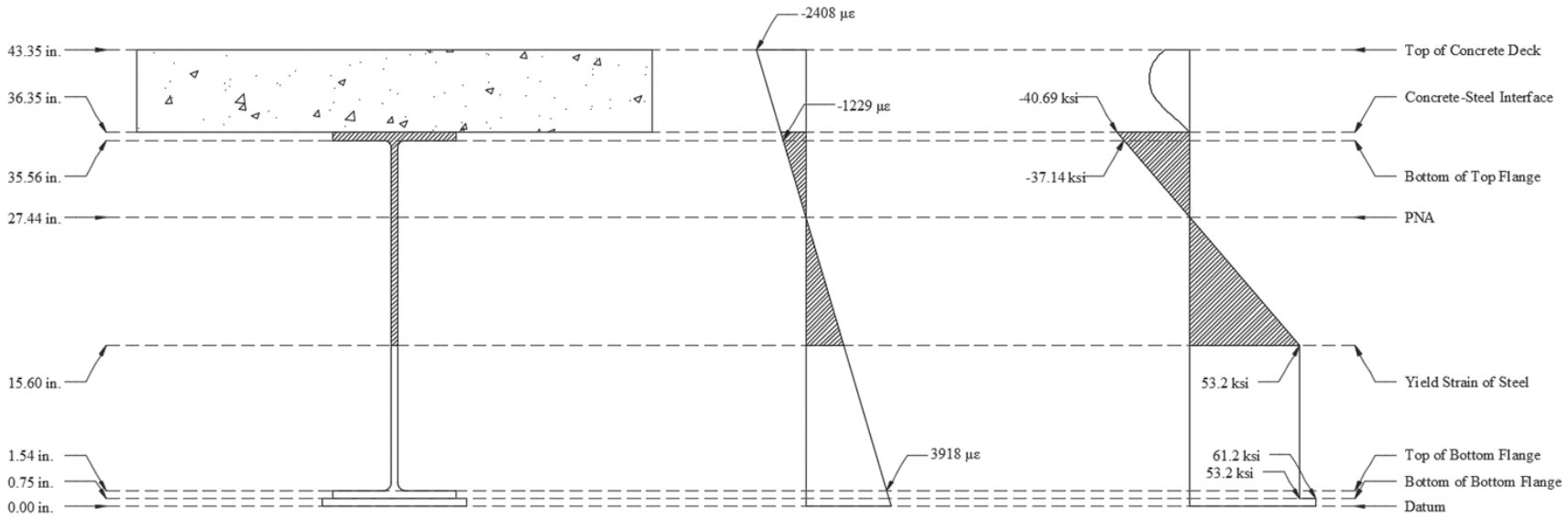

Figure 4.24. Strain and Stress Distribution at Section 2 of Specimen D

The M_{exp} calculated based on equilibrium at ultimate and stress-strain profile are tabulated in Table 4.17. The results from both methods are approximately the same. Compared to the nominal flexural strength, the M_{exp} values are significantly greater than the M_n value, probably due to the material properties of the section. In further discussions only the M_{exp} obtained from equilibrium at ultimate is considered.

Table 4.17. The PNA, M'_P and M'_n of Composite Specimens

Average of P_a of P_b	*Distance to the load from the support, (ft)*	*M_{exp} from the equilibrium at ultimate*	*M_{exp} from the strain profile at ultimate*
344.5	*13.5*	*4651*	*4586*
265.3	*19.875*	*5273*	*5447*
359.4	*16*	*5750*	*5868*
310.4	*16*	*4966*	*4510*

4.6. Validation of the Proposed Method

4.6.1 Relationship between Capacity and Moment of Inertia

The moment of inertia based on measured properties, I'_n and the experimentally estimated moment of inertia, I_{exp} are listed in Table 4.18 as a ratio to the nominal moment of inertia, I_n of each specimen. The I_{exp} and I'_n values are significantly different compared to the I_n value of each specimen. However, the I_{exp}/I_n and I'_n/I_n ratios are approximately equal, suggesting, (1). The difference between I_{exp} and I_n is due to the difference between measured and nominal material properties, and (2). Theory of strength of materials along with measured material properties can be used to accurately estimate the moment of inertia of a steel-concrete composite specimen.

Table 4.18. Comparison of Moment of Inertia Values

Experiment	$I_{exp}/I_n \approx (I_{FEM}/I_n)$	I'_n/I_n
A	*1.16*	*1.04*
B	*1.12*	*1.14*
C	*1.16*	*1.15*
D	*1.09*	*1.12*

Similarly, the flexural strength based on measured properties, M'_n and the experimentally estimated flexural strength, M_{exp} are listed in Table 4.19 as a ratio to the nominal flexural strength, M_n of each specimen. The M_{exp} and M'_n are significantly higher than the M_n. However, the M_{exp}/M_n and M'_n/M_n ratios are approximately the same. This suggests that (1). The difference between M_{exp} and M_n is due to the difference between measured and nominal material properties, and (2). The guide lines given in the Appendix D6.1 of the AASHTO LRFD Bridge Design Specification [50] can be used along with the measured material properties to get an accurate estimate of the flexural strength of the steel-concrete composite sections.

Table 4.19. Comparison of flexural strength Values

Experiment	M_{exp}/M_n	M'_n/M_n
A	*1.25*	*1.26*
B	*1.38*	*1.41*
C	*1.38*	*1.34*
D	*1.19*	*0.99*

4.6.2 Improved Load Rating Factor Calculation

Figure 4.25 (same as Figure 4.7(a)) shows the relationship between moment of inertia and flexural strength of Specimen A. According to Table 4.8 and Table 4.14, I_{exp} of Specimen A can be calculated as 25542 in^4. It is important to remember that the I_{exp} and I_{FEM} represents the same concept, that is the moment of inertia of the specimen under existing condition at the time of the load rating. The possible flexural strength values corresponding to the I_{exp} of the specimen can be obtained from Figure 4.25(a) and shown in Figure 4.25(b). According to Figure 4.25, as an average the M_{imp} values are higher than the M_n of the section, implying that higher the moment of inertia, higher the flexural strength. Also, the flexural strength values correspond to the I_{exp} of the specimen is smaller than the M_{exp} of the section.

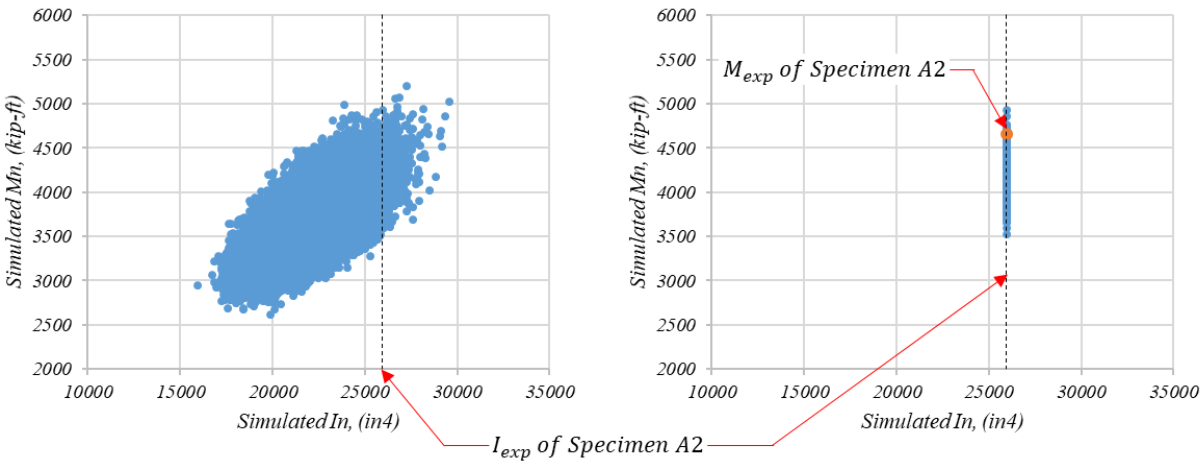

Figure 4.25. Validation of Proposed Procedure with Specimen A2

Similarly, Figure 4.26 shows the relationship between moment of inertia and nominal flexural strength of Specimen B. The improve estimation for the flexural strength, (M_{imp}) is corresponds to the I_{exp} of the section. According to Table 4.8 and Table 4.14, the I_{exp} of Specimen B can be calculated as 27978 in^4. As an average the M_{imp} values are higher than the

M_n of the section. Also, the M_{exp} of the section is larger than the M_{imp} values, suggesting that the M_{imp} values can be used to improve the rating factor calculation process.

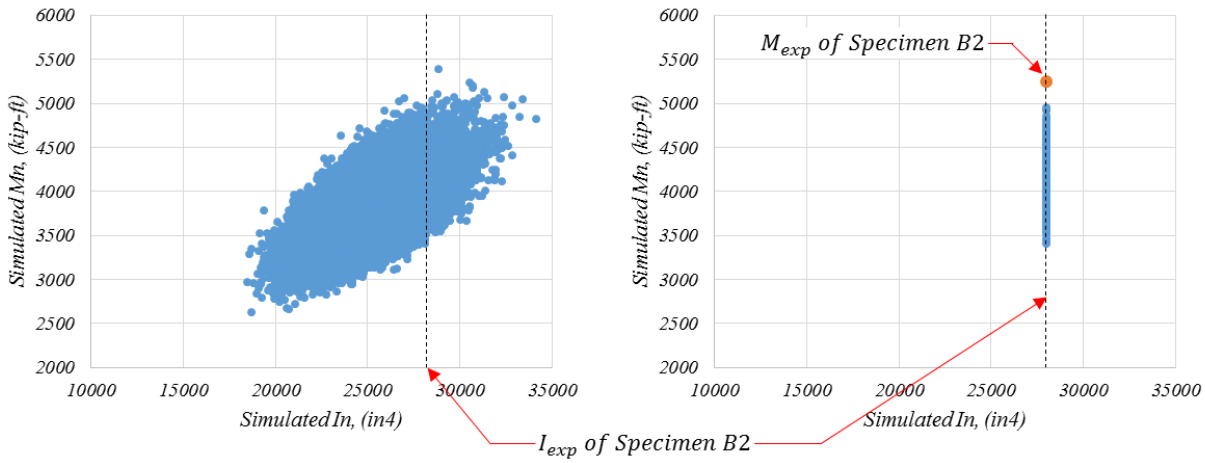

Figure 4.26. Validation of Proposed Procedure with Specimen B

Finally, the relationship between moment of inertia and the flexural strength of Specimen C and Specimen D are shown in Figure 4.27. Both Specimen C and D had the same relationship due to the same nominal properties of the specimen. However, due to the different measured concrete strength, Specimen C shows the higher I_{exp} value than the I_{exp} value of Specimen D. The M_{imp} values corresponding to the I_{exp} of Specimen C shows a larger value compared to it M_n and significantly lower than the M_{exp} of the specimen. Since the I_{exp} of Specimen D is smaller than the I_{exp} of Specimen C and it shows the M_{imp} values are smaller than the M_{imp} values. Again, this suggested that there is a trend, such that when flexural strength increases then the moment of inertia increases and vice versa. Also, the M_{exp} of Specimen D is higher than the M_{imp} values of the section.

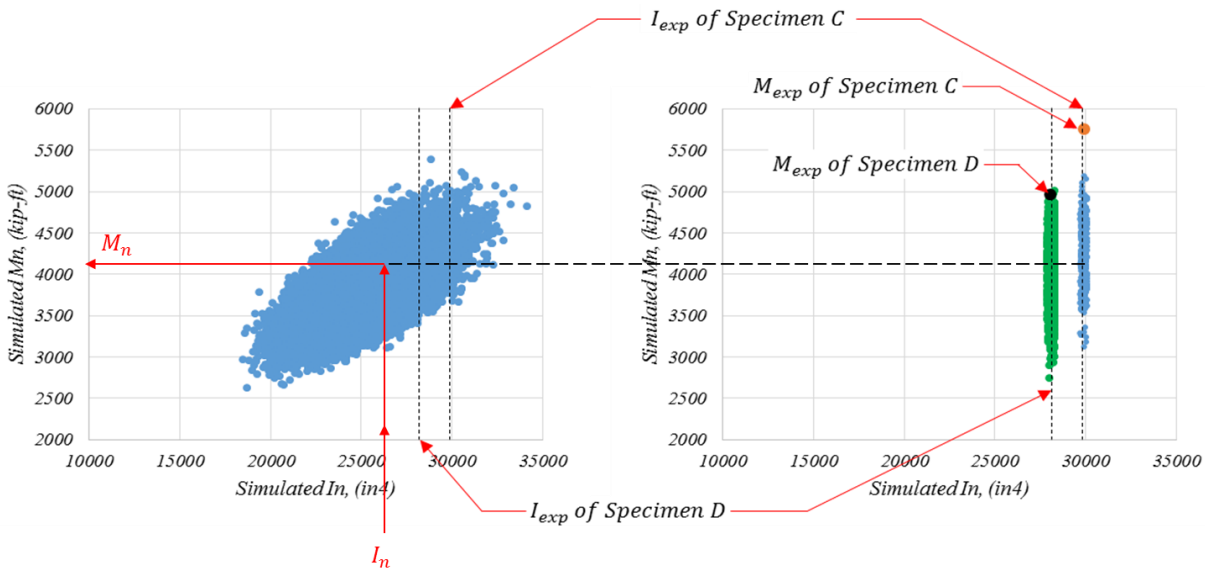

Figure 4.27. Validation of Proposed Procedure with Specimen C and Specimen D

The above results show that the I_{exp} of each specimen can be used in combination with a Monte Carlo simulation to obtain an improved flexural strength of steel-composite section. Since the I_{exp} is calculated similar to the I_{FEM} calculation process, the I_{FEM} can be used to obtain an improve flexural strength of a bridge, without doing a destructive test and interrupting the traffic on the bridge.

CHAPTER 5. PREDICTION OF FUTURE BRIDGE CONDITION RATINGS

5.1. Introduction

According to the American Association of State Highway and Transportation officials (AASHTO) Manual of Bridge Evaluation (MBE) [2], a bridge is defined as a structure that supports moving loads with a length more than 20 ft. over obstructions, such as water, highway, or railway. Elements of a typical bridge can be grouped into three primary components as (1). Deck, (2). Superstructure and (3). Substructure. The deck of a bridge is defined as the component that directly carries the moving loads. The superstructure is defined as the component that supports the deck and connects to the substructure. The superstructure consists of every element below the deck and above the bearings. The substructure is responsible for support of both deck and superstructure of the bridge and responsible for distributing loads to the ground. The substructure consists of every element below the bearings, including diaphragm, piers and components of the foundation. The wing walls and the abutments of a bridge are also considered as substructure components.

Bridges are continuously exposed to the environment and dynamic loading effects due to moving loads. Therefore, bridges can deteriorate relatively quickly. Figure 5.1 shows the leading causes of typical bridge deterioration. Hairline cracks on a bridge deck propagate due to freeze-thaw effects of water, which seeps through the hairline cracks. Also, the water and deicing salt inside the cracks accelerate corrosion of the deck reinforcement. Ineffective drainage systems could accelerate the corrosion of superstructure and substructure. Debris clogged inside the joints may prevent the intended degree of freedoms that leads to misalignment such that the structure may not be able to release the necessary stresses. Scour damages the foundation and washes away the soil under the foundation causing excessive

settlements of the bridge. The continuous dynamic effects, especially from the moving heavy traffic, amplify the stresses and may induced fatigue damage.

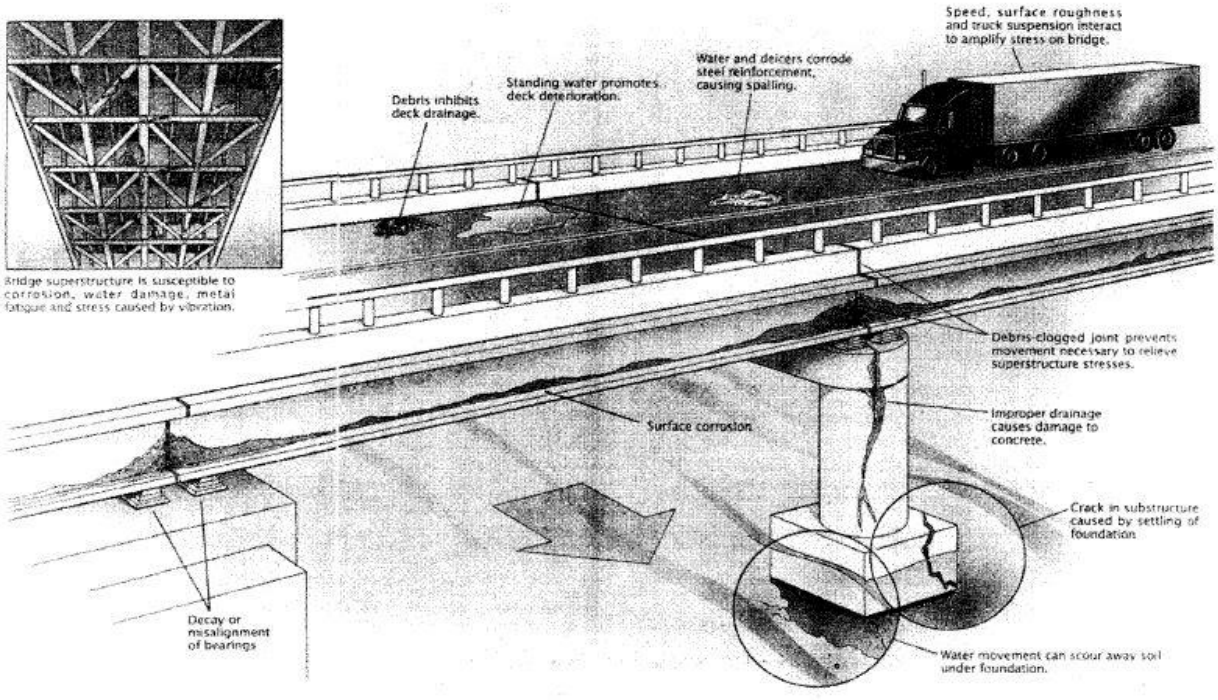

Figure 5.1. Causes of Deterioration of a Typical Bridge [71]

Bridge deterioration is a critical problem in the United States. According to the infrastructure report card of the American Society of Civil Engineers (ASCE) [1], as of 2016, out of 614,387 bridges in the United States, almost 1 in 11 (9.1%) bridges are rated as structurally deficient. A structurally deficient bridge is defined as a bridge with condition rating of 4 or less for either the deck, superstructure, or substructure, where, the condition rating is a condition assessment scale from 0 to 9, where 0 is the failed condition and 9 is the excellent condition. Structurally deficient bridges are not necessarily unsafe to the traffic, but it can quickly become unsafe without proper inspection and maintenance. Even though high traffic volume bridges may have a lower probability to be structurally deficient, in 2016 an average of 188 million trips per day were recorded on structurally deficient bridges [1]. Figure 5.2 shows the total number of bridges and total number of structurally deficient bridges in the

United States from 2002 to 2012. The good news is that, as the number of bridges increases, the number of structurally deficient bridges decrease. However, the bad news is out of 600,000 bridges, approximately 100,000 (1/6) are still rated as structurally deficient.

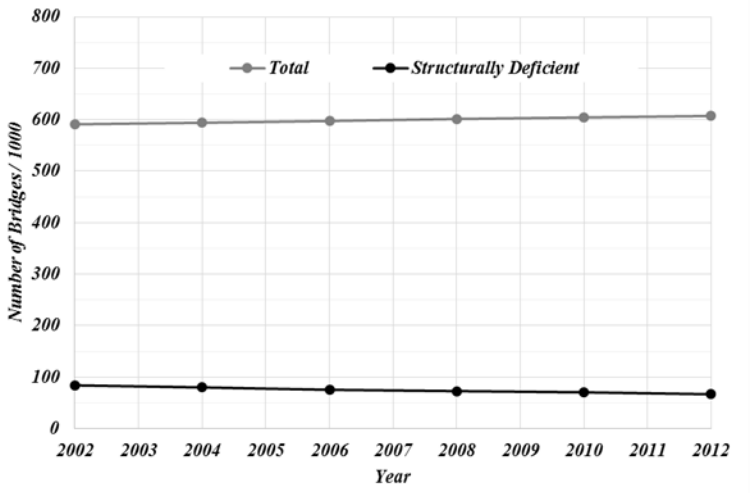

Figure 5.2. Statistical Data of Structurally Deficient Bridges in the United States

Figure 5.3 illustrates the condition of each bridge component in 2012. The bridge components with condition rating greater than 6 are classified as "Good", while the bridges components with condition rating lower than 5 are classified as "Poor". The bridges components with condition rating 5 and 6 are classified as "Fair" condition. According to Figure 5.3, about 40% of each bridge component has a condition rating 6 or less, which implies that there are large amount of bridges getting closer to the structurally deficient limits.

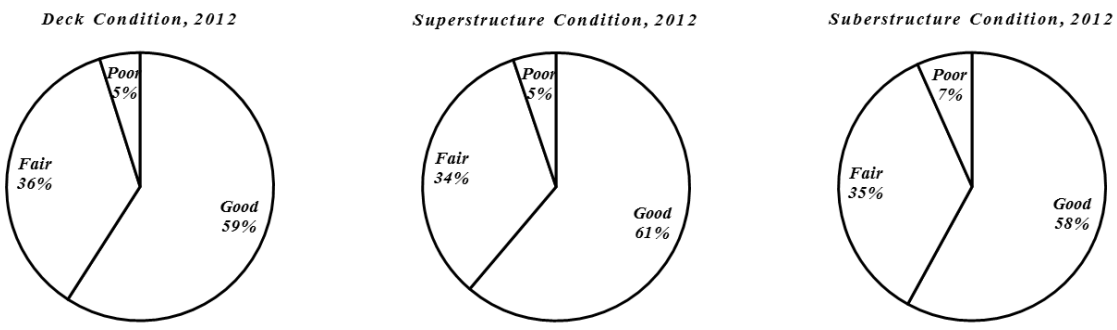

Figure 5.3. Condition of Each Bridge Component in the United States in 2012

The design life of many bridges was originally 50 years. The average age of a bridge in the US is 43 years. Figure 5.4 shows the percentage of bridges in different age groups and the portion of structurally deficient bridges in each age group. According to Figure 5.4, approximately 4 out of 10 (40%) bridges are older than 50 years. As of 2016, the American Society of Civil Engineers estimates that rehabilitation of these bridges could cost about $123 billion, suggesting that even though there is a high repair and maintenance demand, available resources are very limited.

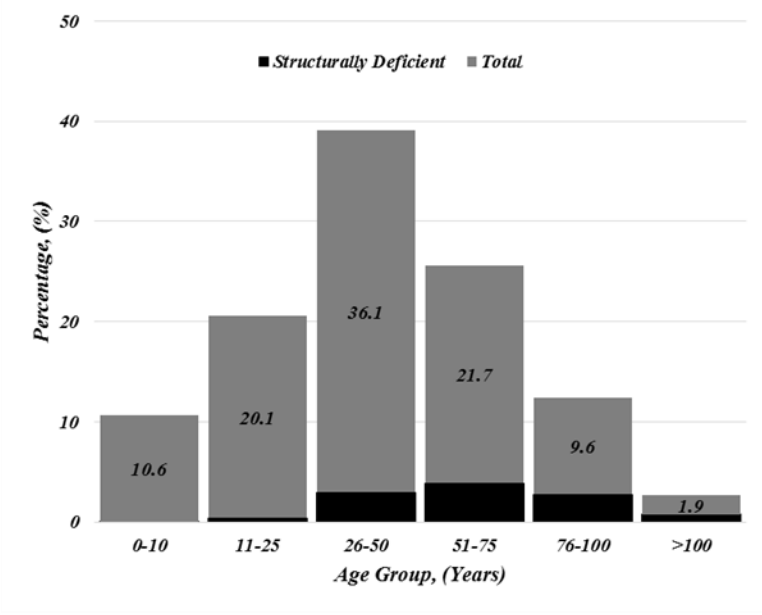

Figure 5.4. Number of Bridges in Each Age Group

This indicates the necessity of proper bridge management plans to keep the nation's transportation system functioning. Prediction of future conditions and estimating the remaining service life are important, so that owners can prioritize the repair and maintenance activities while minimizing the required resources. According to the literature (Section 2.4.1), many researchers carried out different methods to develop future condition rating prediction models. Each method has its own limitations. However, it may be noticed that the best way to predict

the future behavior to estimate the remaining service life is use of NBI bridge condition rating database.

5.2. Historical Behavior of Bridges in the United States

5.2.1 National Bridge Inventory (NBI) Database

The National Bridge Inventory (NBI) database contains historical bridge condition information for bridges in the United States. The NBI database was created after the Silver Bridge collapse in 1967, which was used to connect the State of Ohio and the State of West Virginia across the Ohio River. After the incident, the Federal Highway Administration (FHWA) mandated that every state maintain records of their bridges regarding its (1). Geometric properties, such as span length, width of the deck etc., (2). Operational conditions which includes the traffic volume and age of the bridge, (3). Condition of every component of the bridges with physical inspections. Currently, departments of transportations in each state commonly conduct three types of inspections, namely (1). Initial inspection, (2). Routine inspection and (3). In-depth inspection. The initial inspection of a bridge is conducted after the construction or rehabilitation of the bridge to establish a baseline for the bridge condition and identify any problems that may exists. The regular inspections are performed out at intervals not less than 24 months. The inspection interval can be increased up to a maximum of 48 months with written FHWA approval only if past inspection analysis justifies it. The in-depth inspections are carried out independent of the scheduled routine inspections to identify any problems that are cannot be identified during the routine visual inspections.

Typically, the initial inspection and routine inspection are visual inspections. According to Recording and Coding Guide for the Structure Inventory and Appraisal of the Nation's Bridges, hereafter referred to as the NBI Coding Guide [9], concrete decks should be

inspected for possible cracks, scaling, spalling, leaching, chloride contamination, potholes, delamination, full depth or partial depth failures. The condition of the wearing surface, joints, expansion devises, curbs, sidewalks, parapets are not considered in evaluating the overall deck condition. Also, decks integral with the superstructure will be rated as a deck only and not how they may influence the superstructure rating. The superstructures are inspected for signs of distress, which may include cracking, deterioration, section loss and malfunction and misalignment of bearings. Except in extreme situations, the conditions of bearings, joints and paint systems are not included in the superstructure condition ratings. When the deck is integral with the superstructure, the superstructure condition rating may be affected by the deck condition. All substructure elements should be inspected for visible signs of distress including cracking, section losses, settlement, misalignments, scour, collision damages and corrosions of piers, abutments, piles, footings or other components. Substructure rating is independent of the deck and superstructure ratings.

During the initial and routine inspections, the condition of each component of the bridge is rated according to the condition rating system given in Table 5.1. The rating system ranges scale from 0 to 9 on an integer scale, where condition rating 0 represents a failed condition and condition rating 9 represents an excellent condition. As mentioned in Section 5.1, a bridge with either deck, superstructure or substructure rating of 4 or below is defined as a structurally deficient bridge.

Table 5.1. Description of Condition Ratings for Deck, Superstructure and Substructure

Code	*Rating*	*Description*
N	*Not Applicable*	
9	*Excellent Condition*	
8	*Very Good Condition*	*No problems noted.*
7	*Good Condition*	*Some minor problems.*
6	*Satisfactory Condition*	*Structural elements show some minor deterioration.*
5	*Fair Condition*	*All primary structural elements are sound, but may have minor section loss, cracking, spalling or scour.*
4	*Poor Condition*	*Advanced section loss, deterioration, spalling or scour.*
3	*Serious Condition*	*Loss of section, deterioration, spalling or scour have seriously affected primary structural components. Local failures are possible. Fatigue cracks in steel and shear crack in concrete may be present.*
2	*Critical Condition*	*Advanced deterioration of primary structural elements. Fatigue cracks in steel or shear cracks in concrete may be present or scour may have removed substructure support. Unless closely monitored it may be necessary to close the bridge until corrective action is taken.*
1	*"Imminent" Failure Condition*	*Major deterioration or section loss present in critical structural components or obvious vertical or horizontal movement affecting structure stability. Bridge is closed to traffic, but corrective action may put back in light service.*
0	*Failed Condition*	*Out of service, beyond corrective action.*

5.2.2 Historical Bridge Condition Statistics, Iowa and Wisconsin

The NBI condition rating database is the best available database to describe the historical condition of bridges in the United States. Though the NBI condition rating database was started around 1970, the condition rating data are available from 1982 for the interstate bridges in the State of Iowa and the condition rating data are available from 1990 for the interstate bridges in the State of Wisconsin. The NBI condition rating histories of both Iowa and Wisconsin bridge components were analyzed to understand any possible trend of each

bridge component in each state. Later, the analysis results were also used to strengthen the results of the future condition rating prediction models.

Figure 5.5 shows the frequency of inspection of each bridge component during last three decades. There is no significant difference between any of the bridge components in both the Iowa and Wisconsin databases. According to Figure 5.5, more than 65% of bridges had at least 10 inspections during last three decades. This implies that these condition rating histories describe around 1/3 of bridge life, hence these condition rating histories may be useful in predicting future bridge conditions.

Figure 5.6 illustrates the frequency of each bridge component in five-year age groups. There is no significant difference between the histograms for each bridge component of Iowa condition rating database. Similarly, there is no noticeable difference between the histograms for each bridge component of Wisconsin condition rating database. However, the histograms of Iowa condition rating data and Wisconsin condition rating data show a significant difference. The average age of any Iowa bridge component is about 46.0 years, whereas average age of any Wisconsin bridge component is about 38.5 years. The age of the Iowa bridges is greater than the average age of the nation's bridges (43 years). The age of the Wisconsin bridges is younger than the average age of the nation's bridges. Also, the ASCE Infrastructure Report Card ranked the State of Iowa as the state with highest number of structurally deficient bridges.

Figure 5.7 shows the percentage of each condition rating number given to each bridge component over the last three decades for both Iowa and Wisconsin bridges. According to Figure 5.7 most of the bridge decks in both Iowa and Wisconsin are rated as condition rating 7. Whereas, most of the superstructures and substructures in both Iowa and Wisconsin are rated

as condition rating 7 or condition rating 8. This implies that the deck deteriorates somewhat faster than the substructure and superstructure, probably because the bridge decks are continuously and directly exposed to both traffic and environmental changes. Figure 5.7 also shows that very small amount of bridges are rated as condition rating 3 or below.

Figure 5.8 illustrates the age span of each condition rating for all bridge components in both Iowa and Wisconsin databases. The age span of each condition rating of both Iowa and Wisconsin bridges shows similar trend with some minor differences. The condition rating 6 and 7 has wider age span, ranging from 5years to 100 years. Whereas condition rating 9 has a narrower age span, ranging from 1 year to 15 years.

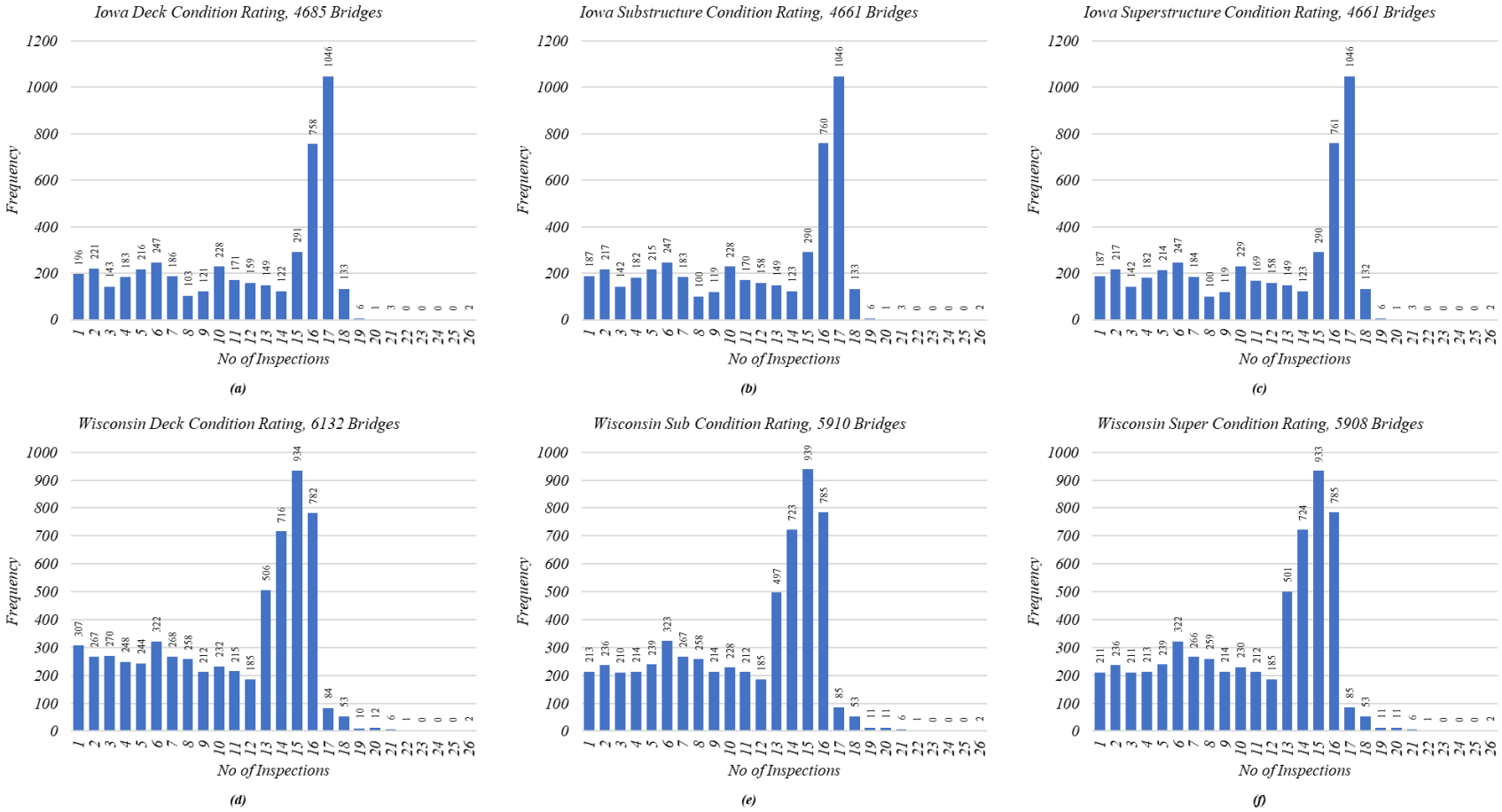

Figure 5.5. Statistics of Frequency vs Number of Inspections

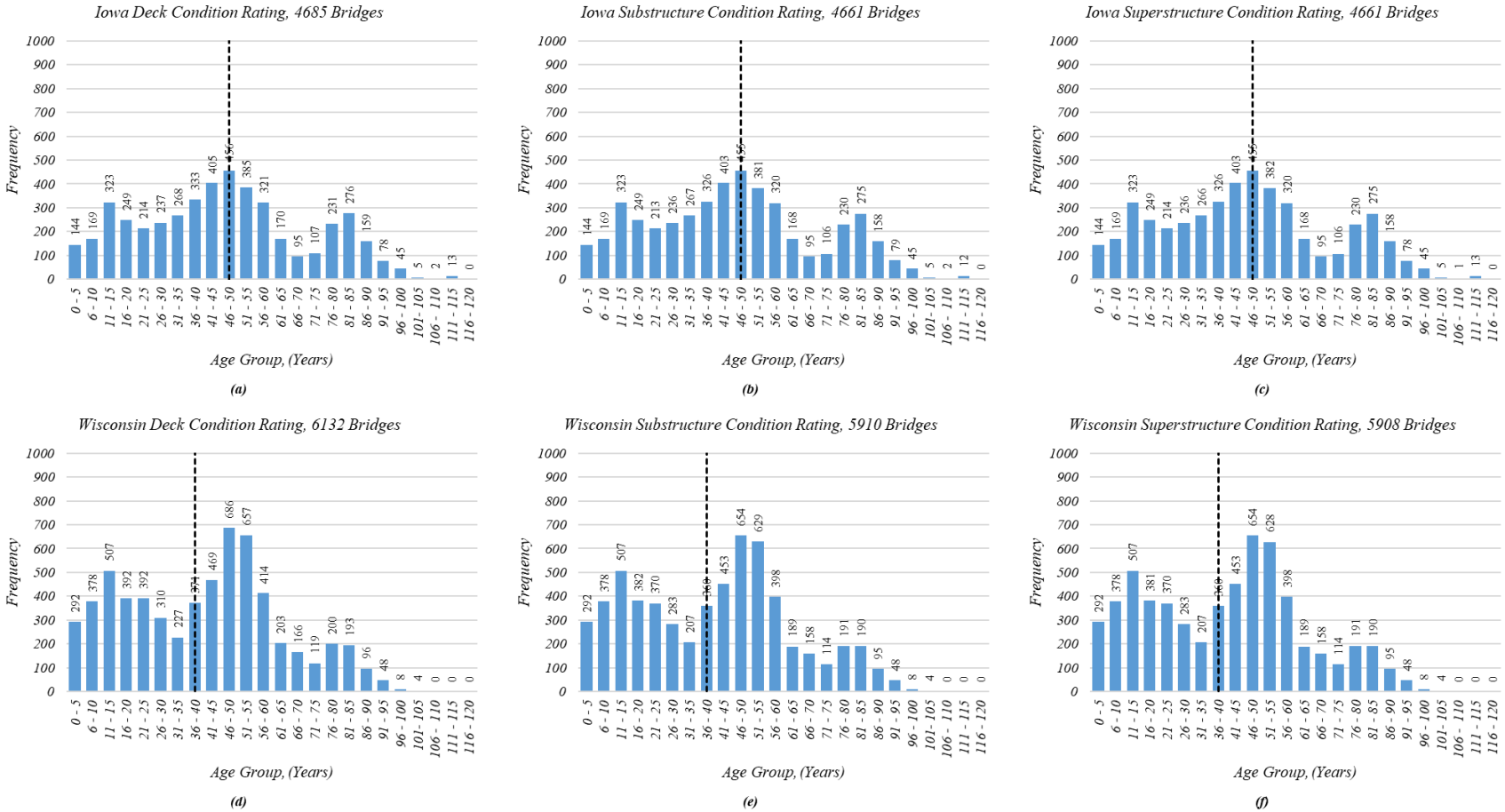

Figure 5.6. Statistics of Frequency vs Age

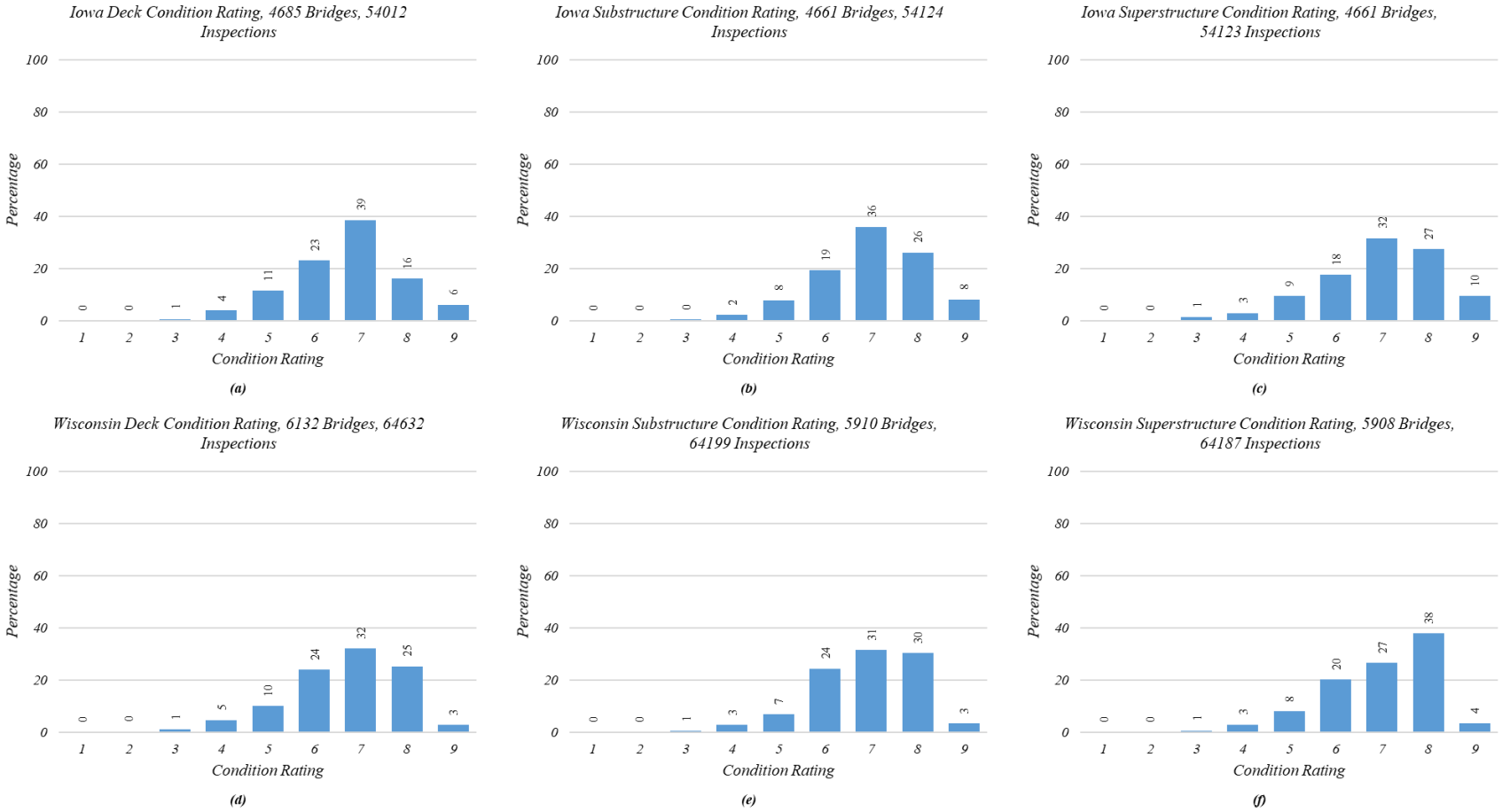

Figure 5.7. Statistics of Frequency vs Condition Rating

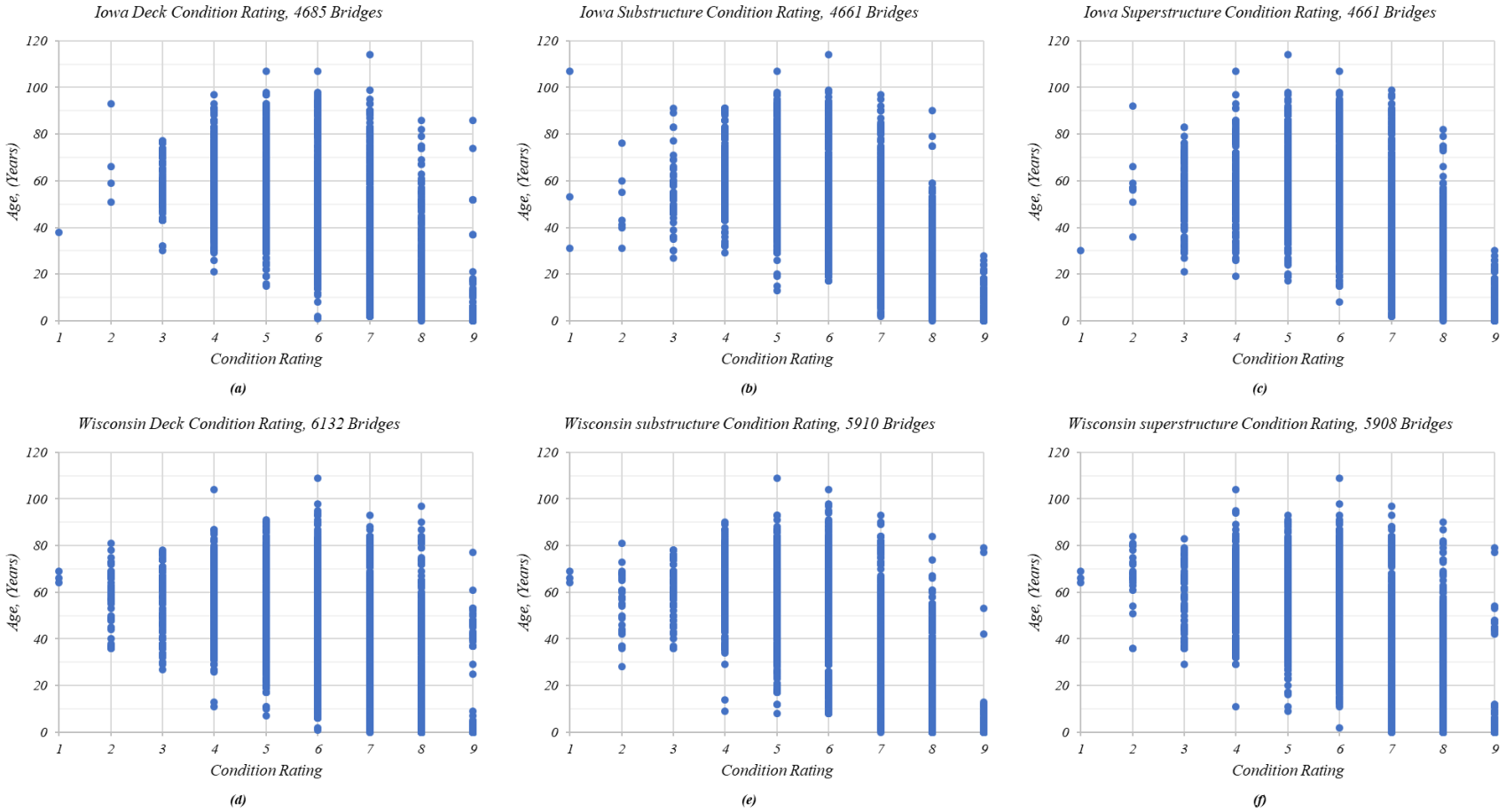

Figure 5.8. Statistics of Condition Rating vs Age

5.3. Objective

The objective of this portion of the project was to develop a mathematical model which can be used to predict future condition ratings of each bridge components, more specifically, to estimate the probability of each bridge component being at any condition rating at any future year. The research group was interested in developing two different types of prediction models. The first type was named as Current Practice Model (CPM), which is capable of simulating the effects of historical maintenance activities when predicting the future condition rating probabilities. The second type was named as Deterioration Prediction Model (DPM), which does not consider the historical maintenance activities when predicting the future condition rating probabilities. Both models could be useful when making bridge management decisions. For example, CPM and DPM can be used to investigate the effects of current maintenance practices while making repair and maintenance decisions, such that bridge management decisions can be optimized while minimizing the required resources.

5.4. Methodology

5.4.1 Current Practice Model (CPM)

The methodology behind the development of Current Practice Model (CPM) is explained in this section. As discussed in previous sections, the models were developed using the historical condition rating data available in the NBI condition rating database. As shown in Section 5.2.2, there are very few bridges rated as condition rating 3 or below. Therefore, this methodology of calculating the probability of bridge component being at any condition rating is limited to between 4 and 9 in any future year.

The NBI condition rating data recorded until 2014 were considered to develop CPM. Therefore, 2014 was assumed as the present year and 2016, 2018, 2020 and etc. were

considered as the future years. Since typical routine-inspection interval is two years, the probability of bridge being at any condition rating between 4 and 9 was calculated in two-year intervals and defined as prediction interval. The most recent inspection year and the most recent condition rating were defined as current year and current condition rating. The subsequent future years at the end of each prediction interval are termed as prediction years. The possible paths to transition from one condition rating to another condition rating are defined as transition paths. Both the condition ratings and transition paths were labeled such that the rating number, year and transition path can directly understandable manner. For an example $CR_{7@2014}$ represents the condition rating of the bridge deck in 2014 is 7. Also, $CR_{7\rightarrow 8@2016}$ indicates the condition rating transition from $CR_{7@2014}$ to $CR_{8@2016}$, whereas $CR_{7\rightarrow 8\rightarrow 5@2018}$ indicates the condition rating transition from $CR_{7@2014}$ to $CR_{8@2016}$ and then $CR_{5@2018}$. Also, the CPM assumes that the pervious maintenance practices will continue. i.e., with respect to the current condition rating, the future condition rating can be increase or decrease or stay at the same.

A hypothetical condition rating history of a bridge deck is used here to illustrate CPM development process (Figure 5.9(a)). As example, methodology of calculating the probability of the bridge deck being at $CR_{8@2016}$ and $CR_{5@2018}$ are discussed. When calculating the probability of a bridge being at a given condition rating, it is very important to identify every possible transition path to reach that condition rating. For an example, Figure 5.9(a) shows that there is one possible transition path available to reach $CR_{8@2016}$, that is $CR_{7\rightarrow 8@2016}$. Also, Figure 5.9 shows that there are six possible transition paths available to reach $CR_{5@2018}$, such as, $CR_{7\rightarrow 9\rightarrow 5@2018}$, $CR_{7\rightarrow 8\rightarrow 5@2018}$, $CR_{7\rightarrow 7\rightarrow 5@2018}$, $CR_{7\rightarrow 6\rightarrow 5@2018}$, $CR_{7\rightarrow 5\rightarrow 5@2018}$, and $CR_{7\rightarrow 4\rightarrow 5@2018}$. This clearly suggests that there are total of 36 possible transition paths are

available when calculating the probability of bridge being at any condition rating in year 2020 (Prediction Year 3). The number of transition paths quickly increase with the number of prediction intervals, such that representation of every possible path in Figure 5.9 is problematic. A tree diagram can be used to clearly represent every possible transition paths for any number of prediction intervals and it can be used to develop the probability theory to calculate the bridge deck being at each condition rating at a given year (Figure 5.10).

5.4.2 Deterioration Prediction Model (DPM)

The development of Deterioration Prediction Model (DPM) is similar to the development of CPM, however, DPM does not assume that the current maintenance practices will continue. i.e., with respect to the current condition rating, the future condition ratings cannot be increased with time, but it can continue to stay the same or decrease with time. The labeling system used in CPM modelling process was used to label condition ratings and the transition paths. The same hypothetical condition rating history was used to illustrate the methodology behind DPM and calculation of the probability of bridge being at $CR_{8@2016}$ and $CR_{5@2018}$ are discussed. As mentioned in Section 5.4.1, $CR_{7\rightarrow 8@2016}$ is the only possible path to reach $CR_{8@2016}$. Since the DPM does not consider current maintenance practices, the $CR_{7\rightarrow 8@2016}$ is not a valid transition path, such that the probability of the bridge deck being at $CR_{8@2016}$ is zero. When calculating the probability of bridge being at $CR_{5@2018}$, three possible transition paths are available, such as, $CR_{7\rightarrow 7\rightarrow 5@2018}$, $CR_{7\rightarrow 6\rightarrow 5@2018}$, $CR_{7\rightarrow 5\rightarrow 5@2018}$. All invalid transition paths are shown in light dashed line (Figure 5.9(b)). Compared to the CPM, the DPM consists of smaller number of transition paths. However, to clearly explain the methodology behind the DPM development process it also illustrated in a tree diagram and shown in Figure 5.10(b).

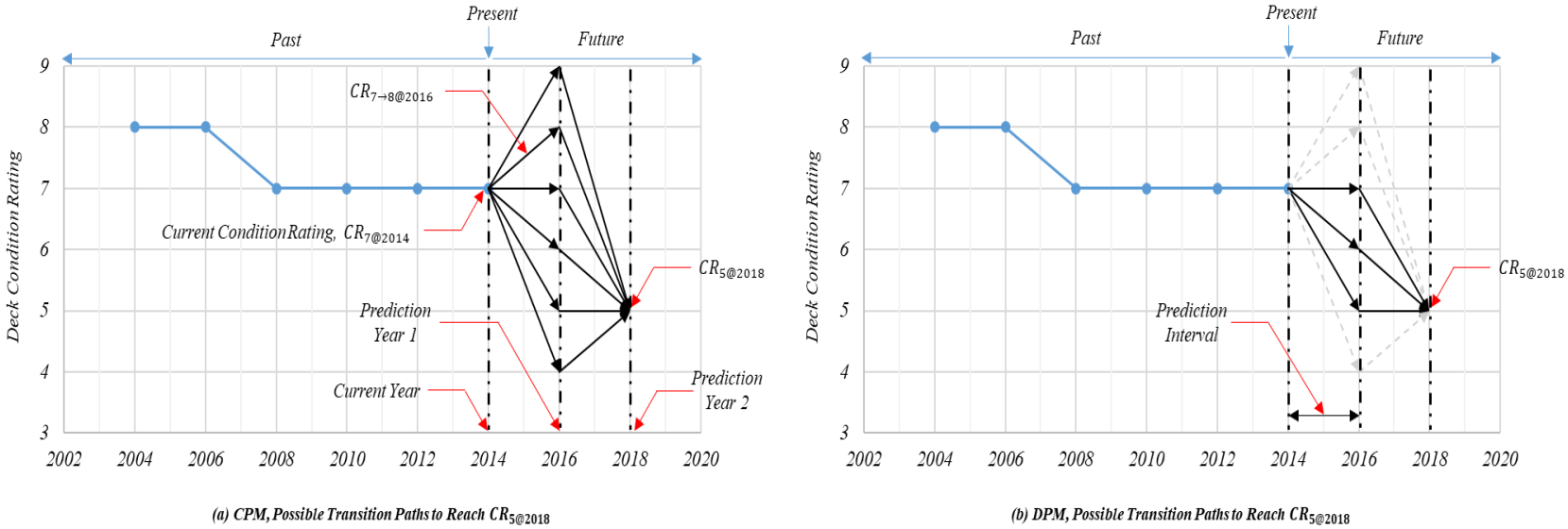

Figure 5.9. CPM Development Process, Possible Future Deck Condition Ratings

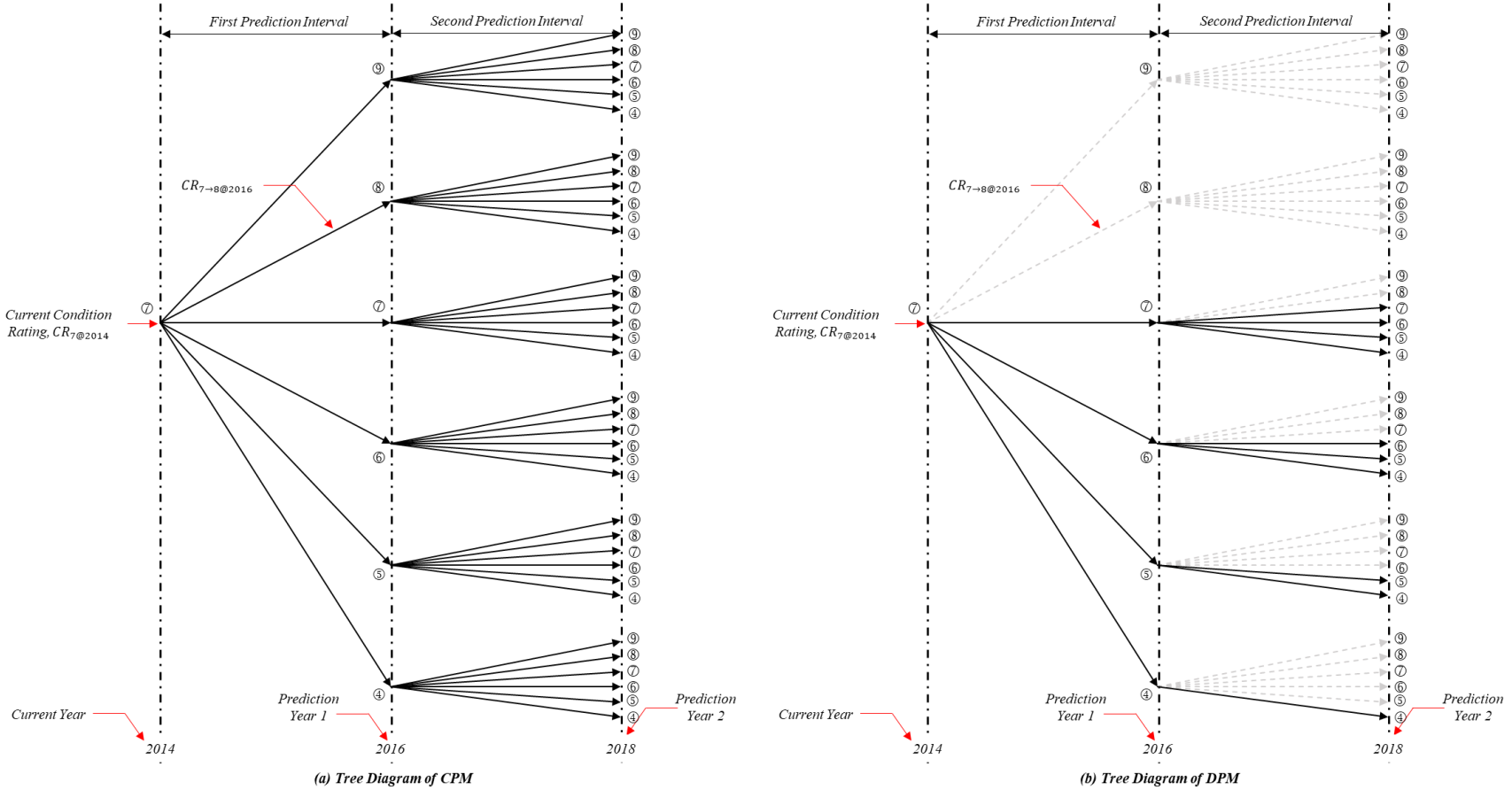

Figure 5.10. Possible Future Condition Ratings Using Tree Diagram

5.4.3 Probability Theory

Use of tree diagrams to calculate the probability of being at each condition rating at a given year consists of two steps, (1). Calculation of probability of each possible transition path (2). Summation of probabilities of every possible transition path. These steps are explained by calculating the probability of the bridge deck being at $CR_{5@2018}$. As a part of the first step of the probability calculation, the probability of having $CR_{7\to9\to5@2018}$ path is calculated and defined it as Event B_9. Event B_9 can be simplified in to two events as Event A_1 and Event A_2, where Event A_1, is defined as $CR_{7\to9@2016}$ and Event A_2, is defined as $CR_{9\to5@2018}$. In statistical terms transition path $CR_{7\to9\to5@2018}$ can be written as shown in Equation 15. The probability of having $CR_{7\to9\to5@2018}$ transition path can be written as shown in Equation 16.

$$\boldsymbol{B_9 = CR_{7\to9\to5@2018} = CR_{7\to9@2016} \cap CR_{9\to5@2018} = A_1 \cap A_2} \quad \ldots. (15)$$

$$\boldsymbol{P(B_9) = P(CR_{7\to9\to5@2018}) = P(CR_{7\to9@2016} \cap CR_{9\to5@2018}) = P(A_1 \cap A_2)} \quad \ldots. (16)$$

According to the probability multiplicative rule, if an experiment consist of dependent events A_1, A_2, A_3,…. A_m, then the probability of having every event is given in Equation 17, where $P(A_2|A_1)$ is the conditional probability of Event A_2 given that Event A_1 is already happened.

$$\boldsymbol{P(A_1 \cap A_2 \cap A_3 \cap \ldots \cap A_m) = P(A_1) \cdot P(A_2|A_1) \cdot P(A_3|A_1 \cap A_2) \cdots P(A_m|A_1 \cap A_2 \cap A_3 \cap \ldots \cap A_{m-1})} \quad \ldots. (17)$$

Event A_1 and A_2 defined above are in depended events because of the probability of Event A_2 is depend upon the occurrence of Event A_1. Following the probability multiplicative

rule, the probability of condition rating transition path $CR_{7\to9\to5@2018}$ can be written as shown in Equation 18 and Equation 19.

$$\boldsymbol{P(B_9) = P(A_1 \cap A_2) = P(A_1) \cdot P(A_2|A_1)} \quad \text{.... (18)}$$

$$\begin{aligned}\boldsymbol{P(CR_{7\to9\to5@2018})} &= \boldsymbol{P(CR_{7\to9@2016} \cap CR_{9\to5@2018})} \\ &= \boldsymbol{P(CR_{7\to9@2016}) \cdot P(CR_{9\to5@2018}|CR_{7\to9@2016})}\end{aligned} \quad \text{.... (19)}$$

According to Figure 5.9(a), there are five other possible transition paths available to reach $CR_{5@2018}$, as $CR_{7\to8\to5@2018}$, $CR_{7\to7\to5@2018}$, $CR_{7\to6\to5@2018}$, $CR_{7\to5\to5@2018}$, and $CR_{7\to4\to5@2018}$. These events were defined as Event $B_8, B_7,\ldots, B_4$, respectively. The same procedure was followed to calculate the probability of these five transition paths to reach $CR_{5@2018}$. In statistical terms every possible path that could reach to $CR_{5@2018}$ can be written as shown in Equation 20. The probability of having $CR_{5@2018}$ can be written as shown in Equation 21.

$$\boldsymbol{CR_{5@2018} = CR_{7\to9\to5@2018} \cup CR_{7\to8\to5@2018} \cup \ldots \cup CR_{7\to4\to5@2018} = B_9 \cup B_8 \cup \ldots \cup B_4} \quad \text{.... (20)}$$

$$\begin{aligned}\boldsymbol{P(CR_{5@2018})} &= \boldsymbol{P(CR_{7\to9\to5@2018} \cup CR_{7\to8\to5@2018} \cup \ldots \cup CR_{7\to4\to5@2018})} \\ &= \boldsymbol{P(B_9 \cup B_8 \cup \ldots \cup B_4)}\end{aligned} \quad \text{.... (21)}$$

However, the bridge deck can take only one possible path to reach $CR_{5@2018}$, implying that these six possible paths are independent from each other. Such events are defined as mutually exclusive events. The probability of mutually exclusive events can be calculated using the additive rule given in Equation 22. Following the additive rule, the probability of being at $CR_{5@2018}$ can be calculated as shown in Equation 23. The same procedure can be applied to calculate the probability of being at any condition rating at any given year.

$$\boldsymbol{P(B_1 \cup B_2 \cup \ldots \cup B_n) = P(B_1) + P(B_2) + \cdots + P(B_n)} \quad \ldots. (22)$$

$$\boldsymbol{P(CR_{5@2018}) = P(CR_{7\to9\to5@2018}) + P(CR_{7\to8\to5@2018}) + \cdots + P(CR_{7\to4\to5@2018})} \quad \ldots. (23)$$

5.4.4 Sojourn Time

When predicting future condition ratings of bridge components, the time spent at each condition rating is important. The time spent at any given condition rating until it transitions to a different condition rating is defined as the Sojourn Time of the condition rating. Throughout this study, the Sojourn Time is designated as A_i, where i represents the condition rating and A represents the time spent at condition rating i. The A_i of a bridge component can be easily calculated by transforming the actual NBI condition rating history to a simplified condition rating history. Whenever the condition rating of a bridge component transitions from one condition rating to another, the former condition rating was assumed to remain just before the latter condition rating, such that the actual NBI condition rating history can be transformed to a simplified condition rating history of the bridge component.

The simplified condition rating history is very useful in defining the Sojourn Time of a bridge component and quantifying the history of the bridge component before and after the Sojourn Time, and thereby mathematically modelling the future condition rating prediction models. Figure 5.11 shows a schematic representation of an actual NBI condition rating history and the simplified condition rating history of a bridge deck. The condition rating of the bridge deck at any inspection was labeled such that the condition rating and the year of inspection can be easily understood. For an example, $CR_{i@t_2}$ represents that the bridge deck is rated as condition rating i in year t_2. As mentioned earlier, the "A_i" value represents the Sojourn Time

of the bridge deck at condition rating i. The "B_i" value represents the condition rating transition of the bridge deck before the $CR_{i@t_2}$, i.e., right before the Sojourn Time A_i. Whereas the "C_i" value represents the condition rating transition of the bridge deck after the $CR_{i@t_3}$, i.e., right after the Sojourn Time A_i. Where the $CR_{i@t_2}$ and $CR_{i@t_3}$ should be the same. Positive B_i or C_i values suggest possible maintenance effects on the bridge deck. Whereas negative B_i or C_i values represent the possible effects due to deck deterioration. Degree of maintenance or deterioration is related to the magnitude of the B_i or C_i values.

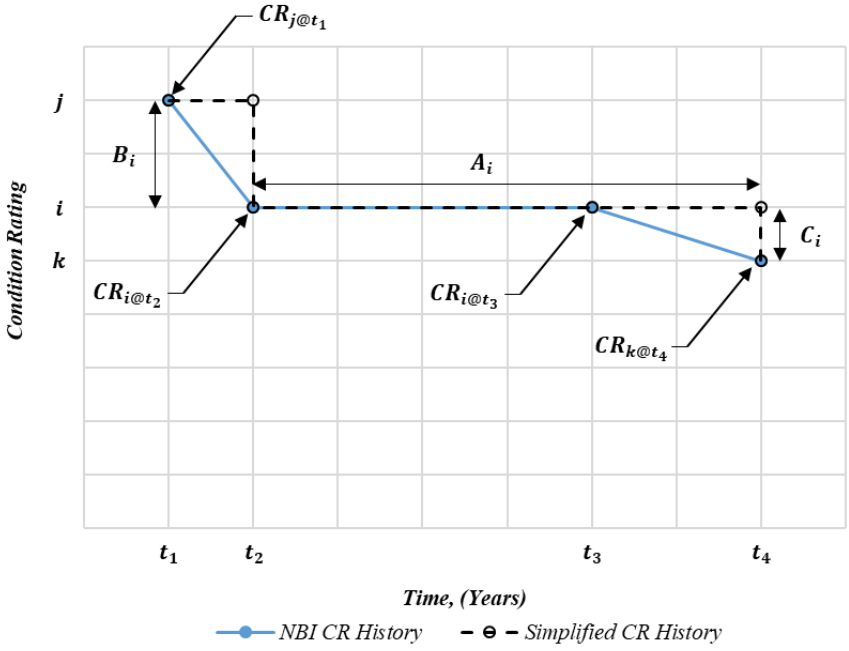

Figure 5.11. Schematic Representation of Actual and Simplified Rating Histories

Depending upon the sign of B_i value and C_i value, nine different types of Sojourn Times can be identified (Figure 5.12). These nine sojourn time types are capable of representing every possible transition in condition rating of a bridge component throughout its entire life.

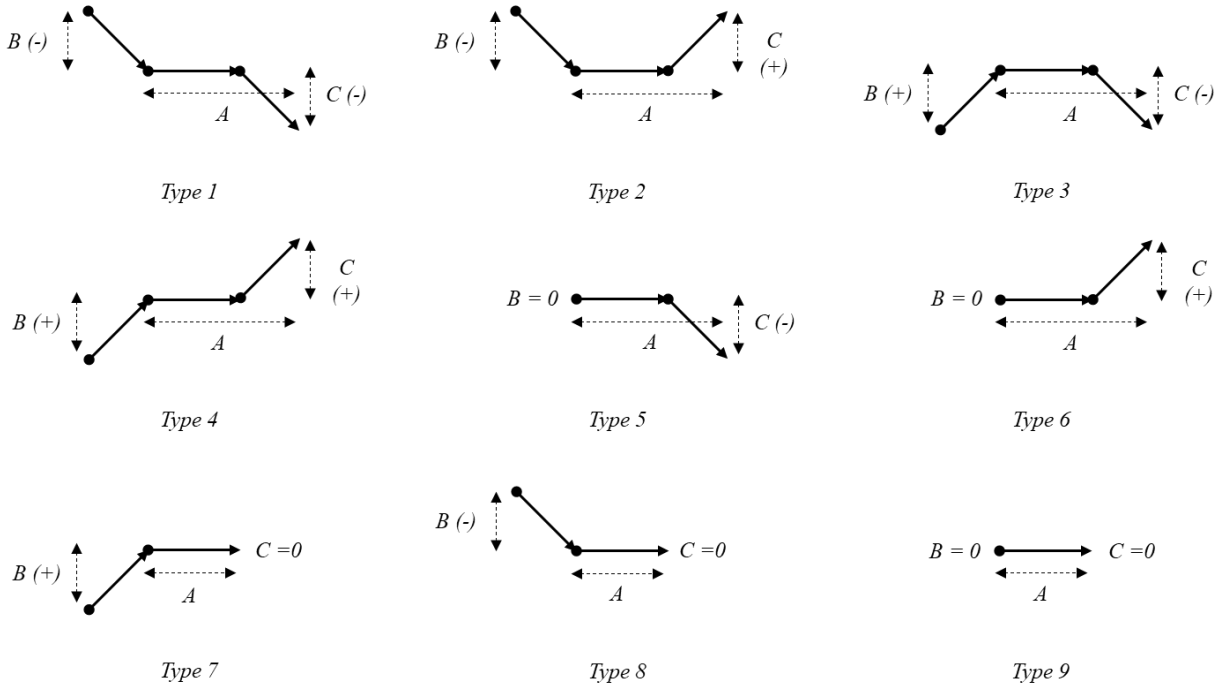

Figure 5.12. Sojourn Time Types

As an example, an actual condition rating history of a bridge deck in Iowa (Figure 5.13) is used to illustrate the concept of simplified condition rating history, Sojourn Time and different types of Sojourn Time. The continuous line in Figure 5.13 shows the actual NBI condition rating history, which is obtained during the routine inspections process. The dashed line shows the simplified condition rating history of the bridge deck. It is obvious that the simplified condition rating history is nothing but the actual condition rating history with instantaneous transitions. As shown in Figure 5.13, six different Sojourn Time types can be identified and used to describe the deck condition rating history of the bridge.

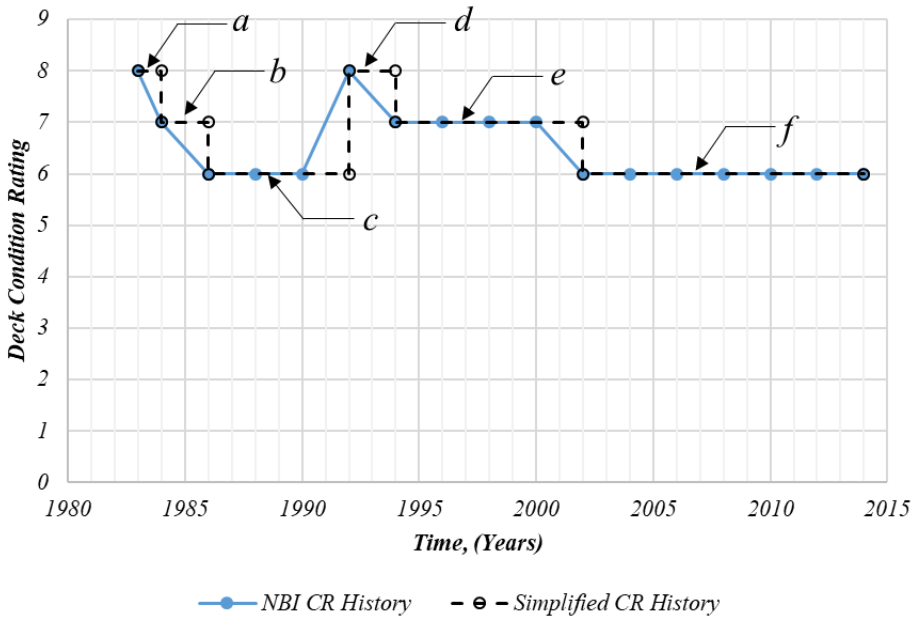

Figure 5.13. Actual and Simplified Rating Histories of an Actual Bridge Deck

A summary of the Sojourn Times shown in Figure 5.13 is tabulated in Table 5.2. The bridge was built in 1980 and the condition rating inspection data was available from 1983. Parameter "Age_i" in Table 5.2 represents the age of the bridge deck at each inspection correspond to condition rating transition of the NBI condition rating history. Table 5.2 suggests that for a given condition rating history there can be several Sojourn Times with different combinations. For example, No: 1 and No: 4 are two different behaviors of the bridge deck at the same condition rating, but different ages. Whereas No: 2 and No: 5 represent the same type of sojourn time for the same condition rating, but at two different ages and two different Sojourn Times (A_i values). Also, Table 5.2 completely describes the historical behavior of the bridge deck in details in numerical format, which would be very helpful to develop the future condition rating prediction models.

Table 5.2. Summary of Sojourn Times

No:	*Year*		Age_i	CR_i	B_i	A_i	C_i	*Sojourn Time Type*
	From	*To*						
a	*1983*	*1984*	*3*	*8*	*0*	*1*	*-1*	*5*
b	*1984*	*1986*	*4*	*7*	*-1*	*2*	*-1*	*1*
c	*1986*	*1992*	*10*	*6*	*-1*	*6*	*2*	*2*
d	*1992*	*1994*	*12*	*8*	*2*	*2*	*-1*	*3*
e	*1994*	*2002*	*20*	*7*	*-1*	*8*	*-1*	*1*
f	*2002*	*2014*	*34*	*6*	*-1*	*12*	*0*	*8*

5.4.5 Sojourn Time Database and Characteristics

As discussed previously, the Sojourn Time, A_i along with parameters B_i and C_i can be used to describe the condition rating history in a quantifiable manner, and it can be used to train the future condition rating prediction models. For the purpose of developing future condition rating prediction models, the parameters listed in Table 5.2 were extracted from each NBI condition rating history of each bridge component.

Characteristics of the Sojourn Time Database were investigated to understand the statistics of Sojourn Times and significance of each Sojourn Time Type. Figure 5.14 shows the time span of Sojourn Time at each condition rating of each bridge component in both Iowa and Wisconsin, regardless the Sojourn Time type. There is no significant difference between the behaviors of Sojourn Time of each Iowa bridge component. Similarly, Wisconsin bridge components shows no noticeable difference between the behaviors of Sojourn Time. However, the Sojourn Time span of Wisconsin bridges are smaller than that of the Iowa bridge components, probably because Wisconsin bridge components have fewer number of inspections than Iowa bridge components.

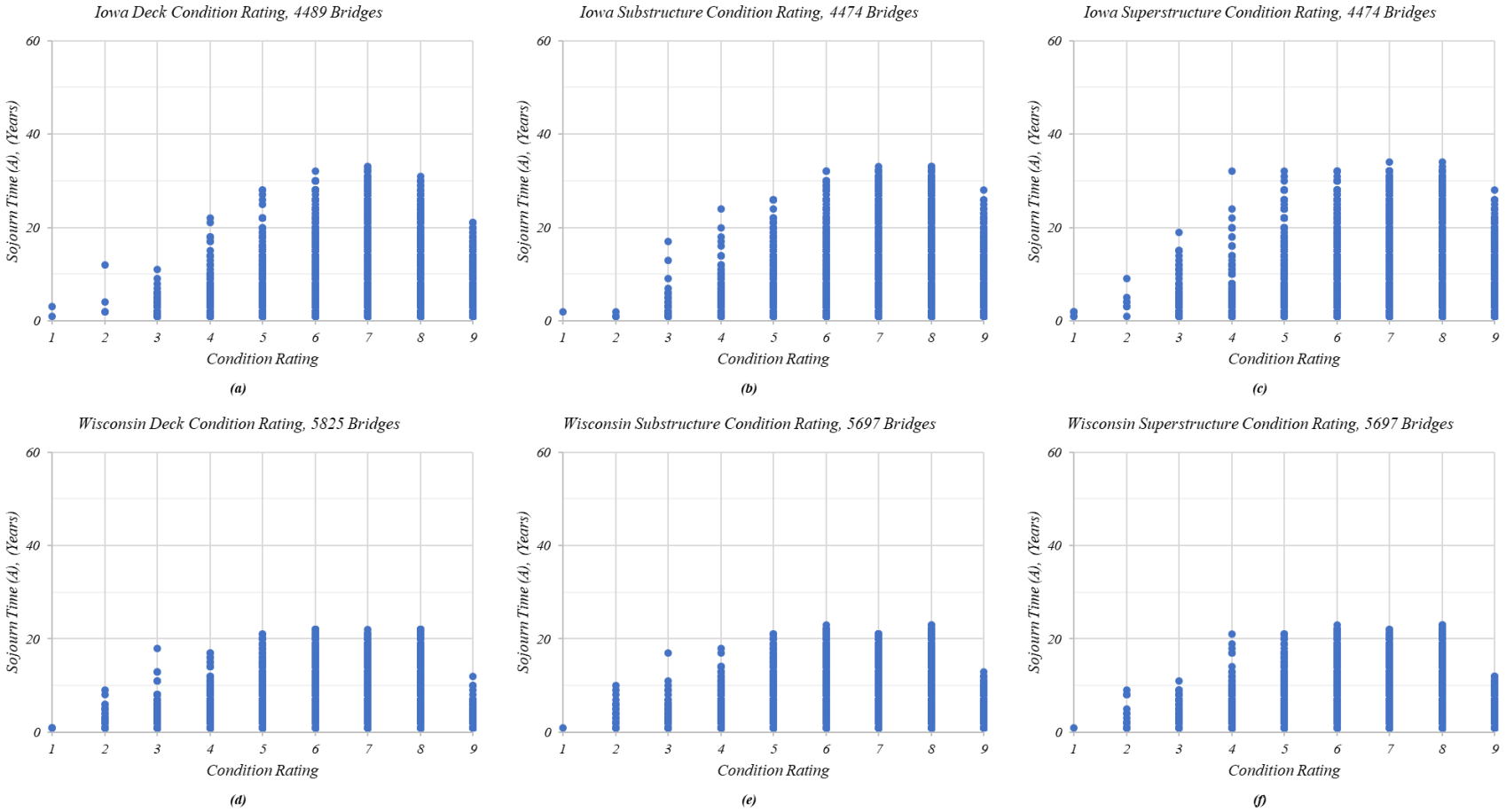

Figure 5.14. Statistics of Sojourn Time of Each Bridge Component

According to Section 5.2.2 and Figure 5.14, the characteristics of condition rating and Sojourn Time of each bridge components are similar in both Iowa and Wisconsin databases. Therefore, only Sojourn Time databases of the deck condition rating of both Iowa and Wisconsin data were used to graphically illustrate the characteristics of Sojourn Times types. Figure 5.15 and Figure 5.16 shows the time span of each Sojourn Time type of both Iowa and Wisconsin deck condition ratings data. The time span of each Sojourn Time of both data sets show similar behavior. Each Sojourn Time type has significant span of Sojourn Time, which implies that each different type of Sojourn Time is important when developing future condition rating prediction models. Also, the time span of each Sojourn Time of condition rating 3 and below is significantly small. The average Sojourn Time of each Sojourn Time type for each condition rating of every bridge component in both Iowa and Wisconsin condition rating data are tabulate from Table 5.3 to Table 5.8.

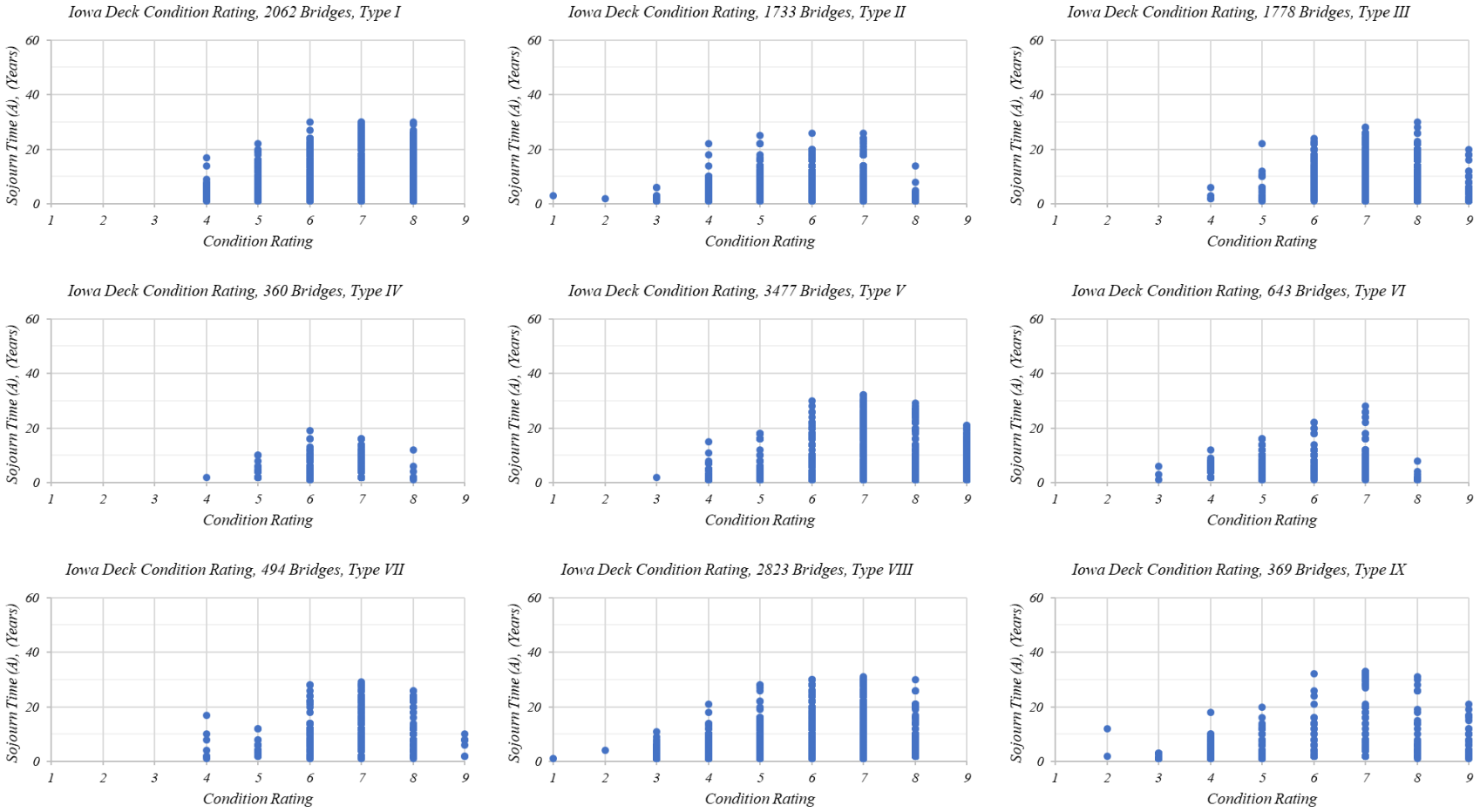

Figure 5.15. Statistics of Sojourn Time Type of Iowa Deck Condition Ratings

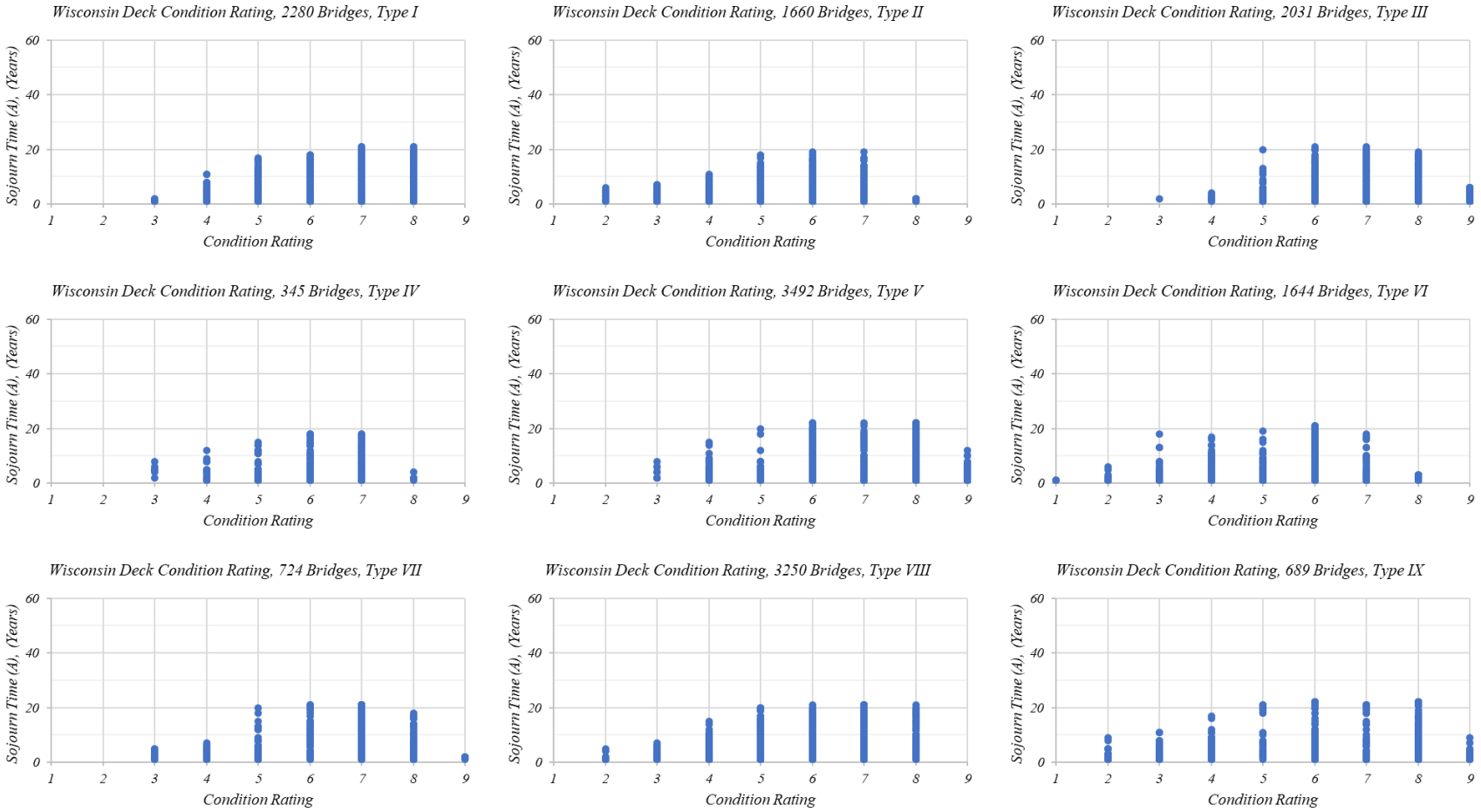

Figure 5.16. Statistics of Sojourn Time Type of Wisconsin Deck Condition Ratings

Table 5.3. Iowa Deck Condition Rating, Average Sojourn Time, (Years)

	Iowa Deck Condition Rating, Average Sojourn Time, (Years)								
	1	2	3	4	5	6	7	8	9
Type I				5.0	5.6	7.1	10.2	8.1	
Type II	3.0	2.0	2.2	3.9	4.6	5.2	6.2	2.9	
Type III				3.3	5.2	7.4	9.0	7.9	4.4
Type IV				2.0	3.7	4.1	4.7	3.9	
Type V			2.0	3.1	3.2	5.0	7.1	3.9	4.2
Type VI			3.3	4.0	4.2	5.8	7.8	2.3	
Type VII				6.3	5.1	7.5	10.1	11.0	6.3
Type VIII	1.0	4.0	3.3	4.8	6.2	7.3	9.0	6.6	
Type IX		7.0	1.7	4.0	5.8	7.5	17.1	9.4	5.9

Table 5.4. Iowa Substructure Condition Rating, Average Sojourn Time, (Years)

	Iowa Substructure Condition Rating, Average Sojourn Time, (Years)								
	1	2	3	4	5	6	7	8	9
Type I			1.0	3.7	5.3	8.3	11.0	10.8	
Type II	2.0	1.0	2.8	4.1	4.2	4.5	5.8	5.7	
Type III				1.0	4.4	7.4	8.9	10.1	7.9
Type IV				2.0	3.7	3.8	4.1	6.4	
Type V			1.0	2.6	3.8	5.9	7.7	7.3	5.3
Type VI		2.0	1.9	5.4	4.5	6.2	8.6	7.3	
Type VII			2.0	6.3	6.1	7.0	12.0	15.6	6.7
Type VIII		1.0	2.8	4.9	6.8	8.9	9.8	8.9	
Type IX			2.8	3.8	5.7	9.9	21.0	18.7	8.6

Table 5.5. Iowa Superstructure Condition Rating, Average Sojourn Time, (Years)

	Iowa Superstructure Condition Rating, Average Sojourn Time, (Years)								
	1	2	3	4	5	6	7	8	9
Type I		9.0	2.0	3.4	4.5	7.4	9.9	10.5	
Type II	1.8	2.5	3.0	3.7	4.0	4.7	5.4	5.9	
Type III			1.0	1.0	4.2	7.1	8.7	9.6	7.4
Type IV				2.0	5.7	4.3	3.4	2.9	
Type V			1.3	3.0	3.5	4.0	7.0	5.6	5.8
Type VI			6.2	4.0	3.7	4.9	7.8	8.4	
Type VII			1.0	6.0	13.6	8.8	13.7	15.5	9.5
Type VIII	1.0	4.0	3.7	4.9	6.8	8.3	9.0	9.0	
Type IX		3.0	3.6	4.0	7.5	13.0	19.8	21.9	8.5

Table 5.6. Wisconsin Deck Condition Rating, Average Sojourn Time, (Years)

	Wisconsin Deck Condition Rating, Average Sojourn Time, (Years)								
	1	2	3	4	5	6	7	8	9
Type I			1.3	3.6	4.3	5.1	5.9	5.7	
Type II		2.9	2.9	3.6	4.3	5.1	4.7	1.7	
Type III			2.0	2.2	3.8	4.9	5.1	4.0	1.9
Type IV			5.0	4.8	4.4	5.0	6.4	2.3	
Type V			4.3	4.5	3.7	5.7	5.6	5.7	2.2
Type VI	1.0	1.7	2.8	3.3	2.2	3.6	2.0	1.5	
Type VII			2.7	3.0	4.6	7.2	8.6	4.7	1.9
Type VIII		2.0	3.0	4.5	5.4	6.8	8.0	6.0	
Type IX		3.0	3.8	4.7	8.7	10.0	8.5	6.4	2.9

Table 5.7. Wisconsin Substructure Condition Rating, Average Sojourn Time, (Years)

	Wisconsin Substructure Condition Rating, Average Sojourn Time, (Years)								
	1	2	3	4	5	6	7	8	9
Type I			1.3	3.9	4.8	5.9	7.1	6.8	
Type II	1.0		2.4	2.8	4.9	5.8	4.2	2.2	
Type III			3.0	2.0	4.4	5.6	5.7	5.3	2.8
Type IV				2.7	5.6	5.9	5.4		
Type V			8.0	4.2	7.3	6.0	5.2	6.7	2.9
Type VI		2.6	3.1	3.4	2.1	4.1	1.7	1.9	
Type VII			1.0	4.8	8.2	8.9	9.6	7.5	7.0
Type VIII		1.7	3.2	3.5	5.7	7.9	9.4	7.7	
Type IX		4.1	4.5	5.1	7.3	13.5	15.6	12.9	3.9

Table 5.8. Wisconsin Superstructure Condition Rating, Average Sojourn Time, (Years)

	Iowa Deck Condition Rating, Average Sojourn Time, (Years)								
	1	2	3	4	5	6	7	8	9
Type I			1.3	3.4	4.9	5.6	6.5	7.3	
Type II	1.0	3.3	4.7	3.2	4.8	5.0	4.5	2.1	
Type III				3.3	4.6	5.6	5.0	5.3	2.3
Type IV			5.0	3.6	5.2	7.6	4.6	1.2	
Type V			5.0	4.1	3.4	5.1	6.6	6.9	3.0
Type VI		1.8	2.5	3.2	4.2	4.0	2.4	1.7	
Type VII			5.0	2.4	7.5	9.4	7.5	7.0	3.8
Type VIII		1.8	3.4	4.6	5.3	7.0	8.9	8.0	
Type IX		3.7	3.9	5.0	8.2	10.3	10.8	13.5	3.9

5.4.6 Transition Probabilities of Condition Ratings

The previous section explained the theory of calculating the probability of being at each condition rating at a given year, given that the transition probability of each individual transition path is known. This current section is focused on calculating the transition probability of each transition path of the tree diagram. The transition probability of each transition path can be represented as the relative frequency of the C_i value for each condition rating. Because, for a given condition rating, the C_i value represents the possible transition paths and the relative frequencies give the probability of taking each transition path and being at any condition rating at the next prediction time. For an example, $CR_{7\rightarrow 8@2016}$ represents the transition path of condition rating goes from $CR_{7@2014}$ to $CR_{8@2016}$ (See Figure 5.9(a)). However, it indirectly represents the C_i value (C_7 = +1) of the transition path with respect to the most recent inspection. Similarly, $CR_{7\rightarrow 5@2016}$ represents C_7 = -2. Since, these models predict condition rating being between 9 and 4, depending on the most recent condition rating, the C_i value could be anything between ±5. In the current example, the most recent condition rating is 7. Therefore C_7 value could be any value between -3 to +2.

The Sojourn Time Database can be used to find the possible C_i values for each condition rating. As mentioned in Section 5.4.4, the Sojourn Time Database of a bridge component consists of Age_i, CR_i, B_i, A_i and C_i. Therefore, the Sojourn Time Database can be filtered with respect to each CR_i and C_i to calculate the relative frequency of C_i of each condition rating, in other words, the probability of bridge component being at any condition rating in the future. As an example, the Sojourn Time Database of the Iowa bridge decks were filtered with respect to each CR_i and C_i to calculate the relative frequency of C_i of each condition rating as shown in Figure 5.17.

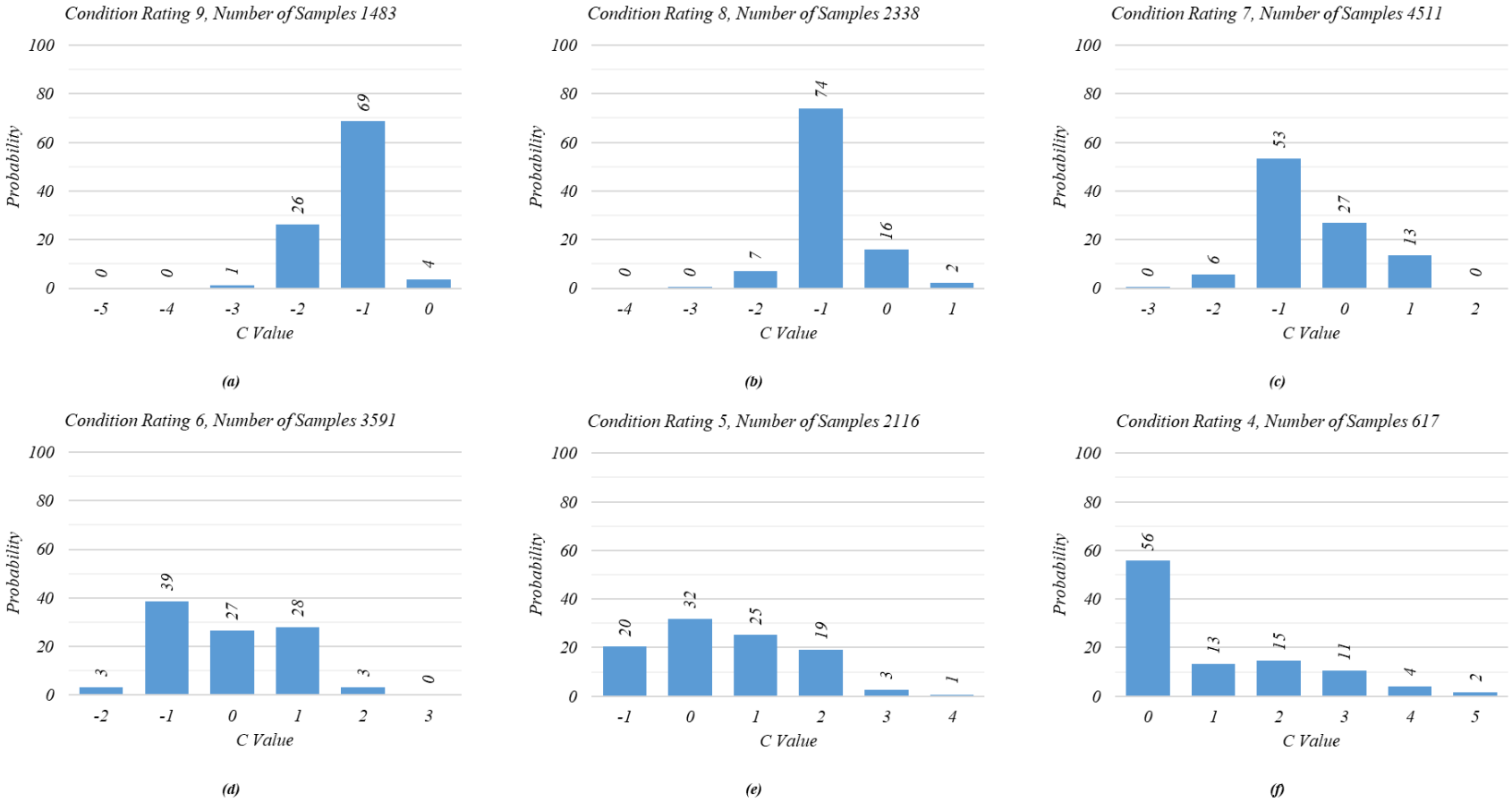

Figure 5.17. Relative Frequency Histogram of C Value for Iowa Bridge Decks

5.4.7 Sample Size

According to Figure 5.17, each probability histogram is based on a different number of samples. In some situations, these sample sizes could be significantly small, raising a question on required minimum sample size to calculate the transition probability. Since the transition probability histograms do not follow any standard statistical distribution, a normal distribution for transition probability histograms was assumed such that a baseline for minimum sample size could be established. To obtain an estimate with $100(1-\alpha)\%$ confident level for mean of a normally distributed population, the required minimum sample size is given in Equation 24. The σ^2 is population variance and E is half width of the confident interval.

$$\boldsymbol{n = \frac{\left(z_{\alpha/2}\right)^2 \sigma^2}{E^2}} \quad \text{.... (24)}$$

Since the population variance is unknown, Equation 25 was used to calculate the reasonable estimate to the population variance. The condition rating changes between six condition ratings, the range can be express as the number of condition ratings minus one.

$$\boldsymbol{\hat{\sigma} = \frac{Range}{4} = \frac{Number\ of\ Condition\ Ratings - 1}{4}} \quad \text{.... (25)}$$

The error E was assumed as 1, implying that the possible error between condition ratings as 1. The minimum required samples were calculated as seven. To be conservative, the minimum required sample size was set as 15 samples.

5.4.8 Filtering Methods

As discussed in Section 5.4.6, the transition probabilities of each transition path can be simply calculated by filtering the Sojourn Time Database with respect to each CR_i and C_i. Even though these probabilities represent an overall idea about future condition rating transitions, it does not entirely represent the effects of historical events occurred in the bridge. To consider the effects of historical events that occurred in the bridge, the Sojourn Time Database can be filtered in many different ways. Future condition rating of a bridge component primarily depends on four factors, namely, (1). Most recent condition rating, (2). Age at most recent condition rating Age_i, (3). Most recent B_i value and (4). Most recent A_i value (Sojourn Time) of the bridge. The most recent condition rating is important because it represents the most recent condition of the bridge component. The age of the bridge component at the most recent condition rating is related to where in the deterioration process the bridge might be. For example, an older bridge component has higher probability of transitioning to a lower condition rating than a new bridge component. Most recent B_i value reflects the most recent deterioration or maintenance activity of the bridge component. As an example, a most recent B_i value of +3 suggests that there was a major maintenance recently. Depending upon the most recent A_i value, the condition rating of the bridge component could go up, down or stay at the same. Further, the longer the A_i value the higher the probability of condition rating transition. To accommodate the effects of historical events occurred in the bridge and to study the effects of the different parameters on the future condition rating, the research group came up with five different filtering methods, and named as Method I to Method V. The filtering methods were applied to both CPM and DPMs.

A sample condition rating history of a bridge (Figure 5.18) can be used to explain each filtering method. Figure 5.18 shows a condition rating history of a bridge deck in Iowa. The objective in this example is to illustrate the five different filtering methods to calculate the probability of the bridge deck being at any condition rating in 2016 (form $CR_{9@2016}$ to $CR_{4@2016}$). The all possible transition paths are shown as dotted arrow lines.

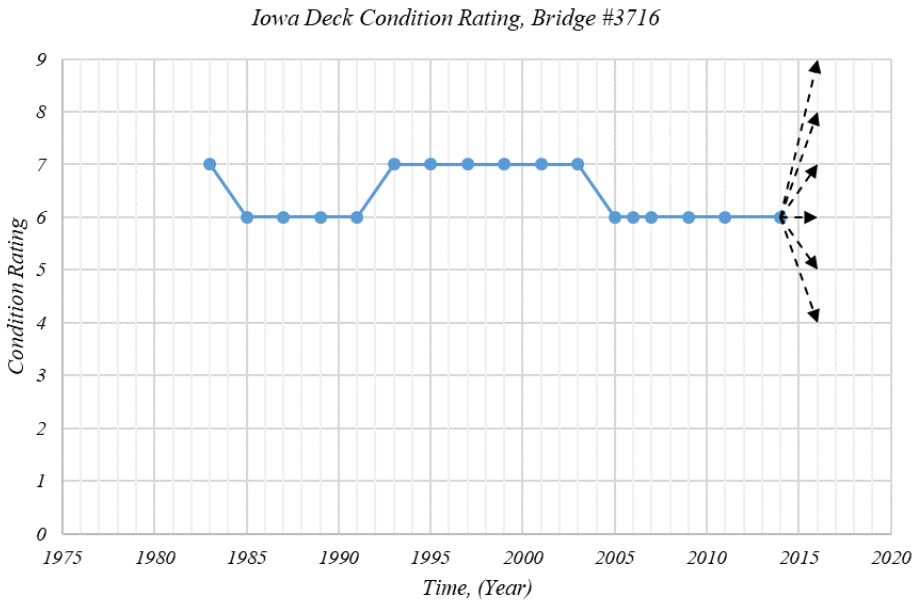

Figure 5.18. Sample Condition Rating Condition Rating History

As mentioned in Section 5.4.6, the probability of the bridge being at any condition rating in 2016 can be simply calculated by filtering the Sojourn Time Database by CR_i and C_i alone. The probability histogram calculated that way is represented in Figure 5.19(a). The probability calculation could be refined based on the age of the bridge deck. The age at the current condition ration ($CR_{6@2014}$) of this bridge deck is 48 years. Therefore, Sojourn Time Database can be filtered based on the age. Filtering Sojourn Time Database by the exact age might give a small amount of numbers of samples. Therefore, the Sojourn Time Database was

filtered in 5 and 15 year age groups. Figure 5.19(b) shows filtering Method II, which considers the large age groups (15 year age groups) and Figure 5.19(c) shows filtering Method III, which considers the small age groups (5 year age groups). Data filtering Method IV was developed to include the effects of Sojourn Time, A_i, and most recent B_i of the bridge deck (Figure 5.19(d)). Data filtering Method V consists of the effects of Sojourn Time, A_i, most recent B_i and Age_i (five-year groups) of the bridge deck (Figure 5.19(e))

Filtering Method I only depends on the CR_i and C_i values. Therefore, transition probability histogram of a given condition rating is constant for the same bridge component. Similarly, the filtering Method II and Method III depend on the CR_i and C_i and Age_i values. Therefore, transition probability histogram of a given condition rating is constant at given age group is constant for the same bridge component. However, the probability values of Method IV and IV is unique at each and every transition path. According to Figure 5.19, different filtering method gives somewhat different probability values. An important thing to notice is that the Number of Samples from Method I to Method V significantly decreases. In some situations, there may not be enough samples (15 samples) to calculate the transition probabilities. In such situations, the transition probabilities were calculated based on the base filtering method, Method I. The accuracy of each filtering method was quantitatively and qualitatively studied in the next sections.

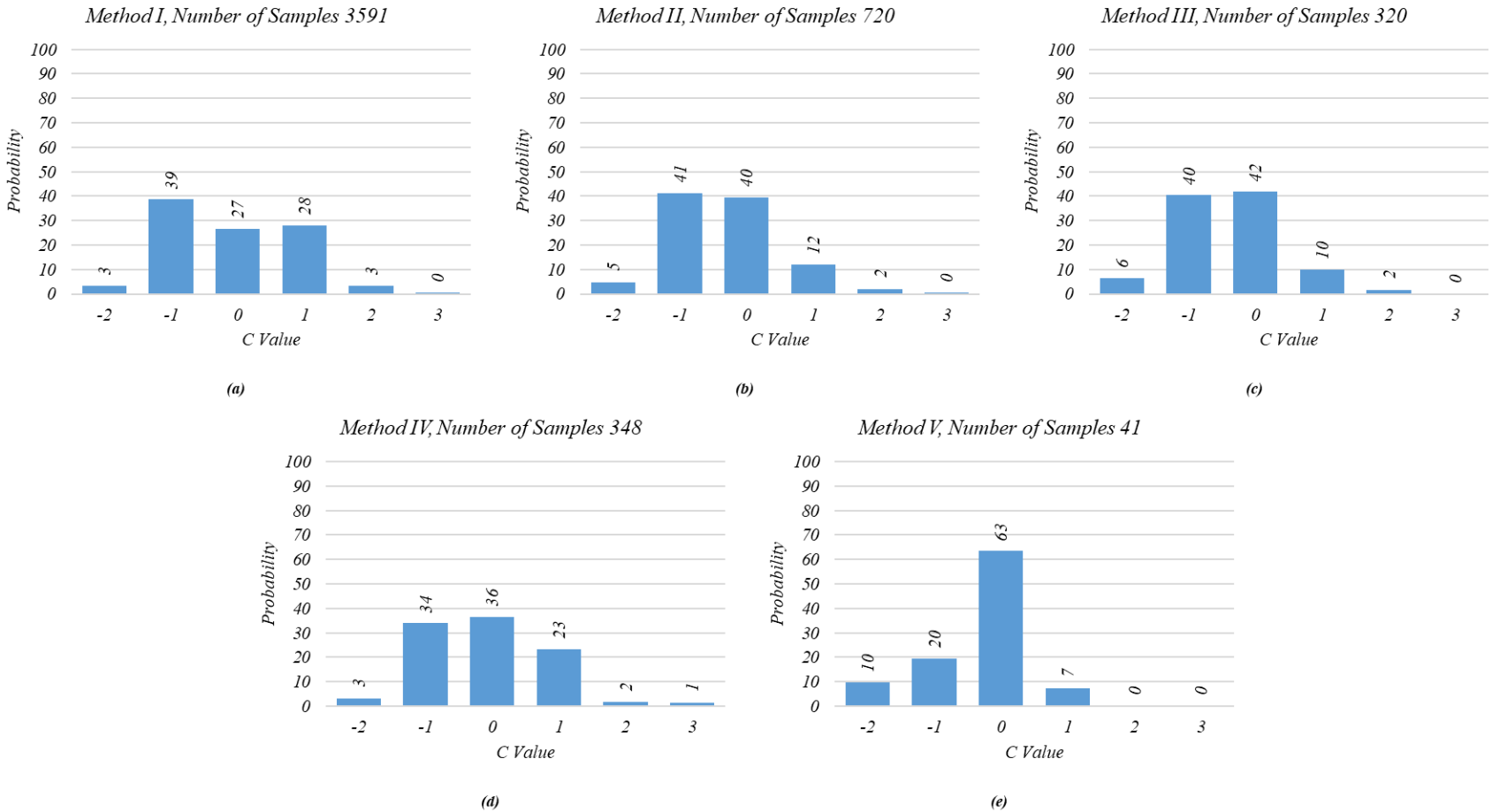

Figure 5.19. Different Filtering Methods

5.5. Validation of Current Practice Model (CPM)

The previous sections illustrate the methodology of developing the Current Practice Model (CPM) and different methods to filter the Sojourn Time Database to calculate the probability of a bridge component being at each condition rating at a given year. This section further describes the representation of CPM, validation of CPM and sample quantitative and qualitative results of CPM validation.

5.5.1 Overview of CPM Predictions

The condition rating history of the bridge deck used in Section 5.4.8 will be used here to explain CPM visual representation. CPM Method I will be shown for easy explanation. However, the same procedure can be applied to all methods. The methodology explained in the Section 5.4 was used to estimate the probability of the bridge deck being at any condition rating in years 2016, 2018 and 2020. The probability histograms obtained using Method I are shown in Figure 5.20(a). The dotted line shown in Figure 5.20(a) represents the line passing through the centroid of each probability histogram, which is a statistical estimate of the most possible future condition rating path of the bridge deck. The most possible condition ratings are not integer numbers like in the NBI condition rating scale. However, the statistical values can be used to understand the future trend of bridge condition, such that it can be used to develop bridge management and maintenance schedules. The predicted and most possible future condition rating path along with historical condition rating data of the bridge deck is shown in Figure 5.20(b).

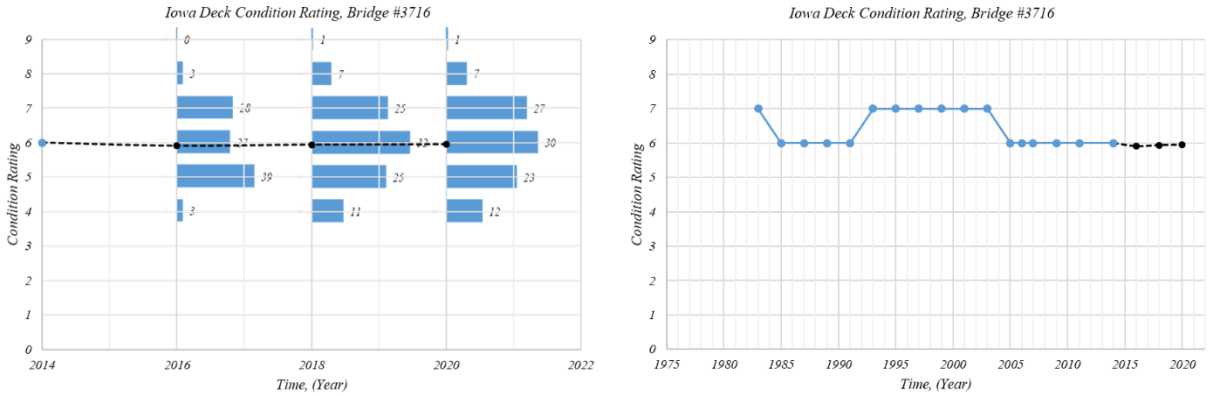

Figure 5.20. Representation of CPM Method I for Iowa Bridge Deck

5.5.2 Hindcasting of CPM

All five different CPMs were quantitatively and qualitatively studied to increase the confidence of using CPMs and to identify the best filtering method. Also, the results are useful in identifying the most important parameters affecting future condition ratings. For the purpose of CPM evaluation, the sub set of condition rating histories were selected from each condition rating database. Each subset of condition rating histories consisted of at least 15 inspections and 30 years of condition rating history. Later, each CPM method was used to hindcast the condition rating. The hindcasting was performed from the middle of the actual condition rating history. Each CPM predication length is 16 years. Figure 5.21 shows the same condition rating history used in previous examples. The dotted line shows the condition rating prediction results of CPM Method I. Both actual condition rating history and prediction results were visually compared to qualitatively evaluate the model. According to Figure 5.21, the prediction and historical condition rating data are in somewhat good agreement.

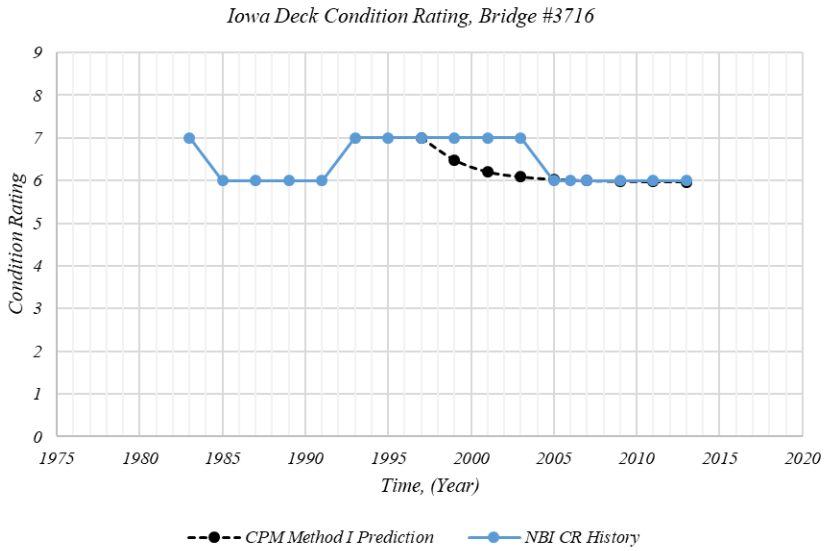

Figure 5.21. CPM Validation Example

According to Figure 5.21, the prediction starts from 1997, the middle of the actual condition rating history of the bridge. The historical condition ratings from 1997 and the predicted condition ratings were used to calculate the Mean Squared Error (Equation 26), such that the models can be quantitatively evaluated. The MSE value between ±1 indicates very good condition rating prediction.

$$\text{Mean Squard Error} = \frac{\sum\left(\text{CR}_{\text{i,Predicted}} - \text{CR}_{\text{i,Actual}}\right)^2}{\text{Number of Inspections}} \quad \ldots. (26)$$

Twenty bridges from the subset of condition rating histories were randomly selected to present the results. The average MSE value of each condition rating database is calculated and tabulated in Table 5.9 and Table 5.10. According to Table 5.9 and Table 5.10, the CPM Method IV shows the lowest MSE value, probably because the Method IV accommodates Sojourn Time, A_i and B_i values. Method V shows the second lowest MSE value. Even though Method V includes the filtering parameters of Method IV, plus Age_i, Method V shows the second

lowest MSE value. This is probably due to not having enough samples to accurately calculate the probability histogram, such that it may occasionally referring to the CPM Method I. In addition to that filtering a bridge with respect to the age does not significantly affect the MSE value, probably because with the maintenance activities throughout the life of the bridge span could alternate the representation of the actual aging process of the bridge.

Table 5.9. CPM validation Results for Iowa Condition Rating Data

Data Filtering Method	*Iowa Condition Rating Data, CPM*		
	Deck	*Substructure*	*Superstructure*
I	*0.82*	*0.72*	*1.19*
II	*0.84*	*0.80*	*1.24*
III	*0.83*	*0.85*	*1.21*
IV	*0.78*	*0.59*	*0.87*
V	*0.74*	*0.62*	*0.89*

Table 5.10. CPM validation Results for Wisconsin Condition Rating Data

Data Filtering Method	*Wisconsin Condition Rating Data, CPM*		
	Deck	*Substructure*	*Superstructure*
I	*0.78*	*0.75*	*1.09*
II	*0.84*	*0.54*	*0.97*
III	*0.84*	*0.58*	*0.93*
IV	*0.81*	*0.75*	*1.20*
V	*0.78*	*0.67*	*0.89*

The CPM validation results for randomly selected six condition ratings for each bridge component for both Iowa and Wisconsin condition rating databases are shown in Figure 5.22 to Figure 5.27 for the purpose of qualitative evaluation.

5.5.3 Example Validations of CPM

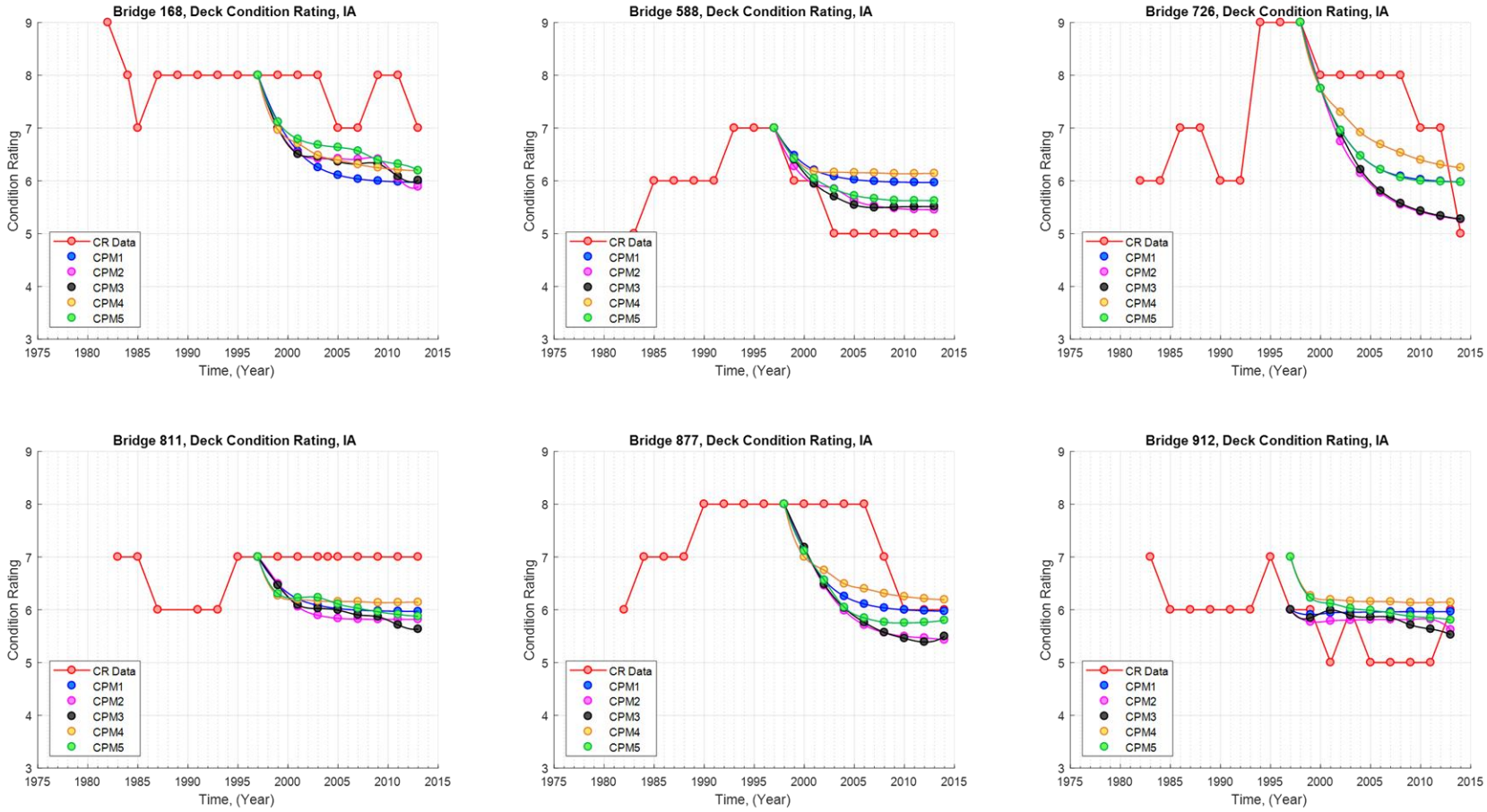

Figure 5.22. CPM validation Results for Iowa Deck Condition Rating Data

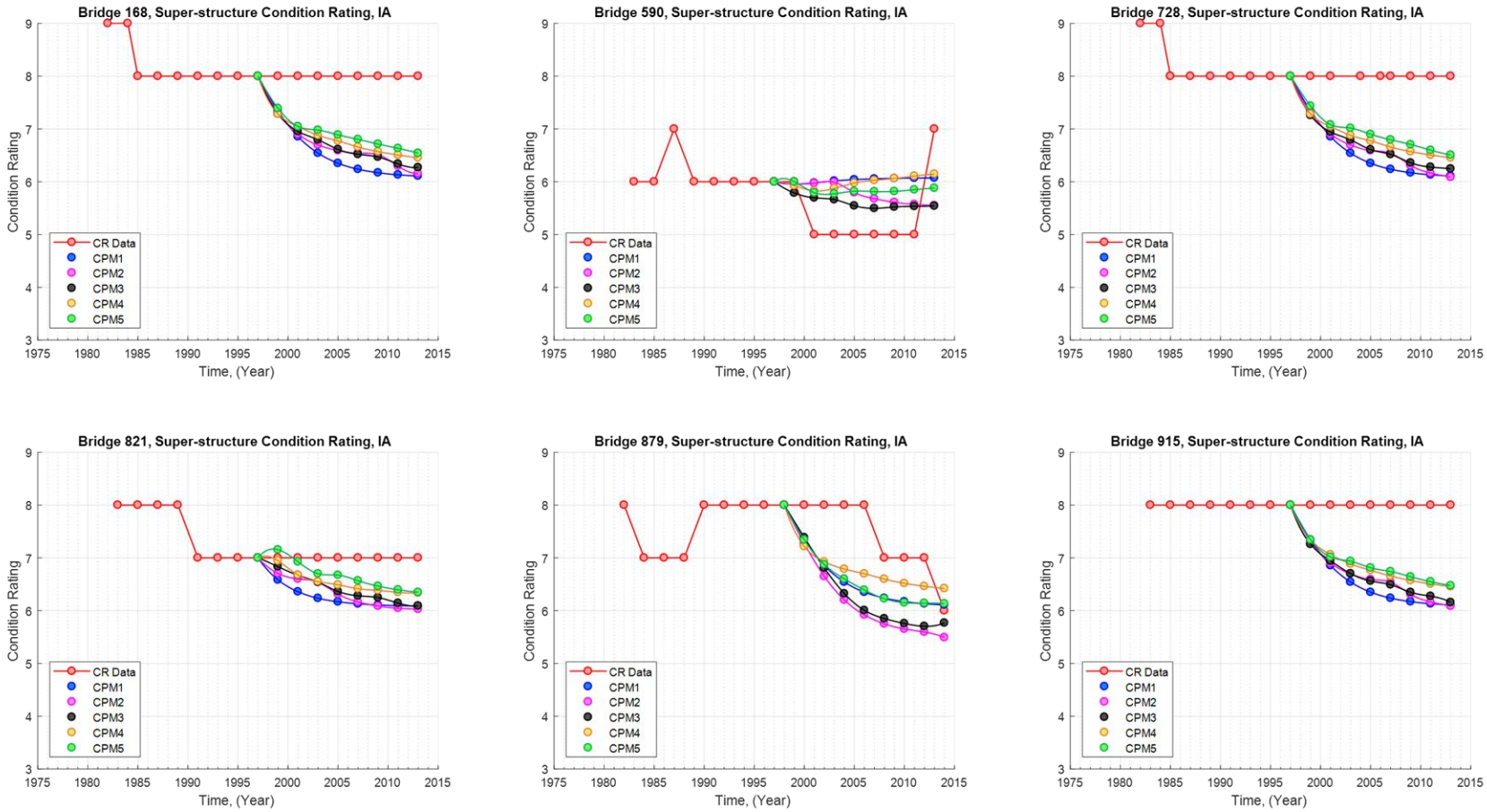

Figure 5.23. CPM validation Results for Iowa Superstructure Condition Rating Data

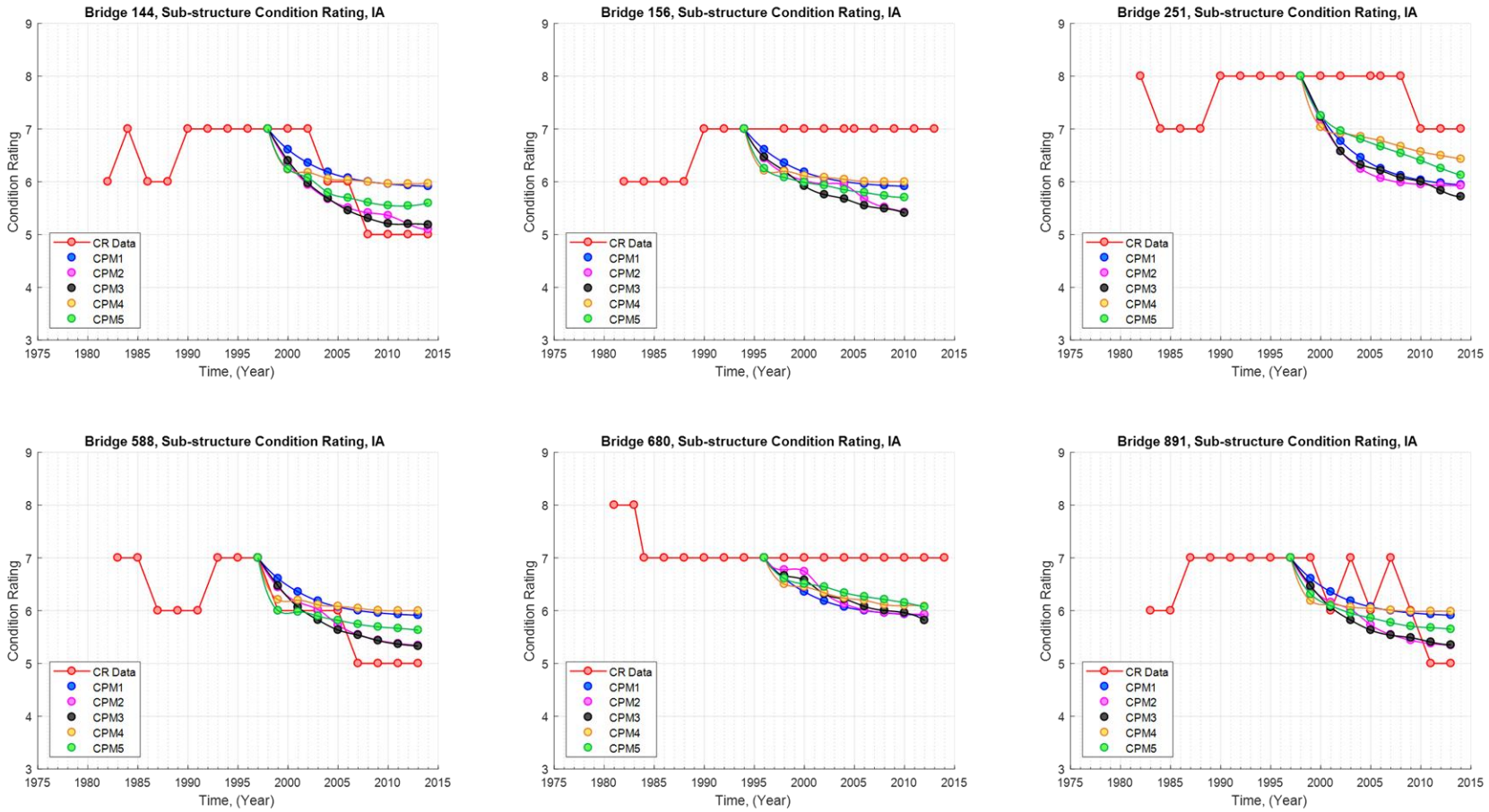

Figure 5.24. CPM validation Results for Iowa Substructure Condition Rating Data

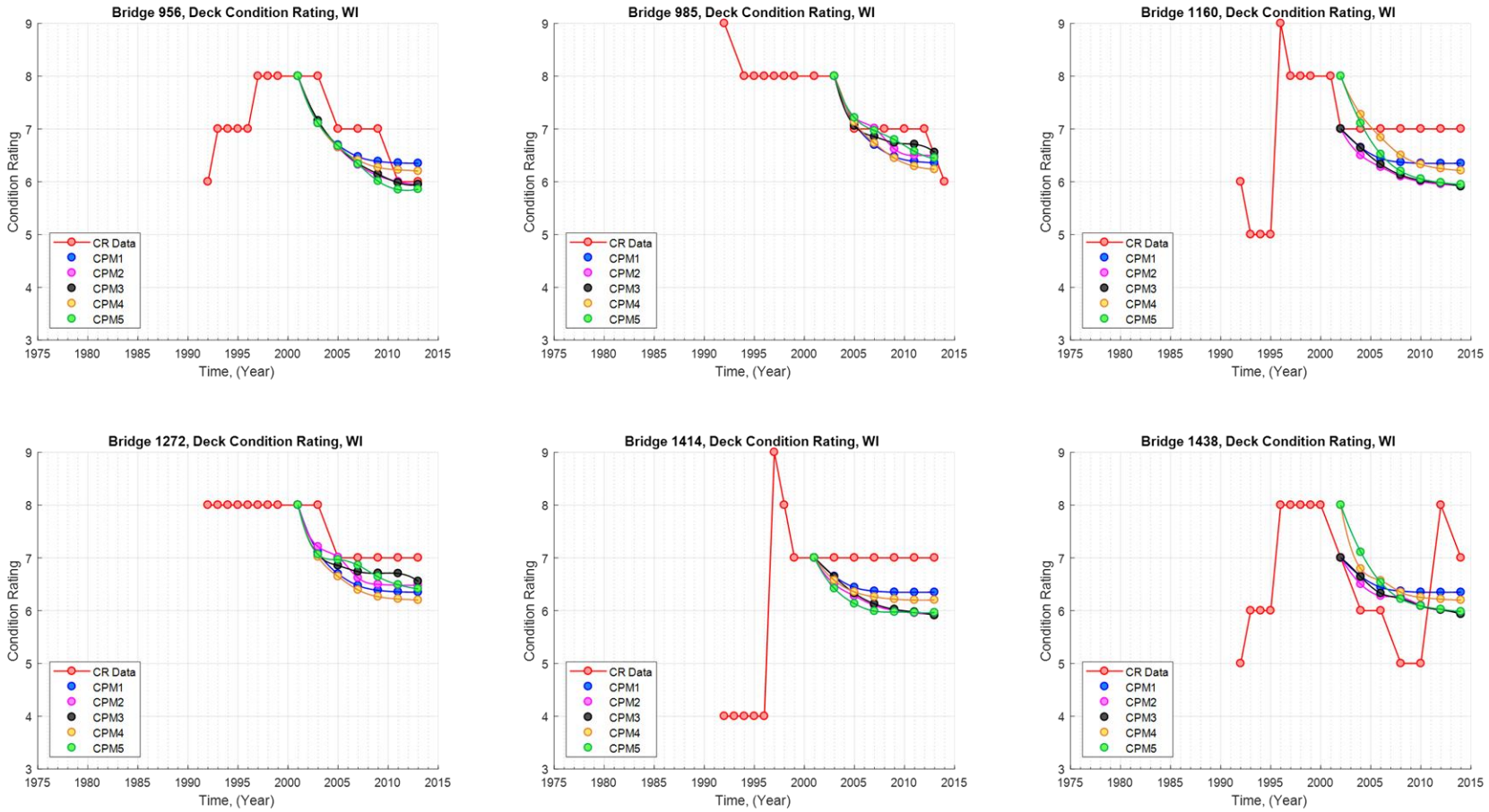

Figure 5.25. CPM validation Results for Wisconsin Deck Condition Rating Data

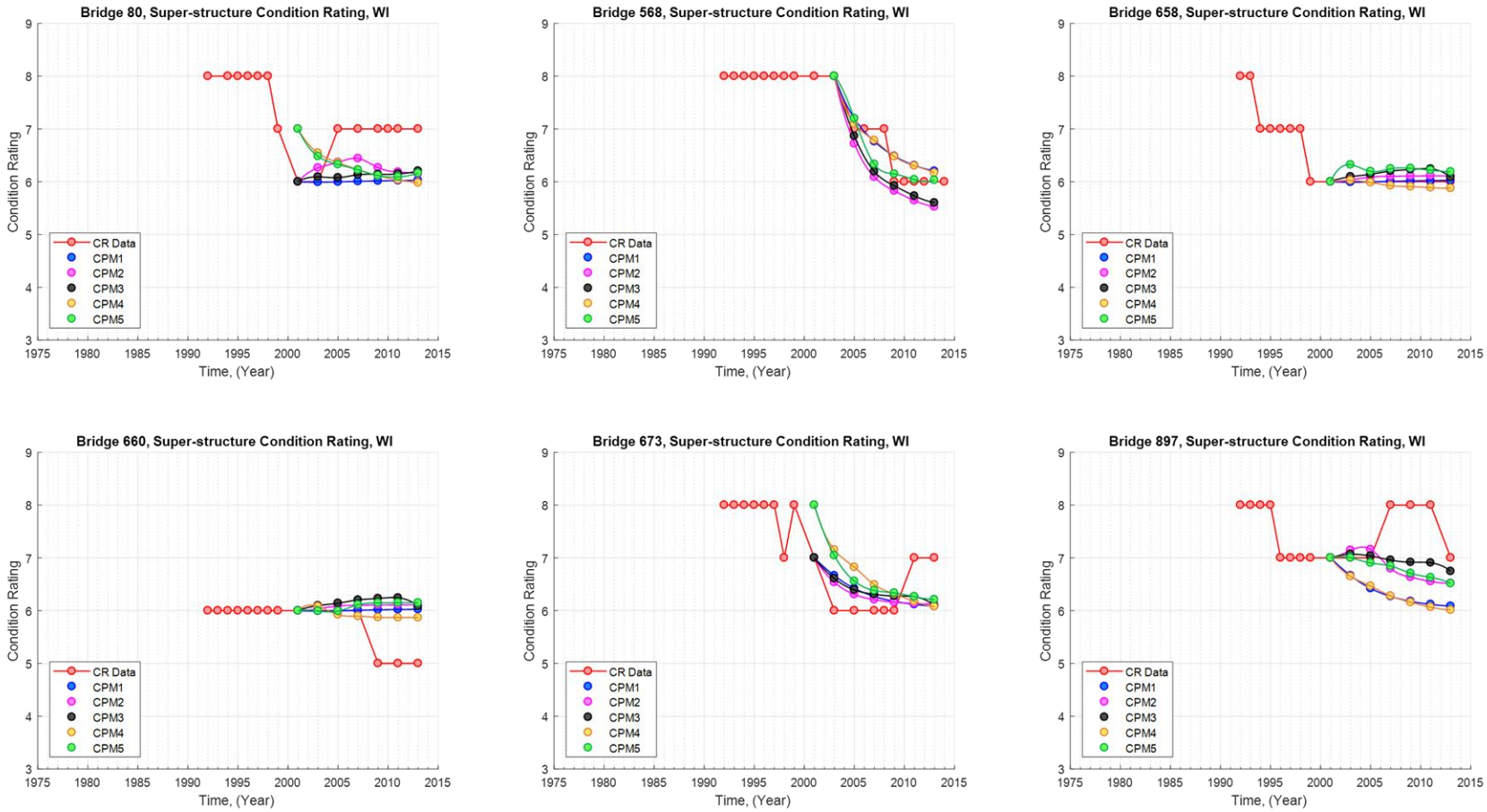

Figure 5.26. CPM validation Results for Wisconsin Superstructure Condition Rating Data

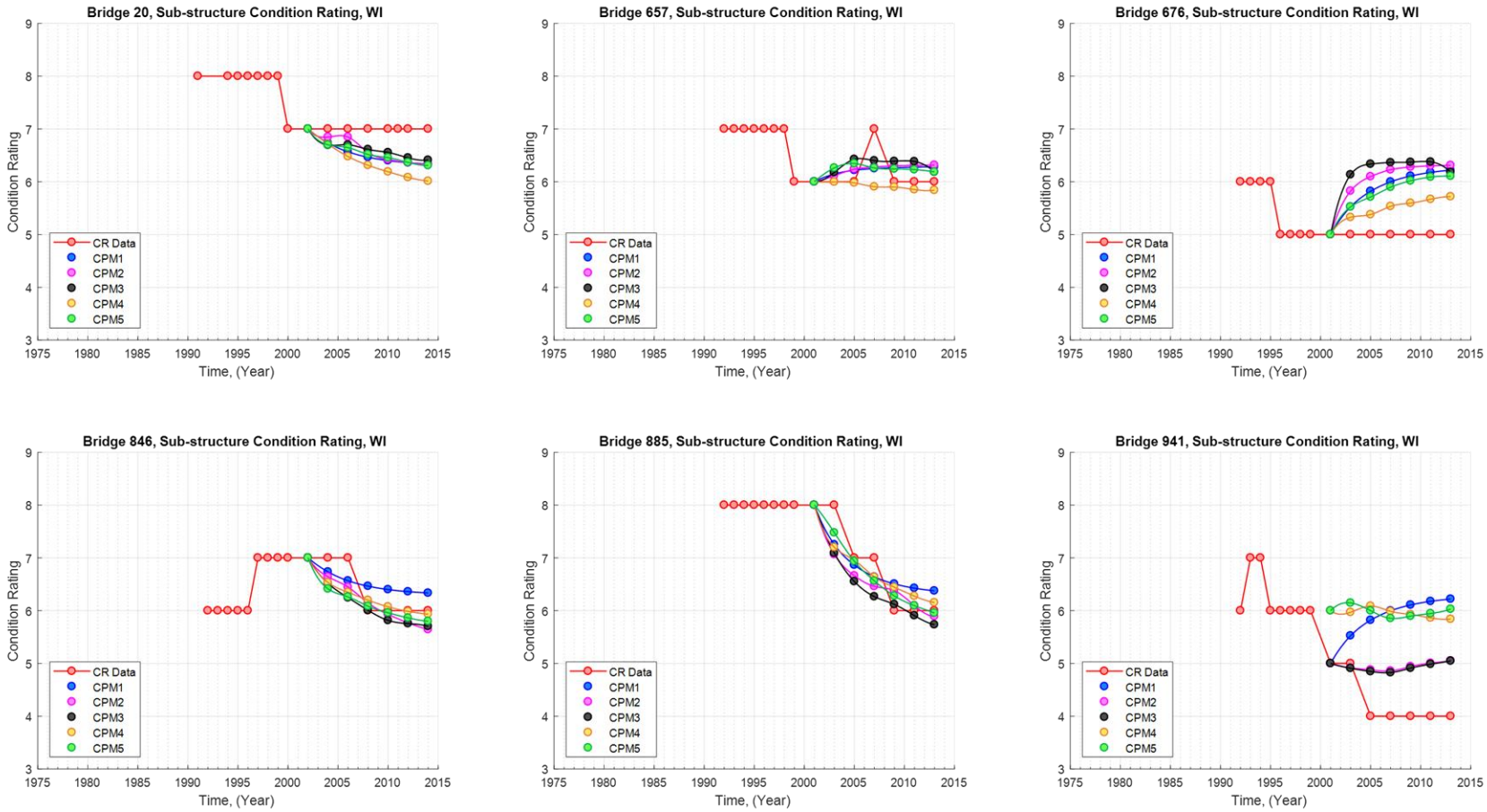

Figure 5.27. CPM validation Results for Wisconsin Substructure Condition Rating Data

5.6. Validation of Deterioration Prediction Model (DPM)

As discussed in Section 5.4, the methodology for developing CPM and Deterioration Prediction Model (DPM) are almost same, but DPM does not consider the effects of maintenance practices. The evaluation of DMP is also similar and the current section describes the visual representation of DPM, DPM validation and sample quantitative, and qualitative DPM evaluation results.

5.6.1 Overview of DPM Prediction

The visual representation of DPM is explained using the same condition rating history used in the previous section. Similar to the previous section, DPM representation is explained with data filtering Method I. The probability histograms obtained using data filtering Method I for years 2016, 2018 and 2020 is shown in Figure 5.28(a). The dotted line shown in Figure 5.28(a) represents the line passes through the centroid of the probability histogram, illustrating the statistical future path of the bridge deck without any maintenance activities. Compared to Figure 5.20(a), Figure 5.28(a) shows the probability of bridge deck being below the current condition rating, $CR_{6@2014}$. Because, DPMs do not consider the condition rating increase with time. The predicted most possible path along with the historical condition rating data of the bridge deck is shown in Figure 5.28(b).

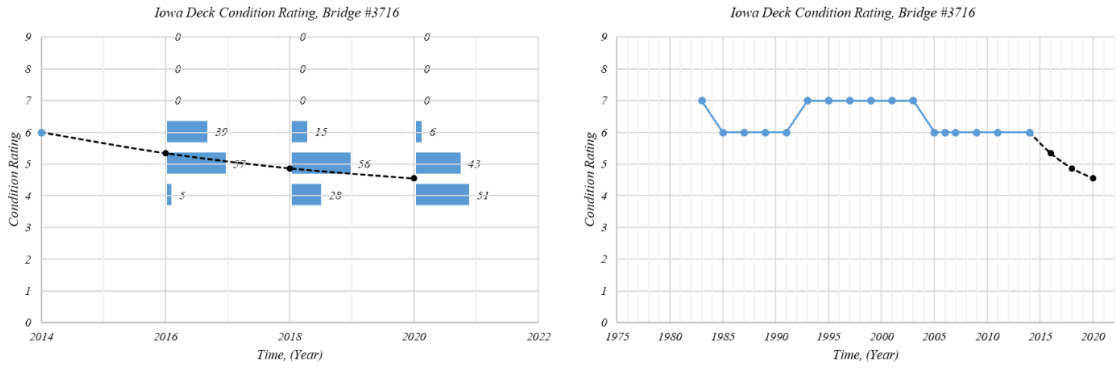

Figure 5.28. Representation of DMP Method I for Iowa Bridge Deck

5.6.2 Hindcasting of DPM

Five different DPMs were quantitatively and qualitatively evaluated to increase the confidence of using the DPM to predict the future bridge condition ratings. For the purpose of validation, a subset of bridge condition rating histories with at least 10 inspections and 20 years of history were selected from each condition rating databases. Each subset of bridge condition rating histories did not contain any condition rating "increasing" events. DPMs were used to predict the probability of condition ratings from the middle of the actual condition rating history of the bridge (Figure 5.29). The prediction length was 16 years. Figure 5.29 shows the example condition rating history and the dotted line shows the condition rating prediction of DPM Method I. Both actual condition rating history and prediction results were visually compared to qualitatively validate the model. Similar to CPMs, the MSE (Equation 26) values were used to quantitatively validate the DPMs.

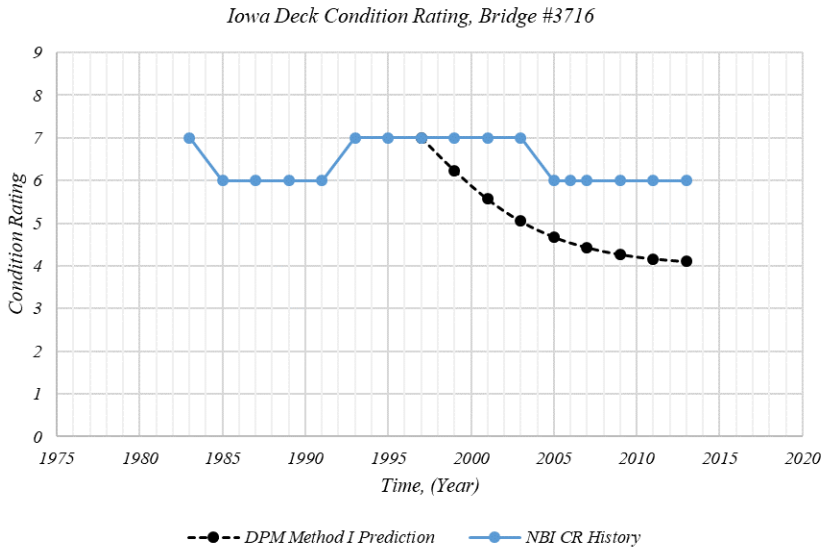

Figure 5.29. DPM Validation Example

Twenty bridges from each condition rating history sub set were randomly selected to present the results here. The average MSE value of each condition rating database was

calculated and is tabulated in Table 5.11 and Table 5.12. According to Table 5.11 and Table 5.12, DPM Method IV shows the lowest MSE value and DPM Method V shows the second lowest MSE value, and the results are consistent with CPM results. This also implies the importance of the use of A_i and B_i values of predicting the future condition rating of a bridge.

Table 5.11. DPM validation Results for Iowa Condition Rating Data

Data Filtering Method	***Iowa Condition Rating Data, DPM***		
	Deck	***Substructure***	***Superstructure***
I	*2.78*	*2.87*	*3.42*
II	*3.16*	*3.59*	*4.20*
III	*3.27*	*3.21*	*4.45*
IV	*2.04*	*1.65*	*2.39*
V	*2.22*	*1.98*	*2.88*

Table 5.12. DPM validation Results for Wisconsin Condition Rating Data

Data Filtering Method	***Wisconsin Condition Rating Data, DPM***		
	Deck	***Substructure***	***Superstructure***
I	*1.09*	*1.40*	*1.47*
II	*1.12*	*1.40*	*1.44*
III	*0.95*	*1.26*	*1.28*
IV	*0.73*	*0.93*	*0.96*
V	*0.86*	*0.95*	*0.88*

The DMP evaluation results for randomly selected six condition ratings for each bridge component history for both Iowa and Wisconsin condition rating databases are shown in Figure 5.30 to Figure 5.35, for the purpose of qualitative validation of DPM models.

5.6.3 Example Validations of CPM

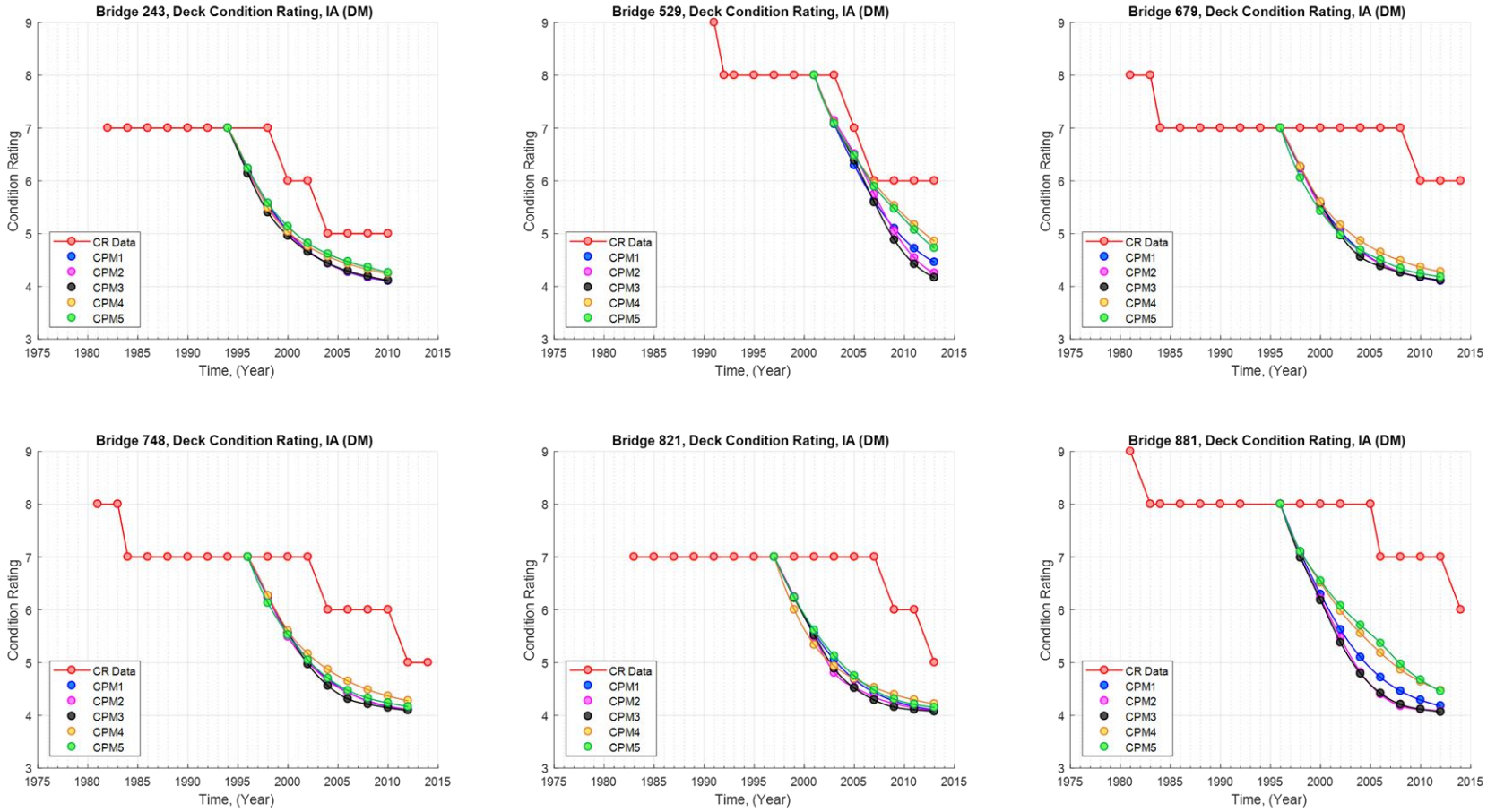

Figure 5.30. DPM validation Results for Iowa Deck Condition Rating Data

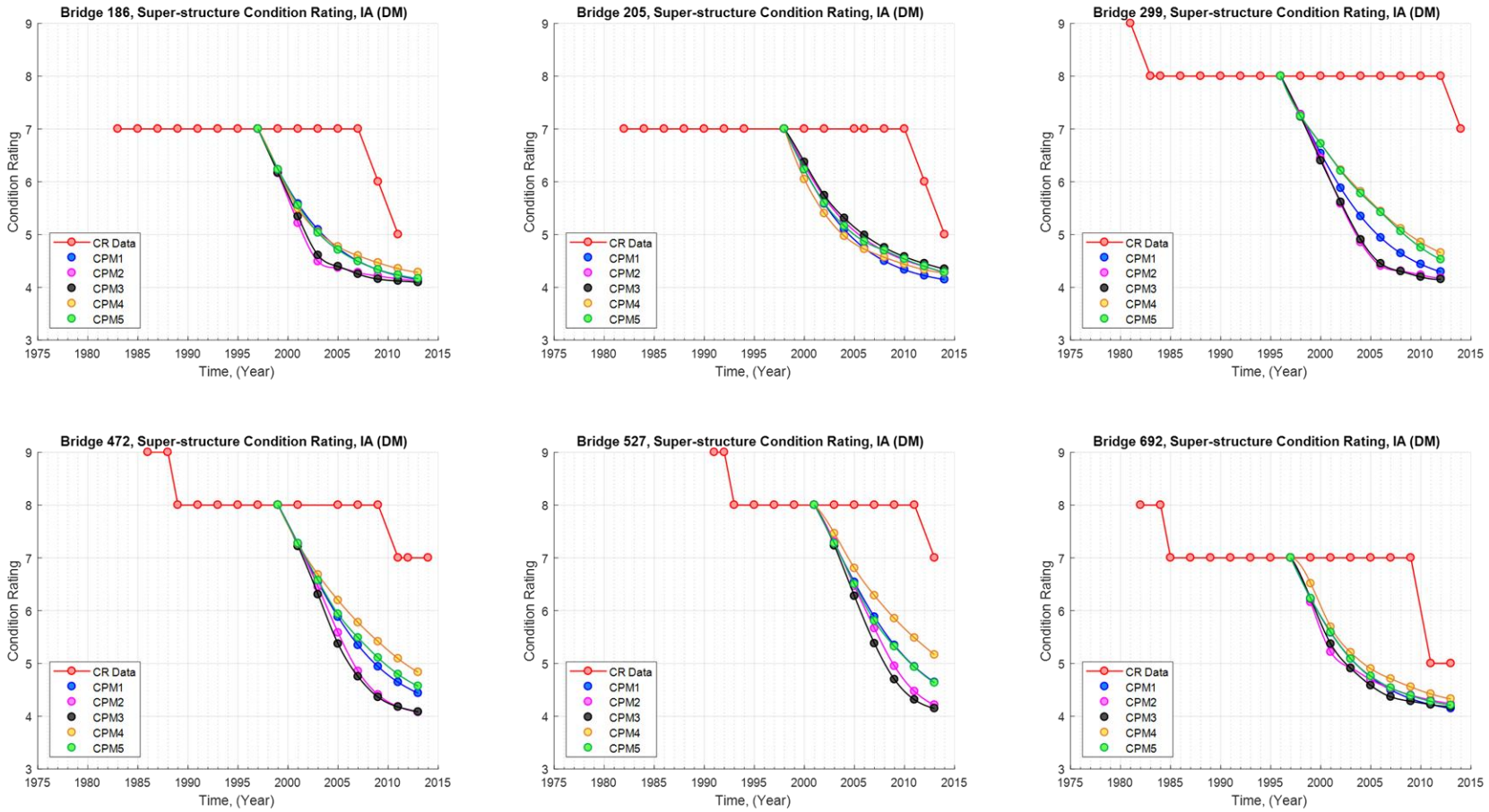

Figure 5.31. DPM validation Results for Iowa Superstructure Condition Rating Data

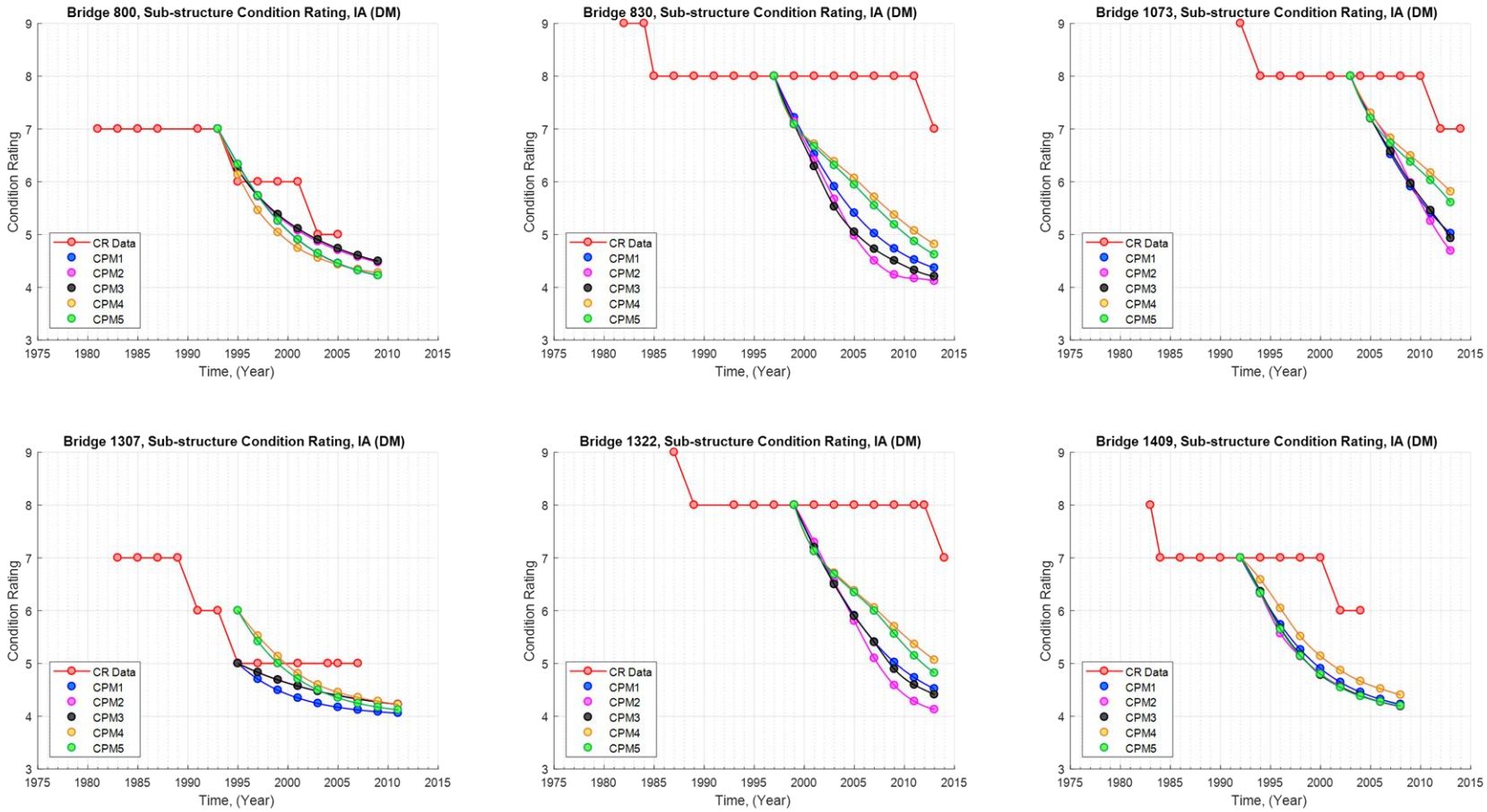

Figure 5.32. DPM validation Results for Iowa Substructure Condition Rating Data

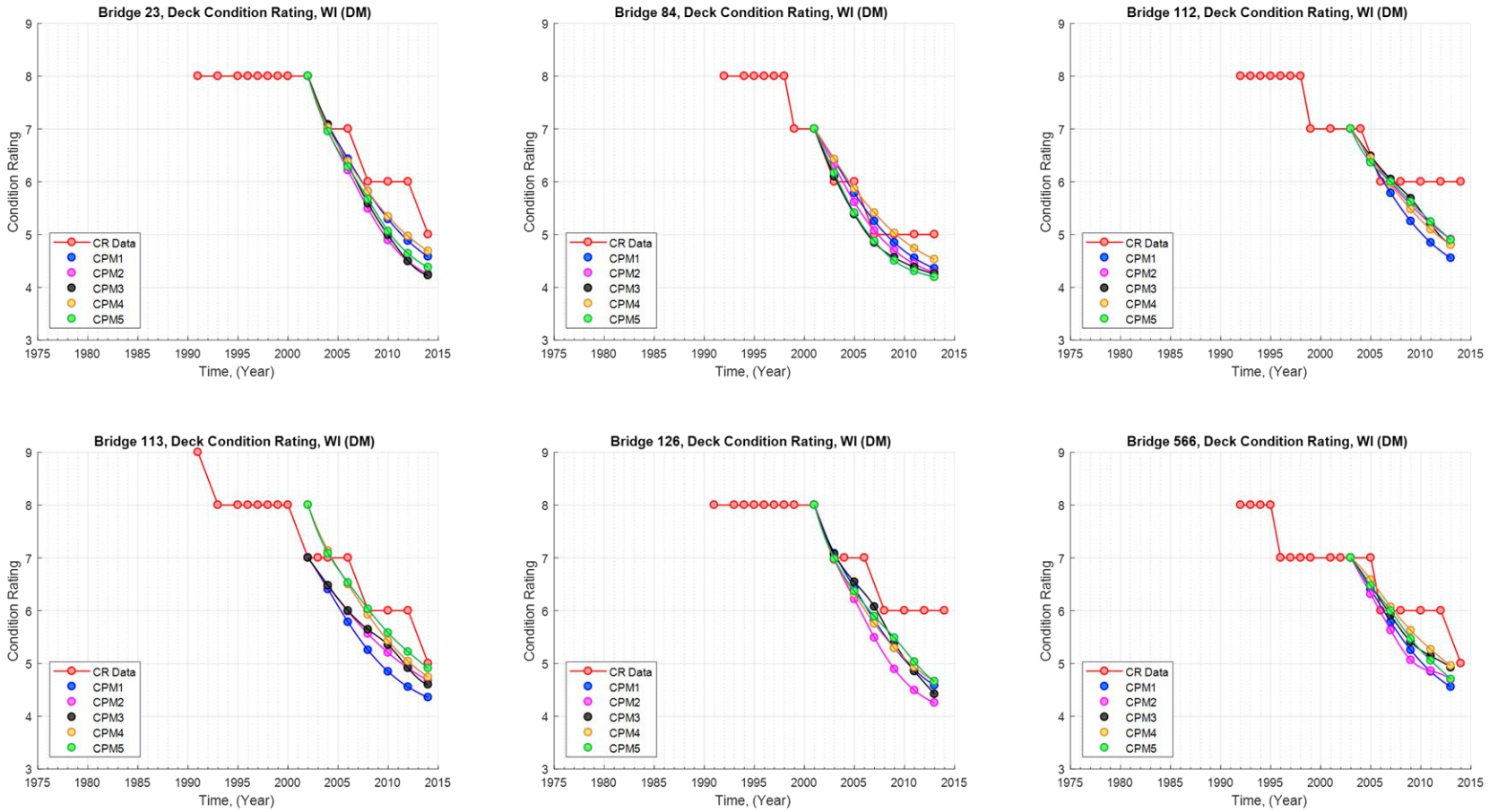

Figure 5.33. DPM validation Results for Wisconsin Deck Condition Rating Data

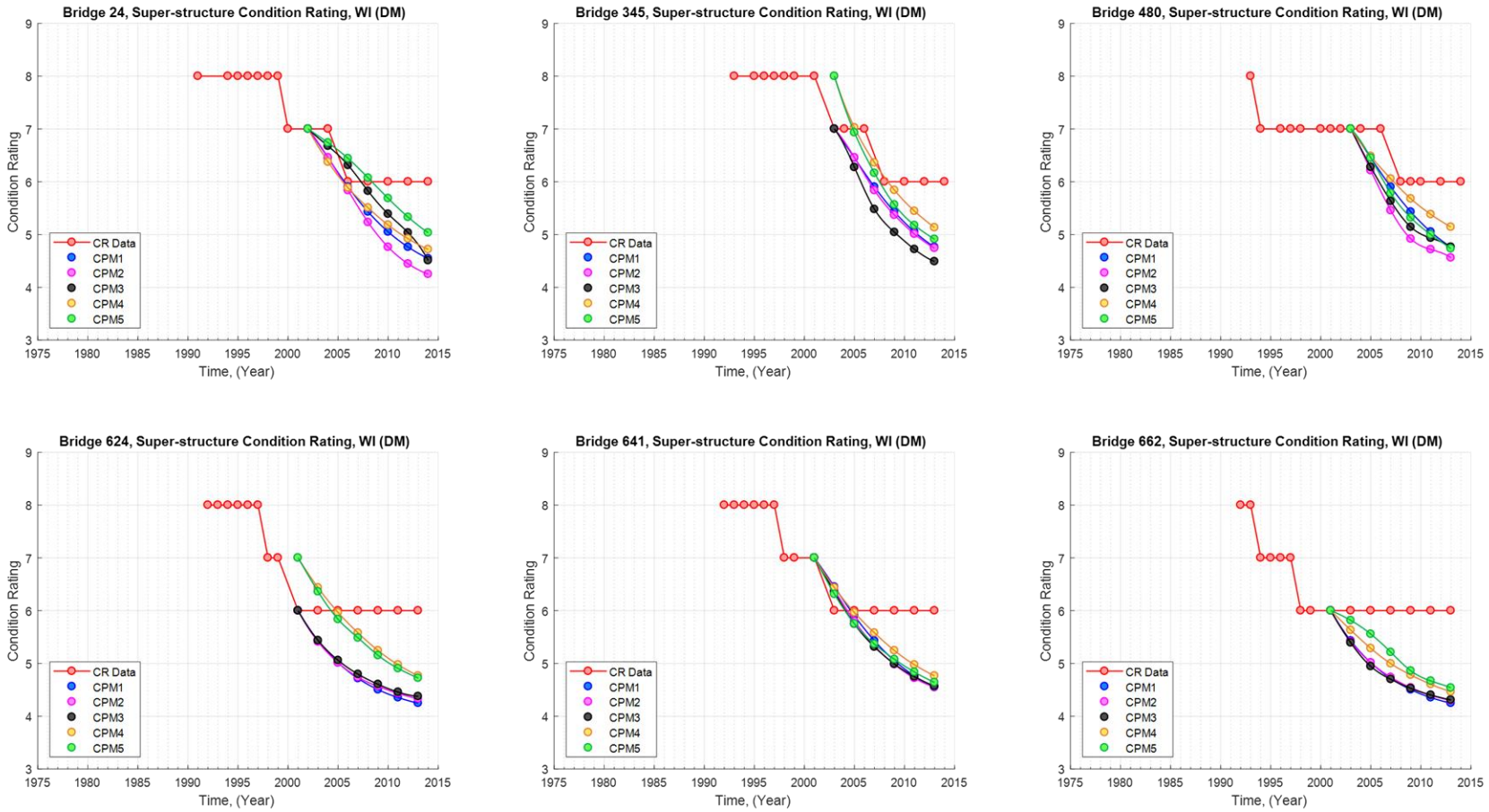

Figure 5.34. DPM validation Results for Wisconsin Superstructure Condition Rating Data

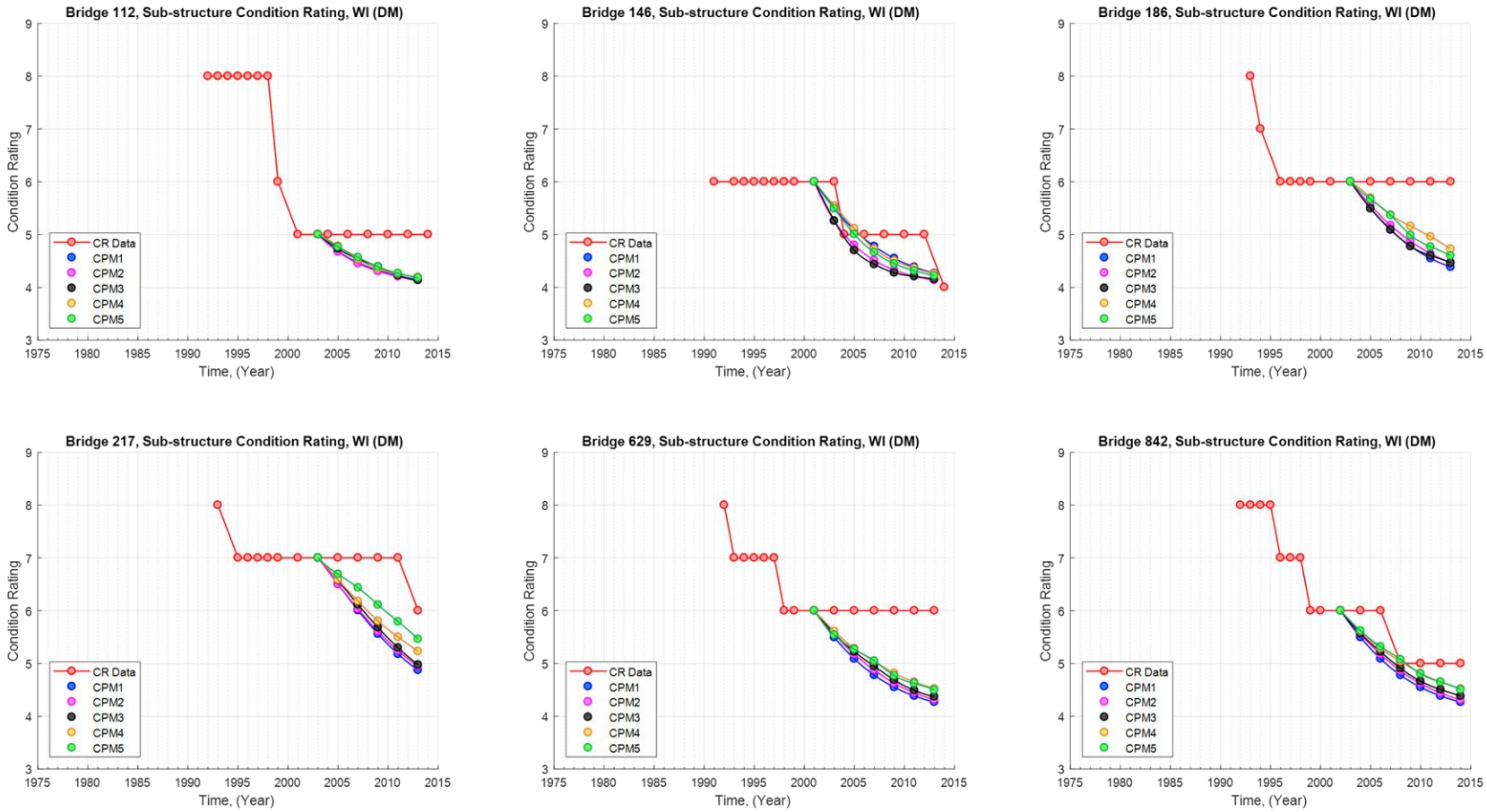

Figure 5.35. DPM validation Results for Wisconsin Substructure Condition Rating Data

CHAPTER 6. SUMMARY AND CONCLUSION

6.1. Summary

6.1.1 Structural Health Monitoring (SHM) Framework

The overview of the SHM framework developed by the Iowa State University Bridge Engineering Center was introduced. The basic components of the SHM framework was illustrated. Damage detection and load rating of the SHM framework is dependent upon a truck detection process. A detailed description of the SHM framework related to truck detection, damage detection, and load rating can be found elsewhere. The damage detection is based on identifying changes in strain responses of the bridge. The load rating calculation process depends on the strain responses of the bridge from single truck events and nominal bridge properties.

6.1.2 Improved Load Rating Factor of SHM Framework

The load rating factor is a measurement DOTs use to describe the load carrying capacity of a bridge, issue permits to heavy trucks, and to determine load postings on bridges. It helps to increase safety by reducing the risk of structural damage and collapse. According to the American Association of State Highway Transportation Officials (AASHTO) Manual of Bridge Evaluation, the rating factor of a bridge can be calculated in two ways, (1) non-destructive load rating method and (2) analytical load rating method. The non-destructive load rating method represent a realistic value for a bridge under existing conditions because it involves load tests on bridges in the field. However, the load tests typically require traffic closures. The Iowa State University (ISU) Bridge Engineering Center (BEC) has developed a method to improve non-destructive load rating method using continuous Structural Health Monitoring (SHM) data coming from an actual bridge site that does not require traffic

disruptions. In the current load rating factor calculation approach, the BEC calculates the live load moments and dead load moments using health monitoring data. However, the M_n is based on the nominal section dimensions and material properties of the bridge and may not represent the actual capacity of the bridge or its elements. The objective of the present research study is to further improve the rating factor calculation process by estimating an improved flexural strength for composite sections. The research group suspected that there is a relationship between moment of inertia and flexural strength of composite sections. The idea, then, is to use the I_{FEM} coming from current load rating process to get an improved estimate of the flexural strength.

To validate the project hypothesis related to capacity estimation, an experimental program was conducted at the Iowa State University Structural Engineering laboratory. Four steel-concrete composite sections were used to obtain the experimentally evaluated moment of inertia of the section and flexural strength, such that research group can (1). Develop a relationship between moment of inertia and flexural strength of steel-concrete composite sections and (2). Validate the use of I_{FEM} to get an improved flexural strength of steel-concrete composite sections. The beams were simply supported, and two concentrated loads were applied to create a constant moment region over the middle of the beam. Instrumentation of the beams consisted of strain gauges on the top of the concrete deck, top flange of the steel girder and bottom flange of the steel girder. Also, displacement gauges were attached to the bottom of each beam.

To calculate the I_{exp}, each specimen was loaded to 40% of the expected yield moment. The strain responses and the measured parameters along with the beam theory was used to calculate the calculated strain. The percent error between the calculated strains and the

measured strain were minimized by optimizing the moment of the inertia of the section. Both strain gauge data and displacement data were used to calculate and compare the I_{exp} results. As expected, the I_{exp} values are significantly higher than the I_n of each specimen. Then loads were applied to each beam until failure of each specimen to obtain the experimentally determined strength of the section. The M_{exp} of each section was significantly higher than the M_n of the section.

According to the experimental results, the theory of strength materials and the guide lines given in appendix D6.1 of the AASHTO Bridge Design Specification along with the actual material properties (if available) of the bridge can be used to evaluate the moment of inertia and the flexural strength of the steel-concrete composite sections. However, in lieu of existing properties of bridge components, Monte-Carlo simulation was used to develop a relationship between moment of inertia and flexural strength of steel-concrete composite sections. The improved flexural strength was noticeably higher than the nominal strength and the improved strength is smaller than the measured ultimate strength of each section thereby giving improved, but conservative estimates.

6.1.3 Prediction of Future Bridge Condition Ratings

Bridges are continuously exposed to environmental changes and dynamic loading effects due to moving loads. As a result, bridge deterioration is a critical problem in the United States. According to the infrastructure report card of the American Society of Civil Engineers (ASCE), as of 2016, almost 9.1% of bridges are rated as structurally deficient. The structurally deficient bridges are not necessarily unsafe to the traffic, but it can quickly become unsafe without proper inspections and maintenance. The average age of a bridge in the US is 43 years and approximately 40% bridges are older than 50 years. The American Society of Civil

Engineers estimates that rehabilitation of these bridges could cost about $123 billion, suggesting that even though there is a high repair and maintenance demand, the available resources are very limited.

The National Bridge Inventory (NBI) database contains historical bridge condition information for bridges in the United States and it is the best available database for describing the historical condition of bridges in the United States. NBI database contain condition rating data of bridges rated during visual inspections, on an integer scale from 0 to 9, where condition rating 0 represents a failed condition and condition rating 9 represents an excellent condition. The condition rating history data of Iowa and Wisconsin bridge components were statistically analyzed to understand the general trend of bridge behavior. More than 65% of bridge components in each state have more than 10 inspections spanning over 20 years. The average age of any Iowa bridge component is about 46.0 years. Most of the bridge decks in both Iowa and Wisconsin are rated as condition rating 7. Most of the superstructures and substructures in both Iowa and Wisconsin are rated as condition rating 7 or condition rating 8.

When predicting future condition ratings of bridge components, the time spent at each condition rating is very important, and it is defined as Sojourn Time of the condition rating of a bridge component. There are nine different types of Sojourn Times that can be defined (See Figure 5.12). These nine sojourn time types are capable of representing every possible transition in condition rating of a bridge component throughout its entire life. The characteristics of Sojourn Time database each bridge component was investigated to understand the effects of importance of Sojourn Time on predicting the future bridge condition ratings of bridges.

The research group developed two different types of future condition rating prediction models, namely Current Practice Model (CPM) and Deterioration Prediction Model (DPM). CPM is capable of simulating the effects of historical maintenance activities when predicting the future condition rating probabilities. Whereas DPM does not consider the effects of historical maintenance activities when predicting the future condition rating probabilities. The Sojourn Time database were filtered in five different ways to calculate the transition probabilities for different prediction methods. Both CPMs and DPMs were quantitatively and qualitatively evaluated to increase the confidence of using CPMs and to identify the best filtering method.

6.2. Conclusion

The experimental results show that the moment of inertia and the flexural strength of steel-concrete composite section calculated based on nominal material properties are significantly different than the actual moment of inertia and the flexural strength of the section. Therefore, the load rating factor calculated using nominal values underestimates the rating factor of bridge by 20% to 40%. The experimental results indicated that the theory of strength of materials and the AASHTO guidelines along with actual material properties (when available) can accurately predict the moment of inertia and flexural strength of the section. In the absence of actual material properties a Monte Carlo simulation along with the I_{exp} from the calibrated load rating model may significantly improve the rating factor of a bridge.

Quantitative evaluation results of both CPMs and DPMs shows data filtering Method IV is the best method for predicting future condition ratings. Also, it shows that Sojourn Time is an important parameter when predicting future condition ratings, whereas the age of the bridges does not play as an important role in predicting the future condition ratings of bridges.

According to the qualitative evaluation results, some bridges show very good agreement with the prediction results and some bridges are not. However, it is important to understand that these predictions are entirely dependent on the original historical data of the bridges, which are subjective. The CPMs tend to converge to condition rating 6 within 15 years, whereas the DPMs tend to converge to condition rating 4 with 15 years. This suggests that conducting current maintenance activities help to keep the nations bridges in at least "Satisfactory Condition". However, without not performing any maintenance could lead bridges to be structurally deficient within 15 years.

REFERENCES

[1] The American Society of Civil Engineers (ASCE), "ASCE Infrastructure Report Card," The American Society of Civil Engineers (ASCE), Reston, Virginia, 2017.

[2] The American Association of State Highway and Transportation Officials (AASHTO), "The Manual for Bridge Evaluation," Washington, DC, 2015.

[3] The American Association of State Highway Officials (AASHTO), "Grand Challenges: A Strategic Plan for Bridge Engineering AASHTO Highway Subcommittee on Bridges and Structures," 2005.

[4] D. Harman, "The Aging Process," *Proceedings of the National Academy of Sciences of the United States of America,* vol. 78, no. 11, pp. 7124-7128, 1981.

[5] R. G. Mishalani and S. M. Madanat, "Computation of Infrastructure Transition Probabilities Using Stochastic Duration Models," *Journal of Infrastructure Systems,* vol. 8, no. 4, pp. 139-148, 2002.

[6] A. E. Aktan, A. J. Helmicki and V. J. Hunt, "Issues in Health Monitoring for Intelligent Infrastructure," *Smart Materials and Structures,* vol. 7, no. 5, 1998.

[7] R. J. Connor and J. R. McCarthy, "Report on Field Measurements and Uncontrolled Load Testing of the Lehigh River Bridge (SR-33) (ATLSS Report No. 06-12)," Advanced Technology for Large Structural Systems, Bethlehem, PA, 2006.

[8] R. J. Connor and B. J. Santosuosso, "Report on Field Measurements and Controlled Load Testing of the Lehigh River Bridge (SR-33) (ATLSS Report No. 02-07)," Advanced Technology for Large Structural Systems, Bethlehem, PA, 2002.

[9] Office of Research Demonstration and Innovation, "The Status of the Nation's Highways, Bridges, and Transit: Conditions and Performance (Report FHWA-PL-93-017)," Federal Transit Administration, Washington, DC, 1993.

[10] N. M. Okasha and D. M. Frangopol, "Integration of Structural Health Monitoring in a System Performance Based Life-Cycle Bridge Management Framework," *Structure and Infrastructure Engineering,* vol. 8, no. 11, pp. 999-1016, 2012.

[11] N. F. Catbas, R. Zaurin, M. Susoy and M. Gul, "Integrative Information System Design for Florida Department of Transportation: A Framework for Structural Health Monitoring of Movable Bridges," Department of Civil and Environmental Engineering, University of Central Florida, Orlando, FL, 2007.

[12] H. Ghasemi, J. Penrod and J. M. Hooks, "Developing Advanced Methods of Assessing Bridge Performance," *The Federal Highway Administration (FHWA), Public Roads, (FHWA-HRT-10-001),* vol. 73, no. 3, 2009.

[13] J. Cadick and G. Traugott, "Condition Based Maintenance: A White Paper Review of CBM Analysis Techniques (Technical Bulletin TB-017)," Cadick Corporation, Garland, Texas, 2009.

[14] Y. Ni and K. Wong, "Integrating Bridge Structural Health Monitoring and Condition-Based Maintenance Management," in *Proceedings of the 4th International Workshop on Civil Structural Health Monitoring*, Berlin, Germany, 2012.

[15] Agency International Atomic Energy, "Implementation Strategies and Tools for Condition Based Maintenance at Nuclear Power Plants (IAEA-TECDOC-1551)," Vienna, Austria, 2007.

[16] Pavement Data Services, "Pavement Condition Assessment (V2.0W)," New York State Department of Transportation, Albany, NY, 2010.

[17] R. Ikegami and E. D. Haugse, "Structural Health Management for Aging Aircraft," in *Proceedings of the International Society for Optics and Photonics*, 2001.

[18] O. Benedettini, T. S. Baines, H. W. Lightfoot and R. M. Greenough, "State-of-the-Art in Integrated Vehicle Health Management," *Proceedings of the Institution of Mechanical Engineers, Part G: Journal of Aerospace Engineering,* vol. 223, no. 2, 2008.

[19] J. Xu and L. Xu, "Integrated System Health Management-Based Condition Assessment for Manned Spacecraft Avionics," *Proceedings of the Institution of Mechanical Engineers, Part G: Journal of Aerospace Engineering*, vol. 227, no. 1, 2012.

[20] J. Xu, F. Guo and L. Xu, "Integrated System Health Management–Based State Evaluation for Environmental Control and Life Support System in Manned Spacecraft," *Proceedings of the Institution of Mechanical Engineers, Part I: Journal of Systems and Control Engineering,* vol. 227, no. 5, 2013.

[21] T. Kijewski-Correa and M. Kochly, "Monitoring the Wind-Induced Response of Tall Buildings: GPS Performance and the Issue of Multipath Effects," *Journal of Wind Engineering and Industrial Aerodynamics,* vol. 95, no. 9-11, pp. 1176-1198, 2007.

[22] T. Kijewski-Correa and J. D. Pirnia, "Dynamic Behavior of Tall Buildings under Wind: Insights from Full-Scale Monitoring," *The Structural Design of Tall and Special Buildings,* vol. 16, no. 4, pp. 471-486, 2007.

[23] T. Kijewski-Correa, D. K. Kwon, A. Kareem, A. Bentz, Y. Guo, S. Bobby and A. Abdelrazaq, "SmartSync: An Integrated Real-Time Structural Health Monitoring and Structural Identification System for Tall Buildings," *Journal of Structural Engineering,* vol. 139, no. 10, 2013.

[24] A. Kareem, T. Kijewski and Y. Tamura, "Mitigation of Motions of Tall Buildings with Specific Examples of Recent Applications," *Wind and Structures,* vol. 2, no. 3, pp. 201-251, 1999.

[25] B. F. Spencer Jr. and S. Nagarajaiah, "State of the Art of Structural Control," *Journal of Structural Engineering,* vol. 129, no. 7, 2003.

[26] B. Oh, Y. Lew and Y. Choi, "Realistic Assessment for Safety and Service Life of Reinforced Concrete Decks in Girder Bridges," *Journal of Bridge Engineering,* vol. 12, no. 4, pp. 410-418, 2007.

[27] T. Kirkpatrick, R. Weyers, M. Sprinkel and C. Anderson-Cook, "Impact of Specification Changes on Chloride-Induced Corrosion Service Life of Bridge Decks," *Cement and Concrete Research,* vol. 32, no. 8, pp. 1189-1197, 2002.

[28] M. Liang, L. Lin and C. Liang, "Service Life Prediction of Existing Reinforced Concrete Bridges Exposed to Chloride Environment," *Journal of Infrastructure Systems,* vol. 8, no. 3, pp. 76-85, 2002.

[29] D. Chen and S. Mahadevan, "Chloride-Induced Reinforcement Corrosion and Concrete Cracking Simulation," *Cement and Concrete Composites,* vol. 30, no. 3, pp. 227-238, 2008.

[30] H. Song, H. Shim, A. Petcherdchoo and S. Park, "Service Life Prediction of Repaired Concrete Structures under Chloride Environment Using Finite Difference Method," *Cement and Concrete Composites,* vol. 31, no. 2, pp. 120-127, 2009.

[31] A. Miner, "Cumulative Damage in Fatigue," *Journal of Applied Mechanics,* vol. 67, pp. 159-164, 1945.

[32] Z. Li, T. Chan and J. Ko, "Fatigue analysis and life prediction of bridges with structural health monitoring data — Part I: methodology and strategy," *International Journal of Fatigue,* vol. 23, no. 1, pp. 45-53, 2001.

[33] Z. Li, T. Chan and J. Ko, "Fatigue analysis and life prediction of bridges with structural health monitoring data — Part II: application," *International Journal of Fatigue,* vol. 23, no. 1, pp. 55-64, 2001.

[34] Y. Zhou, "Assessment of Bridge Remaining Fatigue Life through Field Strain Measurement," *Journal of Bridge Engineering,* vol. 11, pp. 737-744, 2006.

[35] K. Kwon and D. Frangopol, "Bridge Fatigue Reliability Assessment Using Probability Density Functions of Equivalent Stress Range Based on Field Monitoring Data," *International Journal of Fatigue,* vol. 32, pp. 1221-1232, 2010.

[36] A. Caner, A. Yanmaz, A. Yakut, O. Avsar and T. Yilmaz, "Service Life Assessment of Existing Highway Bridges with No Planned Regular Inspections," *Journal of Performance of Constructed Facilities,* vol. 22, no. 2, pp. 108-114, 2008.

[37] M. Bolukbasi, J. Mohammadi and D. Arditi, "Estimating the Future Condition of Highway Bridge Components Using National Bridge Inventory Data," *Practice Periodical on Structural Design and Construction,* vol. 9, no. 1, 2004.

[38] G. Morcous, "Performance Prediction of Bridge Deck Systems Using Markov Chains," *Journal of Performance of Constructed Facilities,* vol. 20, no. 2, pp. 146-155, 2006.

[39] P. Bocchini, D. Saydam and D. Frangopol, "Efficient, Accurate, and Simple Markov Chain Model for the Life-Cycle Analysis of Bridge Groups," *Structural Safety,* vol. 40, pp. 51-64, 2013.

[40] T. Hopper, A. Manafpour, A. Radlinska, G. Warn, F. Rajabipour and Morian, "Bridge Deck Cracking: Effects on In-Service Performance, Prevention, and Remediation," Thomas D. Larson Pennsylvania Transportation Institute, University Park, PA, 2015.

[41] B. T. Adey, L. Klatter and J. S. Kong, "Overview of existing Bridge Management Systems," The IABMAS Bridge Management Committee, 2010.

[42] A. E. Aktan, D. N. Farhey, D. L. Brown, V. Dalal, A. J. Helmicki, V. J. Hunt and S. J. Shelley, "Condition Assessment for Bridge Management," *Journal of Infrastructure Systems*, vol. 2, no. 3, 1996.

[43] A. Rytter, "Vibrational Based Inspection of Civil Engineering Structures, (Ph.D. Dissertation)," Department of Building Technology and Structural Engineering, Aalborg University, Aalborg, Denmark, 1993.

[44] Office of Engineering (Bridge Division), "Recording and Coding Guide for the Structure Inventory and Appraisal of the Nation's Bridges (Report No. FHWA-PD-96-001)," U.S. Department of Transportation, Federal Highway Administration, Washington, DC, 1995.

[45] F. Fanous, L. F. Greimann, D. Petermeier and Z. Yuan, "Essential Parameters for an Iowa Bridge Management System," 1991.

[46] I. (. Bridge Diagnostics, "Integrated Approach to Load Testing Instruction Manual," Bridge Diagnostics, Inc., Boulder, CO, 2003.

[47] T. J. Wipf, B. M. Phares, L. F. Greimann, D. L. Wood and J. D. Doornink, "Evaluation of Steel Bridges (Volume I): Monitoring the Structural Condition of Fracture-Critical Bridges using Fiber Optic Technology," Center for Transportation Research and Education, Ames, IA, 2007.

[48] P. Lu, B. Phares, L. Greimann and T. Wipf, "Bridge Structural Health-Monitoring System Using Statistical Control Chart Analysis," *Transportation Research Record: Journal of the Transportation Research Board*, 2010.

[49] The American Association of State Highway and Transportation Officials (AASHTO), "Standard Specifications for Highway Bridges, 16th ed.,," Washington, DC, 1996.

[50] The American Association of State Highway and Transportation Officials (AASHTO), "LRFD Bridge Design Specification," Washington, DC, 2014.

[51] P. Mans, A. J. Yakel and A. Azizinamini, "Full-Scale Testing of Composite Plate Girders Constructed Using 485-MPa High-Performance Steel," *Journal of Bridge Engineering*, vol. 6, no. 6, 2001.

[52] V. K. Gupta, Y. Okui, N. Inab and M. Nagai, "Effect of Concrete Crushing On Flexural Strength of Steel-Concrete Composite Girders," *JSCE Journal of Structural and Earthquake Engineering*, vol. 63, no. 3, pp. 475-485, 2007.

[53] N. R. Roberts, "Evaluation of the Ductility of Composite Steel I-Girders in Positive Bending (MSc Thesis)," Department of Civil and Environmental Engineering, West Virginia University, Morgantown, WV, 2004.

[54] American Institute of Steel Construction (AISC), "Steel Construction Manual," United States of America, 2015.

[55] J. Melcher, Z. Kala, M. Holicky´, M. Fajkus and L. Rozlı´vka, "Design characteristics of structural steels based on statistical analysis of metallurgical products," *Journal of Constructional Steel Research*, vol. 60, pp. 795-808, 2004.

[56] D. Wiśniewski, P. Cruz, A. Henriques and R. Simões, "Probabilistic models for mechanical properties of concrete, reinforcing steel and pre-stressing steel," *Structure and Infrastructure Engineering*, vol. 8, no. 2, pp. 111-123, 2012.

[57] F. Bartlett, J. Jelinek, B. Schmidt, R. Dexter, M. Graeser and T. Galambos, "Updating Standard Shape Material Properties Database for Design and Reliability," American Institute of Steel Construction, Chicago, IL, 2001.

[58] American Society for Testing and Materials (ASTM) A992/A992M, "Standard Specification for Structural Steel Shapes," West Conshohocken, PA, 2015.

[59] American Society for Testing and Materials (ASTM) A1010/A1010M, "Standard Specification for Higher-Strength Martensitic Stainless Steel Plate, Sheet, and Strip," West Conshohocken, PA, 2013.

[60] American Society for Testing and Materials (ASTM) A709/A709M, "Standard Specification for Structural Steel for Bridges," West Conshohocken, PA, 2016.

[61] American Society for Testing and Materials (ASTM) A370, "Standard Test Methods and Definitions for Mechanical Testing of Steel Products," West Conshohocken, PA, 2015.

[62] American Society for Testing and Materials (ASTM) E8/E8M, "Standard Test Methods for Tension Testing of Metallic Materials," West Conshohocken, PA, 2016.

[63] American Society for Testing and Materials (ASTM) C39/C39M, "Standard Test Method for Compressive Strength of Cylindrical Concrete Specimens," West Conshohocken, PA, 2016.

[64] American Society for Testing and Materials (ASTM) C 469, "Standard Test Method for Static Modulus of Elasticity and Poisson's Ratio of Concrete in Compression," West Conshohocken, PA, 2002.

[65] T. Salama and H. H. Nassif, "Effective Flange Width for Composite Steel Beams," *The Journal of Engineering Research,* vol. 8, no. 1, pp. 28-43, 2011.

[66] J. G. Nie, C.-Y. Tian and C. Cai, "Effective width of steel–concrete composite beam at ultimate strength state," *Engineering Structures*, vol. 30, pp. 1396-1407, 2007.

[67] J. M. Castro, A. Y. Elghazouli and B. Izzuddin, "Assessment of effective slab widths in composite beams," *Journal of Constructional Steel Research*, vol. 63, pp. 1317-1327, 2006.

[68] D. M. Wittry, "An analytical study of the ductility of steel concrete (MS Thesis)," University of Texas Austin, Austin, Tx, 1993.

[69] A. J. Yakel and A. Azizinamini, "Improved Moment Strength Prediction of Composite Steel Plate Girders in Positive Bending," *Journal of Bridge Engineering*, vol. 10, no. 1, 2005.

[70] American Concrete Institute (ACI) Committee 318, "Buiding Code Requirements for Structural Concrete," Farmington Hills, MI, 2014.

[71] G. E. Ramey and R. L. Wright, "Bridge Deterioration Rates and Durability/Longevity Performance," *Practice Periodical on Structural Design and Construction*, vol. 2, no. 3, 1997.